SAND77-1778
Unlimited Distribution

STATUS OF THE DESIGN CONCEPTS FOR A HIGH FLUENCE FAST PULSE REACTOR (HFFPR)

J. S. Philbin, W. E. Nelson, B. Rosenstroch

Sandia Laboratories

SAND77-1778
Unlimited Distribution

STATUS OF THE DESIGN CONCEPTS FOR A HIGH FLUENCE FAST PULSE REACTOR (HFFPR)

J. S. Philbin

Reactor Design and Development Division, 5452

W. E. Nelson

Science Applications, Inc.

B. Rosenstroch

Advanced Reactor Safety Analysis Division, 5424

ABSTRACT

This report describes progress that has been made on the design of a High Fluence Fast Pulse Reactor (HFFPR) through the end of calendar year 1977. The purpose of this study is to present design concepts for a test reactor capable of accommodating large scale reactor safety tests. These concepts for reactor safety tests are adaptations of reactor concepts developed earlier for DOE/OMA for the conduct of weapon effects tests. The preferred driver core uses fuel similar to that developed for Sandia's ACPR upgrade. It is a BeO/UO_2 fuel that is gas cooled and has a high volumetric heat capacity. The present version of the design can drive large (217) pin bundles of prototypically enriched mixed oxide fuel well beyond the fuel's boiling point. Applicability to specific reactor safety accident scenarios and subsequent design improvements will be presented in future reports on this subject.

ACKNOWLEDGEMENTS

The authors would like to thank Paul S. Pickard, Raymond W. Ostensen and Henry C. Monteith of Sandia Laboratories, and Jay P. Odom of Science Applications, Incorporated, for their assistance and advice. We also appreciate the assistance of Allyn R. Phillips of Sandia in the preparation of the computer-drawn graphs.

TABLE OF CONTENTS

TABLE OF CONTENTS--CONT'D

LIST OF TABLES

LIST OF TABLES--CONT'D

LIST OF FIGURES

LIST OF FIGURES--CONT'D

LIST OF FIGURES--CONT'D

CHAPTER 1

Introduction

The progress made on the design of a High Fluence Fast Pulse Reactor (HFFPR) through December, 1977 is documented in this report. This design study conducted on behalf of NRC/RSR is an adaptation of an earlier design study conducted on behalf of Sandia's ERDA/DMA program for a weapon effect simulation facility capable of performance beyond that of the upgraded ACPR. A reactor of the type described would provide a unique capability for large-scale reactor safety research tests as well as for the conduct of the initial requirement--weapon effects tests. However, many weapon effects applications would require an external cavity and other features not emphasized here. This report will not discuss the specifics of the experimental capabilities of HFFPR but will only document some initial design concepts.

The development of a new reactor facility for defense applications would include as a part of the design a large central cavity, about 25 cm in diameter, and an even larger external cavity. During the conceptual design phase of such a facility, performance goals for reactor safety tests were also incorporated. These consisted of an average energy deposition of 2500 joules/gram for a subassembly size test and a radial peak-to-minimum ratio of less than 1.15. For this study it was considered desirable that the normalized spectrum be peaked within the energy range of 100-400 keV, for the minimum positive period to be 1 msec, and for the pulse width to be on the order of 5 msec. Performance based on these initial specifications may not be sufficient for the conduct

of certain types of reactor safety tests. However, as the performance goals for reactor safety tests evolve and as the future directions of advanced reactor safety research become better defined, future designs should reflect these considerations.

Sandia has a successful history of design and development of pulse and steady state reactors for defense-related research programs and more recently for reactor safety research experiments. The history includes the fast burst reactor series (SPR, SPR-II and SPR-III), the steady state Sandia Engineering Reactor (SER), the Annular Core Pulse Reactor (ACPR) and recently the ACPR Upgrade. These facilities have enjoyed a degree of high utilization and have contributed greatly to the development of radiation-hardened weapon systems and components vital to the national defense as well as to LMFBR safety research.

The reactor design concepts for the weapon effects facility as well as those presented here are compatible with the reactor building originally built for the now decommissioned Sandia Engineering Reactor (SER). The design is based on the modification of the lower part of the SER vessel to an outside diameter of approximately 1.25 meters. SER was originally a water-cooled steady state research reactor prior to being decommissioned in 1969. Existing piping, prior utilization of water coolant at the facility, and reduced costs were strong incentives for investigating water-cooled HFFPR designs. However, it was clear that large energy deposition with flat power bundles in large test components or bundles as well as spectral tailoring for such tests are much easier to achieve with a hard spectrum

gas-cooled driver core whose spectrum could be moderated and, therefore, both concepts have been pursued. Slow neutron filters and fueled converters were introduced into some of the models to achieve better power distribution in the test section, but this always resulted in significant sacrifices in total energy deposition. The filter/converter concepts have great potential, particularly with larger, more dilute cores, but optimization of the filter/converter concepts was beyond the scope of this report.

At this time, the favored core for the HFFPR design is a gas-cooled Class I system. A Class I system is defined as one which is capable of generating a power burst, or some form of shaped transient, without the need for significant reactor heat removal during the test; although post test heat removal is required to lower the initially high core and clad temperature. Modest cooling capability would be produced by a helium cooling system operating at 10 atmospheres, and would be sufficient to allow steady state operations sufficient for post accident heat removal experiments, but preconditioning at prototypic power levels would not be possible with the design presented here.

The design choice for the reactor fuel at this point in our study is 35 w/o (or 14 v/o) UO_2 in a BeO matrix. The UO_2 is 40% enriched. This is a higher loading than the ACPR Upgrade fuel which has 21.5 w/o, 7 v/o and 35% enriched UO_2 in BeO. It is expected that the harder spectrum of the gas-cooled system and the nearly flat fission profiles across the driver fuel cell will allow these loading increases without difficulty, but additional fuel testing work will be required to substantiate this

fact. Sandia has just completed the fuel development of the ACPR Upgrade fuel and has contributed to the development of the converter fuel for the Argonne STF.* The HFFPR fuel would be a logical result and possible extension of our experience with the ACPR Upgrade fuel development. At this stage in the calculations, the fuel elements are roughly 1.8 m high and consist of an active core region of 1.2 m with graphite axial reflectors making up the difference. The outer diameter of the core is <1 m, and the inside diameter of the cavity is 0.287 m. A 20 cm graphite radial reflector surrounds the core. Reference design data at this point in our study are described for gas and water-cooled systems in Tables 1-1 and 1-2.

The principal performance criteria for this stage in the design as applied to reactor safety tests has been an average radial energy deposition of 2500 j/gm into a 217-pin sodium cooled fuel bundle with a period of 1 msec. The cell geometry of the fuel bundle and the isotopic concentrations of the heavy nuclides in the mixed oxide fuel were modeled after the Clinch River Breeder Reactor Project (CRBRP) fuel at the beginning of equilibrium cycle (BOEC), i.e., the Pu-239 fraction and the total fissile fraction of heavy isotopes were 0.30 and 0.31, respectively.

The conceptual design, as reported here, falls slightly short of simultaneously meeting the 2500 j/g energy deposition and flux depression requirements for full subassembly test

---

* Safety Test Facility

bundles of prototypic enrichment (<1.15). This is due primarily to constraints on core size (<1.2 m OD) and excess reactivity required for fuel motion slots. Extensive core, converter/filter, or experiment optimization have not been done, however. There is ample excess reactivity to reduce the fissile loading of the driver, for example, and thereby increase the energy deposition in the test assemblies by another 5-10%. If the depositions can be boosted sufficiently, filters can be utilized to reduce the radial peak-to-minimum ratio. Future efforts should be directed toward these ends.

Moreover, the design, as presented, will satisfy energy and flux depression requirements for a majority of the desired safety tests using intermediate size bundles (37 pins) of medium enrichment. The cooling capacity of the reactor is determined by the steady-state heat removal requirements for PAHR type experiments.

The reactor has been designed with sufficient excess reactivity to accommodate two viewing slots through the driver fuel for observation of fuel motion in the test section. These slots are nominally 10 to 12 cm thick. The fuel motion diagnostic technique has not been selected at present but would likely be selected from coded aperture or x-ray cinematography.

Applicability of these reactor concepts to specific reactor safety accident scenarios is not discussed in this report. Specific test requirements will continue to be an evolutionary process and this evolution is expected to impact the final performance requirements for an HFFPR if ever developed. Subsequent

design improvements conducted in the final stages of this study and applications to reactor safety tests will be discussed in future reports on this subject.

TABLE 1-1

INTERIM REFERENCE REACTOR DESCRIPTION -- GAS COOLED
1 Region Driver

FUEL: BeO/UO_2	
Molecular Ratio of BeO to UO_2	20/1
Enrichment of UO_2	40%
Volume percent UO_2	14%
Weight percent UO_2	35%
Peak Operating Temperature	1500°C
CLAD	SS 316 or Inconel 718
COOLANT	He at 10 atms. pressure
DIMENSIONS	
Cavity I.D.	0.28 m
Core O.D.	0.96 m
Core Height	1.22 m
Core volume	0.8 m^3
RADIAL REFLECTOR (GRAPHITE)	
Thickness	0.2 m
Outer Diameter	1.4 m
Volume fraction graphite	1.0
AXIAL REFLECTOR	
Thickness	0.3 m
Volume Fraction Graphite	0.6592
Volume Fraction Gas Coolant	0.25
NEUTRONICS & KINETICS	
K_{eff} (no control elements or slots)	1.184
Generation time	12 μsec
Min. period	1 msec
Pulse width	4.5 msec
Reactivity insertion	$3.00
β_{eff}	0.0069
Core energy release	3000 MJ (ACPR = 108 MJ)
Average isothermal temperature coefficient (300K-900K)	-0.39 ¢/°C

REFERENCE REACTOR DESCRIPTION -- GAS COOLED
1 Region Driver (Cont'd)

MASS OF BeO/UO_2 Fuel -- no converter	2120	kg
Mass of UO_2	740	kg
Mass of U-235 Heavy Metal	260	kg
Mass of BeO	1380	kg
# of elements (3/4" dia.)	1520	

TABLE 1-2

INTERIM REFERENCE REACTOR DESCRIPTION -- WATER COOLED
2 Region Driver

FUEL: BeO/UO_2	
Molecular Ratio	35/1
Weight Percent UO_2	23.57%
Enrichment of UO_2	20%
Volume Percent UO_2	15.56%
Peak Operating Temp.	1500°C
CLAD: SS 304, SS 316	
COOLANT: H_2O	
Volume Percent	15%
CONVERTER: Fe-17 w/o Cr,	
4 w/o UO_2 93% Enriched	
Peak Operating Temp.	1200°C
Coolant	Air
DIMENSIONS:	
Converter I.D.	.28 m
Cavity I.D.	.38 m
Core O.D.	1.12 m
Core Height	1.22 m
RADIAL REFLECTOR: BeO	
Thickness	0.10 m
Outer Diameter	1.22 m
Volume Fraction BeO	0.6602
AXIAL REFLECTOR: BeO	
Thickness	0.3 m
Volume Fraction	0.6602
MASS OF BeO/UO_2 FUEL:	
BeO/UO_2	2540 kg
Mass of UO_2	600 kg
Mass U-235	120 kg
Mass BeO	1940 kg
NEUTRONICS AND KINETICS	
ℓ^*	30 μsec
β_{eff}	0.0069
Min. Period	1 msec

Chapter 2

Description and Comparison of Candidate Fuels -- Gas Cooled System

A number of fuel materials were considered as potential drivers or converters. A sampling of these is given in Table 2-1. The converters consisted of UO_2 and UO_2 dispersions in iron as well as in iron-aluminum, nickel-aluminum, and iron-chromium alloys, plus metallic solid solutions of niobium and uranium. The driver fuels were principally limited to a range of UO_2 loadings and enrichments in BeO and Al_2O_3. There was some one dimensional exploration of mixing metallic/ceramic fuels within core regions in varying fractions from the inside to the outside (envisioned in practice as alternating pellets in the appropriate ratio within a fuel element) as an alternative to separate converter/driver regions for hardening the spectrum. These concepts showed promise of improved energy deposition for a given radial peak-to-minimum in the test section but this idea was not pursued because of time limitations, generally low reactivity worth of the few configurations selected, and the uncertainty of problems associated with such a design.

A number of two-region cores of the driver/converter type were calculated with a one-dimensional transport code and cell-weighted Hansen-Roach 16 group cross sections during the early phase of this study. Within each region the fuel-clad-coolant cell was homogenized according to the volume fractions in Table 2-2.

Based on initial studies (typical parametric results are reported in References 1 and 2) niobium clad for BeO/UO_2 gas cooled systems and Nb-U cermet fuels were rejected because they could not meet reactivity requirements. The BeO/UO_2 fuels with stainless steel or

TABLE 2-1

Survey of Gas Cooled Fuels Considered

Fuel	Favorable Points	Unfavorable Points
BeO/UO_2 Molecular ratio Range: 15 - 70	High volumetric heat capacity.	Spectrum is fairly hard but filters or converters may still be required.
Enrichment: 30-93	High Temperature	
	Good Reactivity	
	Fuel Development experience available at Sandia.	Additional fuel development work is required.
Fe-Al/UO_2 Converter UO_2 wgt. percent ~12.5 Enrichment 40-60%	Good volumetric heat capacity due to high per atom heat capacity of iron and good atom density.	Fuel development effort required. Properties not well known.
	4 atom percent aluminum in iron melts at ~1510°C and does not have the α phase transformation at 910°C observed for pure iron.	
Nb/U	Metallic, solid solution fuel. High temperature. Sandia had studied material properties for previous reactor applications. Considered as a possible driver.	----- Reactivity too low at low fissile loadings required for a reasonable figure-of-merit.
Al_2O_3/UO_2 Molecular ratio 9.4/1	Gives hard spectrum, flat peak-to-min, good energy deposition based on steady state neutronics.	Low reactivity worth.
Enrichment ~50%	Al_2O_3 is a widely used and well-characterized material.	No history as a reactor fuel. Development effort required.
	---	Poor negative temperature coefficient as presently modeled.

Fuel	Favorable Points	Unfavorable Points
Ni-Al alloys	High melting point. Higher than either constituent, and single phase for 50% Al and 50% Ni, T_{melt} = 1638°C.	Brittle, properties not well known.

Inconel 718 clad stood out as the most promising driver fuel candidate from the initial neutronics and materials evaluation. The spectrum of the BeO fuel was softer than we desired as shown in Table 2-3 and Fig. 2-1, but other criteria from Table 2-1 could easily be satisfied. The Al_2O_3 fuel was selected for more extensive finite geometry evaluation because it did yield a harder spectrum and the properties of the Al_2O_3 material are well known. However, the negative temperature coefficient of reactivity and the k_∞ of the Al_2O_3 fuel were both lower than desired. A description of the fuels, as studied, is given in Table 2-4. All fuels will require a fuel-development or test program to verify their performance under repeated pulsing conditions.

Figure 2-2 is a graph of the integrated fissions using the fission cross section of U-235 and four multigroup flux spectra representative of the BeO and Al_2O_3 driver fuels, the Fe-Al converter fuel and the mixed oxide test fuel. At any given energy, decreasing along the abcissa, one can evaluate the fraction of the total fissions that occur above and below that energy for each fuel type. The mixed oxide test fuel (curve 1) has the hardest spectrum and in order to have reasonably flat radial energy deposition profile ($P/M \leq 1.15$) in the test section, the free-field

TABLE 2-2

Cell Descriptions for Gas-Cooled Models

Cell Region	Volume Fraction	Radium, cm
fuel	0.66 (to 0.71)	0.9525
gap (void)	0.035	0.9779
clad	0.055	1.016
gas coolant (void)	0.25 (to 0.20)	1.1732

TABLE 2-3

Comparison of BeO/UO_2 and Al_2O_3/UO_2 Energy Spectrum*

(gas cooled)

Gp	Lower Energy Bound of the Group	Normalized Flux	
		BeO	Al_2O_3
1	3.0 meV	0.0243	0.0205
2	1.4 meV	0.0774	0.0634
3	0.9 meV	0.0399	0.0481
4	0.4 meV	0.0947	0.1238
5	0.1 meV	0.1556	0.2269
6	17 keV	0.2106	0.2434
7	3 keV	0.1361	0.1404
8	0.55 keV	0.1292	0.0782
9	100 eV	0.0816	0.0272
10	30 eV	0.0294	0.0058
11	10 eV	0.0103	0.0016
12	3 eV	0.0056	0.0005
13	1 eV	0.0037	0.0002
14	0.4 eV	0.0010	0.0
15	0.1 eV	0.0005	0.0
16	0.025 eV	0.0	0.0

*Derived from S_n calculations using the reference fuels described in Table 2-1.

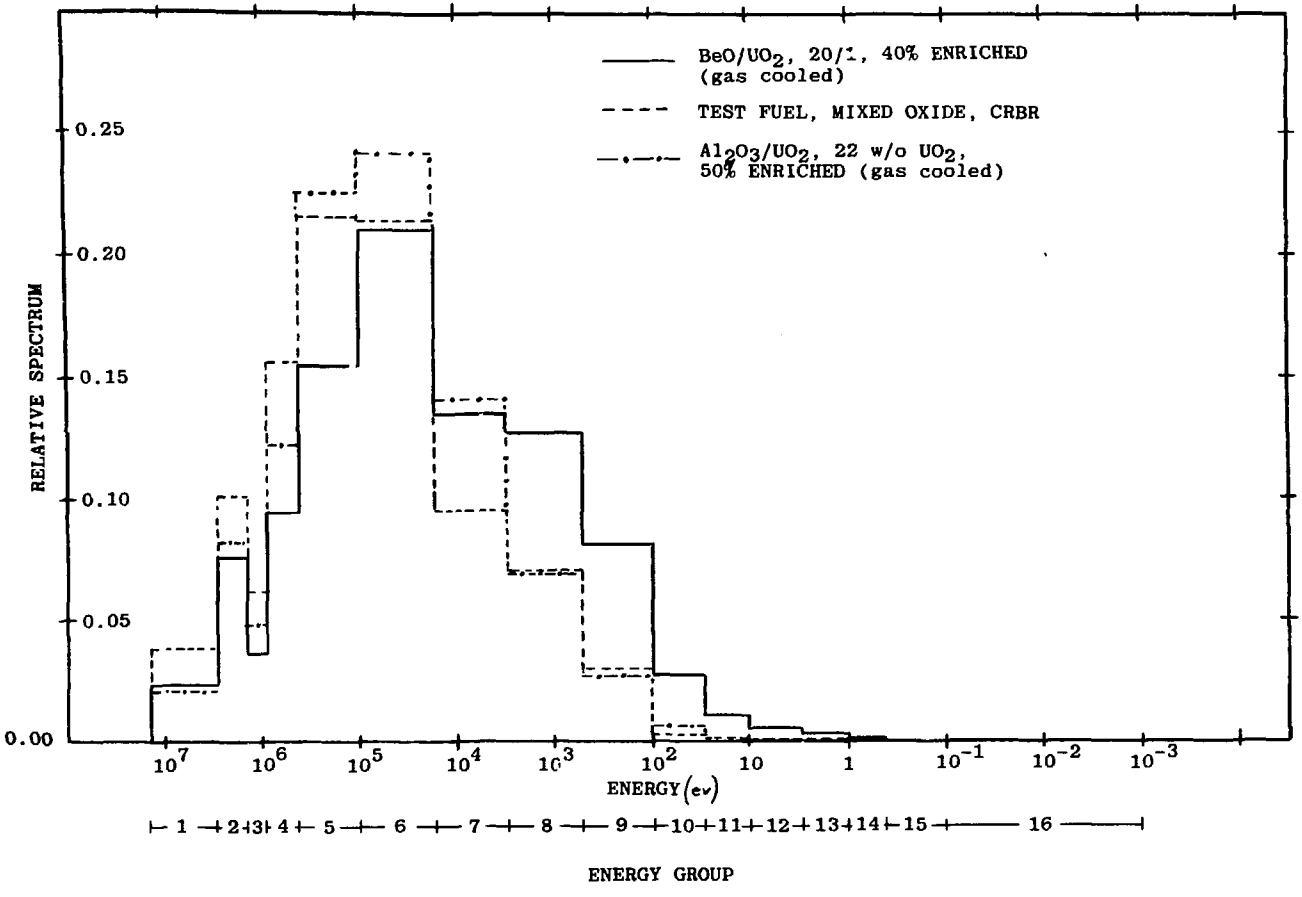

FIGURE 2-1 MULTIGROUP NEUTRON SPECTRUM OF TEST FUEL AND DRIVERS

TABLE 2-4

Reference Fuel Specifications for BeO and Al_2O_3 and Fe-Al Fuels

(gas cooled)

BeO/UO_2 ceramic fuel - k_∞ (from XSDRNPM cell calculation, 123 groups) = 1.53
(infinite media, H-R X-sects) = 1.41

Molecular ratio, 20/1
Weight percent UO_2, 34.9%

UO_2 Enrichment, 40%

Fissile atom fraction, C_D, 0.0093

Composite fuel density, 3.998 g/cc
Peak operating temperature, 1500°C

Al_2O_3/UO_2 ceramic fuel - k_∞ (from XSDRNPM) = 1.39

Molecular ratio, 9.4/1
Weight percent UO_2, 21.85%

UO_2 Enrichment, 50%

Fissile atom fraction, C_D, 0.01

Composite fuel density, 4.567 g/cc
Peak operating temperature, 1250°C

Fe-Al/UO_2 metal converter - k_∞ (16 group CHILE calculation) = 1.33

4% Al in iron
Weight percent UO_2, 12.5%

UO_2 enrichment 50%

Fissile atom fraction, C_D, 0.0133

Composite fuel density, 7.81 g/cc
Peak operating temperature, 1250°C

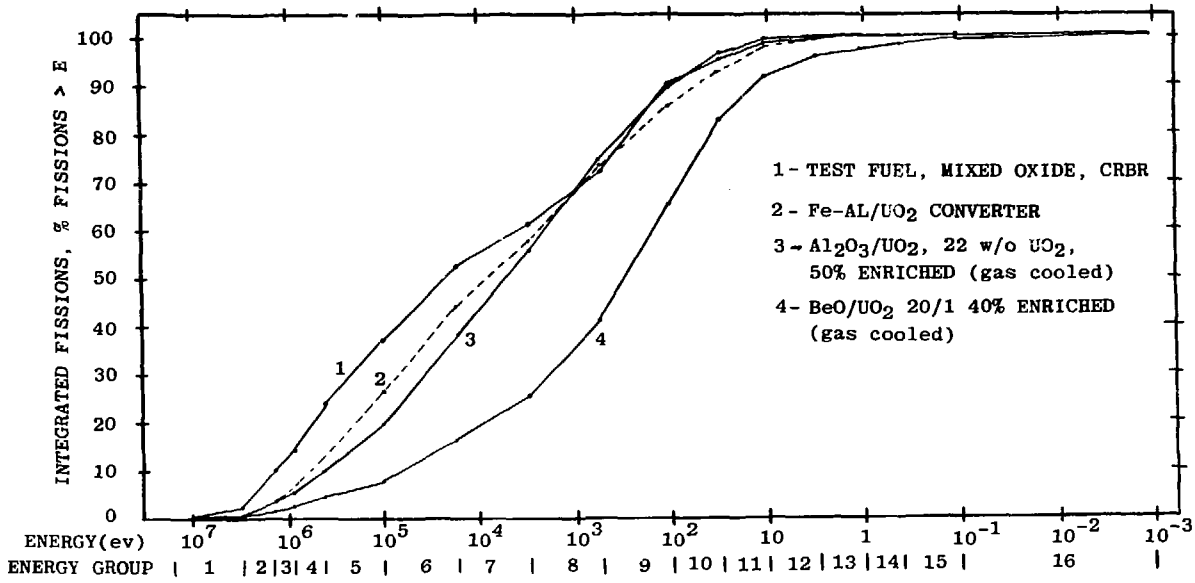

FIGURE 2.2 INTEGRATED FISSION ACTIVITY

cavity spectrum for the experiment should be at least as hard as curve 4 for the unfiltered 20-to-1 BeO/UO_2 (40% enriched) driver. The radial peak-to-minimum for the unfiltered BeO/UO_2 driver is 1.2.

A comparison of the performance characteristics of the various fuels and fuel concepts, gas-cooled, is presented in Table 2-5. Details of the neutronics calculations used in deriving these results are presented in subsequent sections.

Table 2-5
Comparison of Gas Cooled Reactor Characteristics
(Non-Optimized)

Characteristic	Be/UO_2	BeO/UO_2 with Converter	BeO/UO_2 (Filter)	Al_2O_3/UO_2	Nb/U
Energy Deposition (profile (P/M)) (30% Pu-239)	1.19	1.03	--	1.04	<1.0
Energy Deposition (Maximum) j/g	2380	1720	--	2410	750
Min. Period (msec)	1.0	1.0		<4.0	--
Core Volume (m^3)	0.8	1.09	--	>1.35	3.2
Neutron Generation Time (μsec)	12	12	12	2-20	0.2
Maximum Temperature (°C)	1500	1500 Driver 1250 Converter	1500	1250	1400

Chapter 3

Description and Comparison of Candidate Fuels - Water Cooled System

As with the gas cooled system, a number of fuel materials were studied as potential drivers or converters (see Table 3-1). The converter was limited to fully enriched UO_2 dispersed in SS430 (Fe/17% Cr). The driver fuel of greatest promise was the BeO/UO_2 ceramic fuel, although the Al_2O_3/UO_2 and $Fe\text{-}Al/UO_2$ fuels were studied as possible fuel candidates.

Two region cores of the driver/converter type for the light water cooled cores and one region driver cores with cadmium filters for both light and heavy water cooled cores were studied. Specifications of the fuels studied can be found in Table 3-2. Volume fractions for the homogenized fuel cells can be found in Table 3-3.

The Al_2O_3/UO_2 and $Fe\text{-}Al/UO_2$ fuels were not considered for the light water system because of the possibility of severe peaking in the fuel cells. However, they were studied for the heavy water system where they showed some promise because of their harder spectra which leads to lower peak-to-minimum in the test package. A set of histograms in Figure 3-1 show the spectra from heavy and light water moderated BeO fuel along with the harder spectrum from the centerline of the test fuel.

Because of the softness of the BeO spectrum, it is necessary to have some method of hardening the cavity spectrum. This can be accomplished by the use of a dry converter or a filter. Also, one can use a moderator/coolant with a lower moderating power. Table 3-4 is a comparison of light and heavy water moderated drivers with a cadmium filter.

TABLE 3-1

Survey of Water Cooled Fuels

Fuel	Favorable Points	Unfavorable Points
BeO/UO_2	High volumetric heat capacity	Soft spectrums for water systems. Filters or converters required to reduce P/M ratios.
	High temperature	
	Good reactivity Fuel development experience available at Sandia.	Additional fuel development work is required.
Al_2O_3/UO_2	Hard spectrum	Low reactivity worth high U-235 loading reduces energy deposition in test package.
	Flat P/M ratio for D_2O moderated system.	No history as reactor fuel, fuel development effort required.
	Al_2O_3 is a widely used and well-characterized material.	Peaking problems possible in the fuel cell for H_2O moderated system.
Fe-Al/UO_2	Hard spectrum	Fuel development needed.
	Flat P/M ratio for D_2O system.	
	Good volumetric heat capacity.	Peaking problems possible in fuel for H_2O moderated.
Air-cooled converter: Fully enriched UO_2 in 85% dense SS430	Fuel development studies from ANL-STF.	Fluence reduction in cavity due to converter presence.
	Hard spectrum low P/M ratios.	Air cooling required.
	Potential converter fuel	

TABLE 3-2

Candidate Fuel Specifications for Water Cooled HFFPR

BeO/UO_2 ceramic fuel

Molecular Ratio - 35/1
Weight Percent UO_2 - 23.6%

UO_2 enrichment - 10%-50%

Fissile atom fraction C_D = 0.0014 - 0.0068

Composite fuel density = 3.620 g/cc
Peak operating temperature = 1500°C

Al_2O_3/UO_2 ceramic fuel

Molecular Ratio - 9.4/1
Weight Percent UO_2 - 21.9%

UO_2 enrichment - 25%-50%

Fissile atom fraction C_D = 0.0050 - 0.0100

Composite fuel density 4.57 g/cc
Peak operating temperature 1250°C

Fe-Al/UO_2 metal fuel

Molecular Ratio 34.5/1
Weight Percent UO_2 - 12.5%

UO_2 enrichment - 50%-93%

Fissile atom fraction C_D = 0.0069 - 0.0129

Composite fuel density 7.81 g/cc
Peak operating temperature 1250°C

Fully enriched UO_2 in Fe/17% Cr (SS430) metal converter

Molecular Ratio - 35/1
Weight Percent UO_2 6.48%

UO_2 enrichment - 93.15%

Fissile atom fraction C_D = 0.0128

Composite fuel density 6.77 g/cc
Peak operating temperature 1200°C

TABLE 3-3

Cell Description for Water Cooled Models

Region	Volume Fraction	Radius
Fuel	0.6602	2.24 cm
Gap	0.1055	2.41 cm
Clad	0.8423	2.54 cm
Coolant	0.1500	2.76 cm

TABLE 3-4

Comparison of relative spectra for H_2O and D_2O moderated core with BeO/UO_2 fuels, and cavity spectra after filtering with cadmium.

Gp	Lower Energy Bound	Driver: BeO/UO_2 = 35/1 20% Enriched H_2O Mod.		Driver: BeO/UO_2 = 35/1 25% Enriched D_2O Moderated	
		Driver	Cavity	Driver	Cavity
1	1.35 MeV	0.1184	0.1126	0.0829	0.0749
2	0.40 MeV	0.1330	0.1566	0.0980	0.1090
3	86.5 KeV	0.1394	0.1689	0.1375	0.1489
4	0.13 KeV	0.3206	0.3773	0.4960	0.5129
5	1.86 eV	0.1326	0.1469	0.1396	0.1353
6	0.65 eV	0.0320	0.0311	0.0214	0.0168
7	0.16 eV	0.0366	0.0033	0.0155	0.0019
8	0.06 eV	0.0444	0.0014	0.0063	0.0003
9	0.005 eV	0.0430	0.0020	0.0028	0.0002

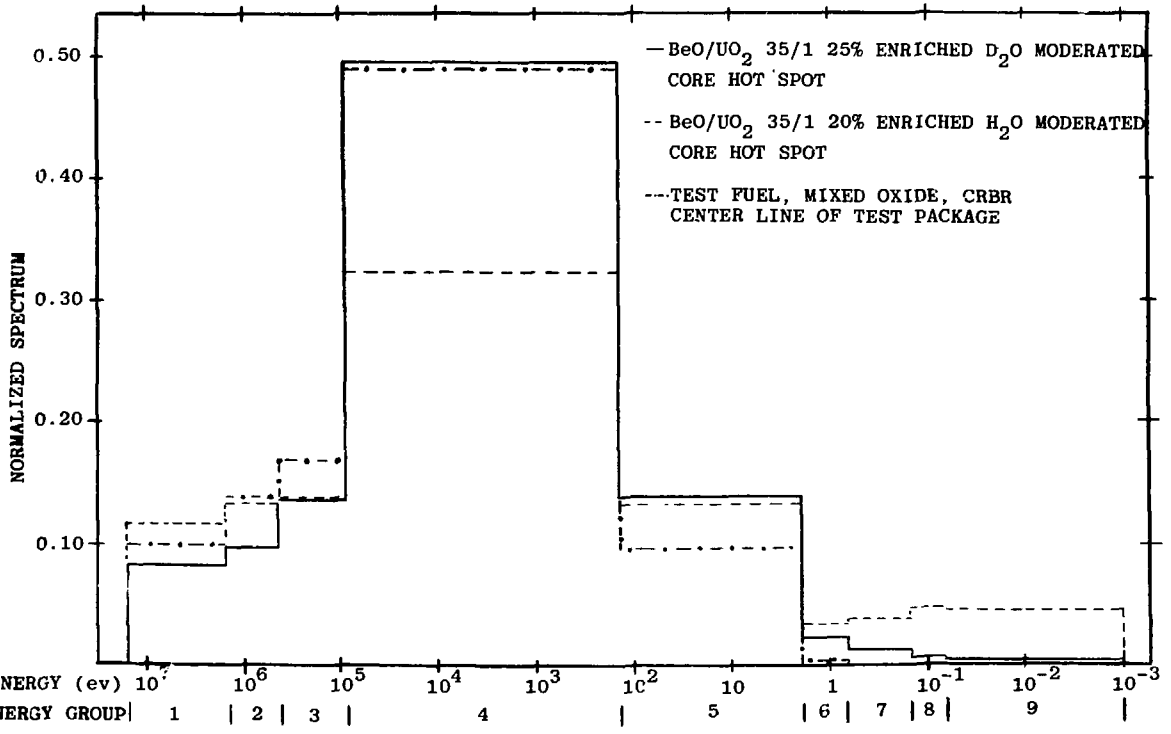

FIGURE 3-1 NORMALIZED SPECTRA FOR HEAVY WATER AND LIGHT WATER MODERATED CORE PLUS TEST PACKAGE CENTER LINE SPECTRUM

It should be noted that the cavity spectrum after filtering with cadmium for the D_2O moderated system is slightly harder than for the H_2O moderated system. This in turn will lead to better peak-to-minimum ratios in the test package.

Figure 3-2 is a graph of the integrated fissions in the driver cores (light and heavy water moderated) and the test package center line. As is apparent, the driver core spectra for both the light and heavy water moderated cores are much too soft to give reasonable peak-to-minimums in the test package.

A comparison of the performance characteristics of various BeO/UO_2 fuels, light and heavy water moderated, and converter/filter systems is found in Table 3-5.

Figure 3-3 is a comparison of the volumetric energy deposition in a H_2O cooled two region core driver/converter type and a D_2O one region core with cadmium filter.

Further details of the neutronic calculations and more extensive results will be found in subsequent sections for the water-cooled concept.

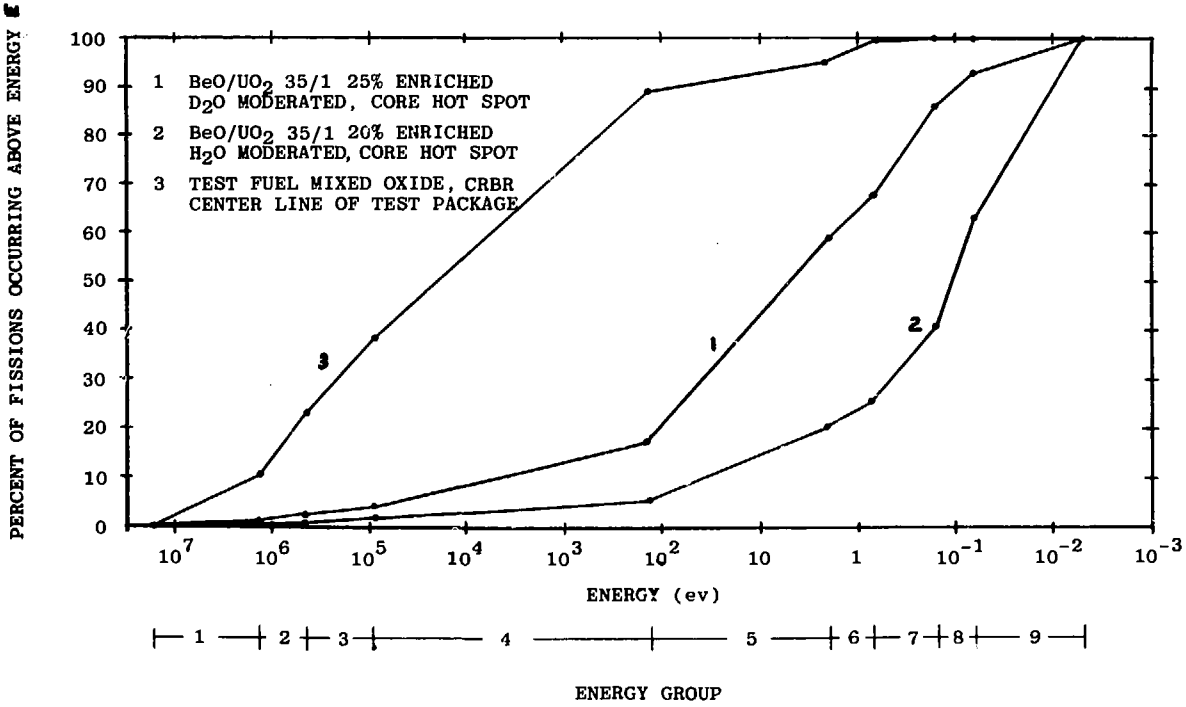

FIGURE 3-2 PERCENTAGE OF FISSIONS OCCURRING ABOVE ENERGY E

TABLE 3-5

Comparison of Water-Cooled Reactor Designs for 61 Pin Bundle Tests

	Driver Core						
	Fuel	En.%	Mod	Convertor/ Filter	Outer Diameter, m	Energy Deposition, J/g	Profile (P/M)	k eff
1.	UO_2 - BeO	20	H_2O	5.08 cm Fe (Dry)	1.22	1100	1.18	1.17
2.	UO_2 - BeO	20	H_2O	2.54 cm Fe (Dry)	1.22	1575	1.60	1.17
3.	UO_2 - BeO	20	H_2O	*Cd Filter	1.22	1375	1.47	1.16
4.	UO_2 - BeO	10	H_2O	*Cd Filter	1.83	1625	1.74	1.05
5.	UO_2 - BeO	25	D_2O	*Cd Filter	1.83	1950	1.17	1.07
6.	UO_2 - BeO	50	D_2O	*Cd Filter	0.91	1550	1.05	1.06

* Areal density ≡ density * thickness = 8.65×10^{-5} g/cm.

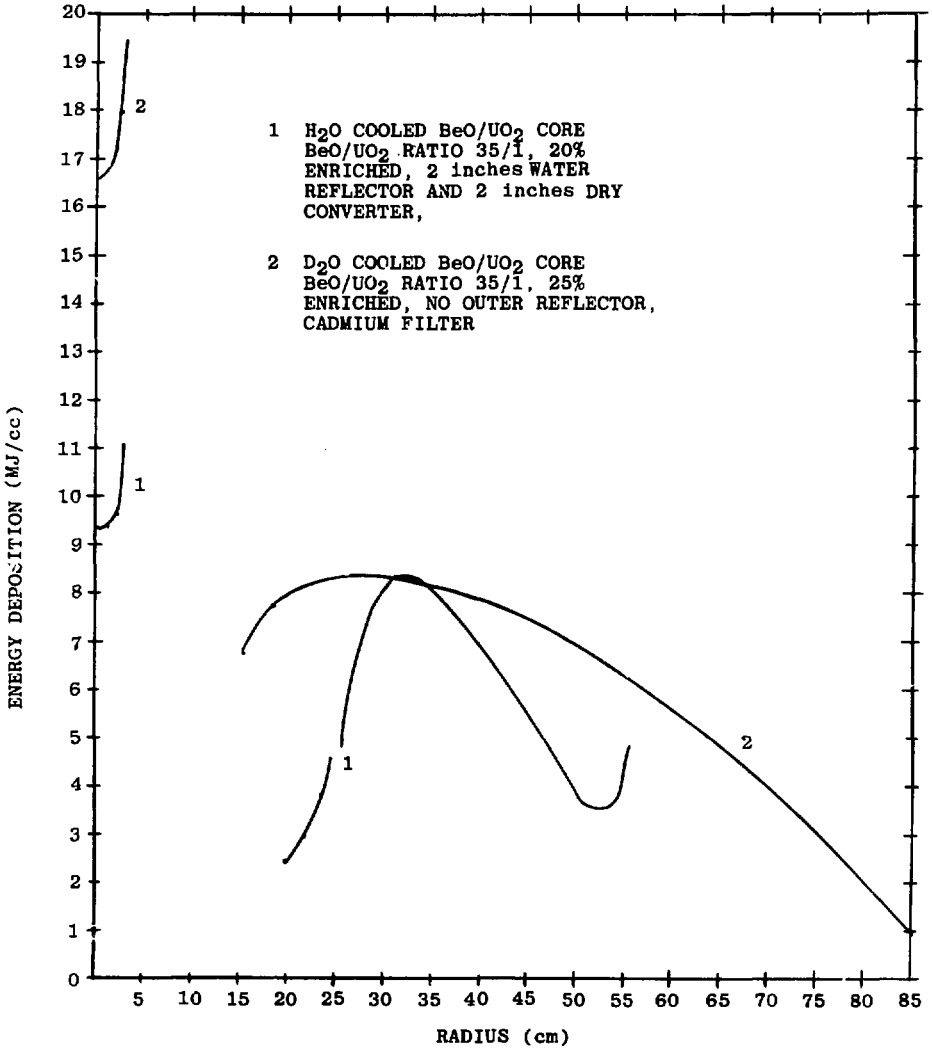

FIGURE 3-3 COMPARISION OF VOLUMETRIC ENERGY DEPOSITION OF H_2O COOLED BeO/UO_2 CORE AND D_2O COOLED BeO/UO_2 CORE

Chapter 4

Cross Section Development

Temperature dependent multigroup cross section sets were developed for use in the neutronic calculations. The modular code AMPX [3] was used to process the raw ENDF/B data in order to catalog the necessary temperature dependent cross section sets. The AMPX modules can be used to (1) generate multigroup neutron cross section sets; (2) generate multigroup gamma cross section sets; (3) generate gamma yields for gamma producing neutron interactions; (4) produce coupled neutron, gamma, and gamma yield cross section sets; (5) perform one dimensional discrete ordinates transport or diffusion theory calculations for neutrons and gammas and also use the one dimensional results as weighting functions for collasping the fine group cross sections to broad group structure; and (6) output multigroup group cross sections in convenient formats for other codes. The basic modules in AMPX that were used to produce the temperature dependent, multigroup neutron cross section sets were (1) XLACS, (2) NITAWL, (3) XSDRNPM, and (4) AID. Special modules that were employed include (1) JUANITA, (2) CONVERT, and (3) LAVA. The Sandia version of AMPX is described in Reference 4.

XLACS was used to reduce the ENDF/B data to a 123 energy group master library. XLACS can be used to produce neutron cross sections of desired group structure, scattering order, and a variety of weighting functions. For most resonance nuclides, XLACS will perform a preliminary processing of the resonances and pass any unresolved parameters to NITAWL for final resonance resolution. NITAWL is used to produce an AMPX working library that is suitable for use in XSDRNPM and

also KENO-IV [5]. For resonance nuclides with unresolved parameters, NITAWL uses the Nordheim Integral treatment to reduce any unresolved resonance parameters. XSDRNPM is a one-dimensional discrete ordinates code that has the capability of doing spectrum weighting and collapsing of the fine group cross section sets to broad group structure. These collapsed sets can be produced as cell-weighted or a variety of region-weighted sets. The cross sections from XSDRNPM were in ANISN format, suitable for use in the code TWOTRAN-II [6]. AID was used to convert from ANISN format to DTF format and also to label the sets as to fuel type (driver, converter, test package, etc.).

JUANITA and CONVERT were used to process cross section sets from an old XSDRN library to sets compatible with the format now in use in the AMPX modules. These sets were in the form of a master library and could then be updated onto the master library produced from XLACS.

LAVA was used to produce AMPX working libraries from ANISN cross section sets. The working libraries were then concatenated with NITAWL so that they could be used in KENO-IV.

Chapter 5

Reactor Studies

5.1 General

Since final fuel element design was beyond the scope of this report and since the general neutronic properties are not particularly sensitive to the cell model in a gas-cooled system, a single cell geometry was selected and used in generating all cell-dependent cross sections. Initially in the 1-D calculations the fuel/coolant volume fractions were adjusted, as noted in Table 2-2, to increase or decrease reactivity, but a 0.66 fuel fraction was used in all of the 2-D calculations reported here.

The basic 1-D and 2-D calculational models are shown in Figs. 5.1-1 and 5.1-2. The central irradiation cavity of 28 cm was assumed for all cases, but the outer core radius and the reflection thicknesses were varied as part of a parametric study.

The fuel cell specifications used for the generation of cell-weighted cross sections were fixed for all of the neutronic calculations. The fuel element size was chosen by considering the thermal-hydraulic, stress, and heat removal characteristics of a combination of fuel materials, fuel element diameters, gap sizes, gap fill gases, clad thicknesses, and coolant heat transfer coefficients under both pulse and steady state operating conditions. See Chapters 2 and 3 plus Section 5.3.

The analytic tools and approach to the reactor design are presented in Table 5.1-1. A brief description of the codes is given below:

DTF-IV [7] was used for the performance of survey calculations. It solves the multigroup, one-dimensional Boltzmann

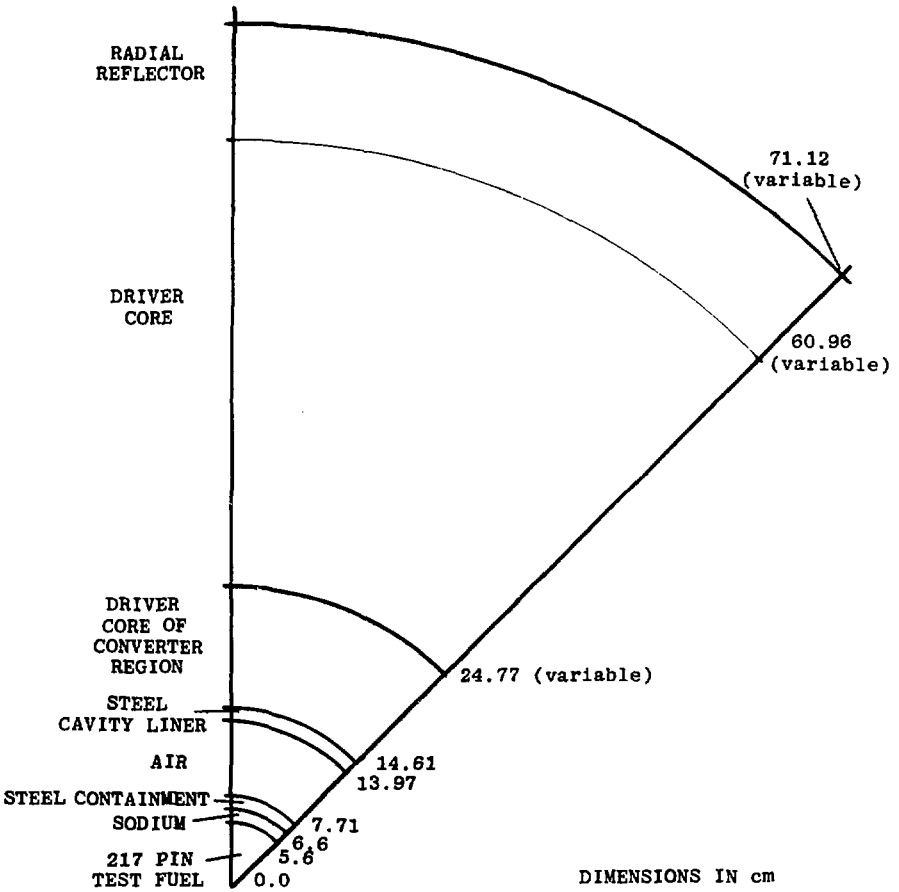

FIGURE 5.1-1 1-D MODEL, GAS COOLED SYSTEM, 217 TEST PINS

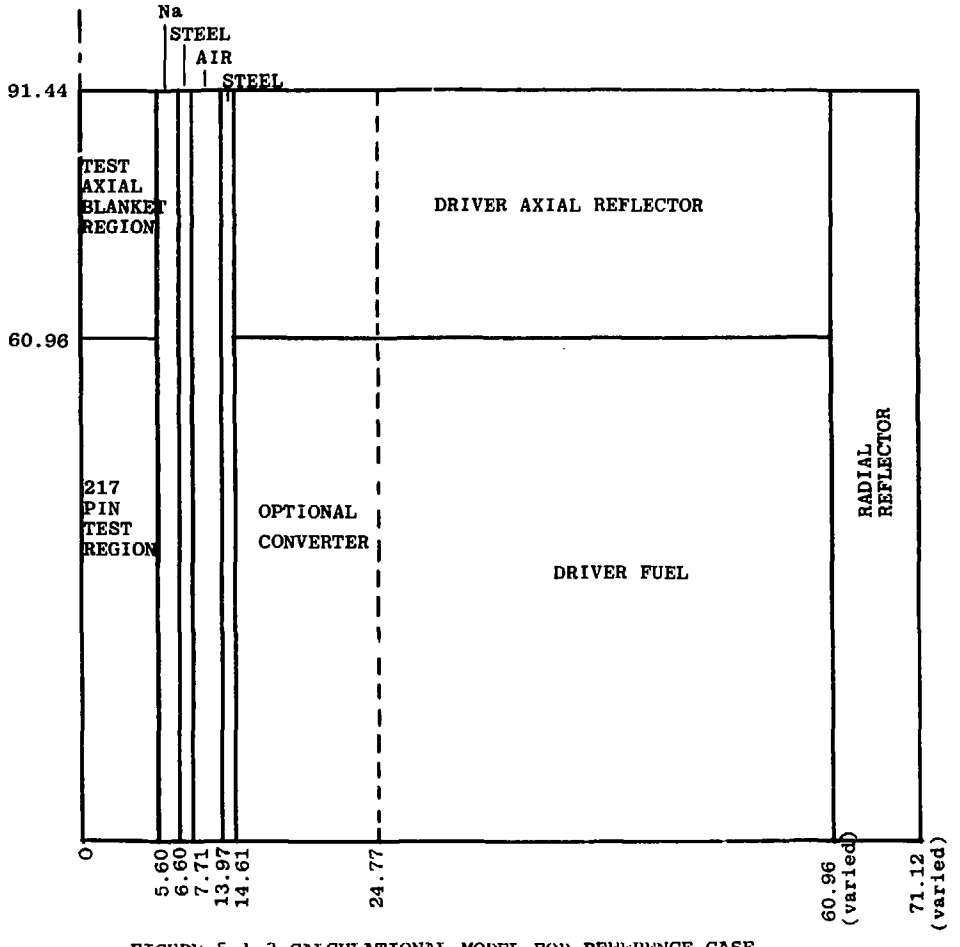

FIGURE 5.1-2 CALCULATIONAL MODEL FOR REFERENCE CASE

Table 5.1-1

Analytic Approach for HFFPR Design Studies

Survey Calculations	1D - DTF
Preliminary Design Calculations	1D - DTF
	2D - TWOTRAN-II
	3D - KENO-IV
Kinetics	KENO-IV - (ℓ)
	SAK - (α)
	TWOTRAN-II (α)
	PK1D, SAK (Kinetics)
Heat Transfer	TAC2D PK1D, SAK
Cross Sections	AMPX (ENDF) (Hansen/Roach)

transport equation, including anisotropic scattering. TWOTRAN-II [6] was used to solve the two dimensional multigroup transport equation. Like DTF it uses the S_N discrete ordinates formulation of of the Boltzmann equation.

KENO IV [5] is a multigroup Monte Carlo criticality program which calculates k_{eff}, lifetime, energy dependent leakages and absorptions, fluxes, and fission densities. This code was used primarily for calculating prompt neutron generation times and to confirm some TWOTRAN-II results for k_{eff}.

Kinetics calculations were done with the help of the SAK and PK1D computer codes [8].

The Sandia Kinetics code (SAK) is a one-dimensional, time dependent code which couples thermal hydraulic with neutronic analysis in order to simulate reactor transients. Time dependent changes in material properties are provided for, as is radiative heat transfer. The Point Kinetics One-Dimension Heat Transfer Code (PK1D) solves the point kinetics equations. It uses the same heat transfer routines as SAK, and couples the heat transfer equations with the point kinetics equations by the temperature dependent reactivity feedback.

The prompt neutron generation time for SAK and PK1D were derived from KENO IV and the temperature feedback coefficients for PK1D were derived from SAK. Isothermal temperature coefficients were obtained from TWOTRAN II as a check on the SAK results. SAK allowed for distributed temperatures in the core.

Heat transfer calculations were also performed with the TAC2D code [9], a two-dimensional code for calculating steady state and

transient temperatures by the finite difference method in rectangular, cylindrical, or polar coordinates. As in the SAK code, the thermal properties may be functions of time, local temperature, or local position.

Operations required to generate and collapse multigroup neutron and gamma cross section sets are provided by the AMPX system [13], which utilizes neutron and gamma cross section data obtained from ENDF/B libraries. Use of the AMPX system to generate cross section sets is discussed in Chapter 4.

5.2 Neutronics Calculations - Gas Cooled System

5.2.1 General

During the development of our ENDFB-IV/AMPX, temperature-dependent cross section library, described in Chapter 4, infinite media, as well as 1-D and 2-D S_n calculations were performed using the Hansen-Roach (HR) cross sections [10]. These results will not be reported in detail here. However, in order to make comparisons and to illustrate certain trends that we feel are important, we have chosen to include some of the results calculated with the HR cross sections. In such cases, graphs will be clearly marked and table entries will be footnoted to alert the reader to inconsistencies between these results and later calculations with the newer cross section sets. For the gas cooled systems, the group structure selected for the AMPX-generated cross sections was matched as closely as possible to the sixteen group HR energy boundaries.

5.2.2 Single Region Driver Cores

On the basis of the two-dimensional neutron transport calculations with the HR cross sections, several single region driver cases were selected for evaluation with the new cross sections. The 2-D model was introduced earlier in Fig. 5.1-2.

A description of the various systems and their performance characteristics, including comparisons using the HR cross sections, are given in Table 5.2.2-1. The fuels used in the calculations are described in Table 5.2.2-2. All cases were normalized to the peak operating temperatures of the driver fuels.

Note that for the BeO fuel, the newer cross section set results in a softer spectrum, a higher eigenvalue (6%), a steeper radial

Table 5.2.2-1
Performance Characteristics of Initial BeO and Al_2O_3 Driver Fuels

Case No.	Driver Description	Driver Fuel Outside Diameter (cm)	Radial Reflector[a]	K eff	Generation Time Λ (10^{-6} s)	Edge Energy Deposition (J/gm)	Edge-to-Center Ratio at Midplane	Axial Peak-to-Min. at ℄	Comment
1	BeO-1[f]	121.92	Ni	1.236 (1.160)	2.7 —	2315 (2578)	1.21 (1.12)	2.24 (2.47)	( ) indicates using Hansen-Roach X-sects.
2	BeO-2[f]	121.92	Ni	1.184	3.1	2582	1.22	2.24	
3	BeO-1	115.92	Ni	1.222	--	2333	1.20	2.24	
4	BeO-1	103.92	Ni	1.185	2.7	2370[b]	1.195	2.26	
5	BeO-1	103.92	Ni	1.210	—	6752[b]	1.43	2.09	Test bundle is is fully enriched.
6	BeO-1	121.92	on	1.222 (1.148)	2.6	2327 (2586)	1.21 (1.12)	2.24 (2.44)	H-R comparison case
7	BeO-1	121.92	4-in. Graphite	1.213	4.8	2338	1.20	2.08	
8	BeO-1	121.92	8-in. Graphite	1.253 (1.200)	12.0 —	2300 (2519)	1.21 (1.13)	2.04 (2.14)	H-R comparison case
9	BeO-1	121.92	BeO	1.258	10.4	2313	1.21	1.87	
10	BeO-1	121.92	Be	1.254	13.3	2312	1.21	1.92	
11	Al_2O_3-1[f]	121.92	Ni	1.098	2.3	2410	1.04	2.06	
12	Al_2O_3-1	121.92	Ni	1.141	--	7486[b]	1.19	1.974	Test bundle is fully enriched.
13	Al_2O_3-1	121.92	Iron	1.073	2.1	2507	1.05	2.11	
14	Al_2O_3-1	121.92	8-in. Graphite	1.141	17.3	1986[c]	1.06	1.87	
15	Al_2O_3-1	121.92	BeO	1.155	15.7	2033[d]	1.07	1.65	
16	Al_2O_3-1	121.92	Be	1.150	20.7	1788[e]	1.07	1.70	

a Reflector thickness is 4 in. (101.6 mm) except where indicated otherwise. Axial reflectors are the same material but have a fixed height of 12 in. (305 mm) and a volume fraction of 0.6592 to match that of the fuel elements.
b The 217-pin test bundle for this case contains fully enriched (93.2%) UO_2.
c Limited by thermal flux peaking at the outer edge of the driver. This can be reduced by reducing the reflector size. Normalizing to the interior driver hot spot gives 2446 J/gm as the potential yield.
d Same as above but peaking less severe. Potential yield 2452 J/gm.
e Same as above but peaking more severe than the BeO. Potential yield 2459 J/gm.
f See Table 5.2.2-2 for definition of these fuel types.

Table 5.2.2.-2
Fuel Specifications and Core Volume Fractions

A -- Fuel Specifications

Fuel Title	Molecular Ratio HOST/UO_2	Composite Density (gm/cm)	Weight Percent UO_2	Enrichment	Fissile Atom Fraction	Peak Operating Temperature
BeO-1	20/1	3.998	34.9%	40%	0.0093	1500°C
BeO-2	20/1	3.998	34.9%	35%	0.0081	1500°C
Al_2O_3-1	9.4/1	4.567	21.85%	50%	0.01	1250°C
Prototypic Test Bundle	--	10.0	Mixed Oxide	Heavy Atom %		
				30.16	Pu-237	
				4.06	Pu-240	
				0.59	Pu-241	
				0.07	Pu-242	
				0.15	U-235	
				64.97	U-238	
Enriched Test Bundle	--	10	100%	93.2	U-235	
				6.8	U-238	

B -- Volume Fractions

Driver:	Fuel	0.6592
	Gas Coolant + Gap	0.2856
	Clad	0.0552
Test Section:	Fuel	0.4340
	Gap	0.1436
	Clad	0.0113
	Na Coolant	0.4111

profile (7%), and a lower energy deposition (10%). So basically, except for the self-multiplication factor, the performance predictions are lower with the new cross sections. One can improve on the design by optimizing the fuel loading and the BeO/UO_2 molecular ratio. The energy deposition can be increased by reducing the driver fissile fuel loading since there is plenty of excess reactivity in the reference cases. The radial profile can be reduced by reducing the BeO/UO_2 molecular ratio, increasing enrichment, filtering, or using a converter, any of which will harden the spectrum; but these changes will also reduce the deposition. The excess reactivity exhibited indicates that there is room for substantial improvement with the BeO fuel. Some additional calculations showing the effects of enrichment reduction and converters are given in Section 5.2.3.

The Al_2O_3 fuel is not as reactive but due to its harder spectrum its radial and axial profiles are much less severe, and the deposition values meet the design goals of 2500 j/g and 5000 j/g for prototypic and fully enriched test fuels, respectively.

Table 5.2.2-1 indicates that a flexible range of neutron generation times--2 to 20 microseconds--is possible with different reflectors. The generation times were calculated with KENO IV [5]. Kinetic studies indicate that these generation times are sufficient for producing 5 msec pulse widths at the desired energy levels; see Section 5.3.3.

The effect of the neutron multiplication factor, k_{eff}, on the calculated prompt neutron generation time was investigated for a single region BeO/UO_2 driver using the 20-to-1 molecular ratio and

a 40 percent enrichment. The reflector was graphite. The excess reactivity was controlled by introducing poison into an annular control ring and also by reducing the outside diameter. The data is shown in Fig. 5.2.2-1. A least squares fit of the data gives the following relationship for prompt neutron generation time as a function of k_{eff}.

$$\Lambda(\mu sec) = 46.32 - 27.6\ k_{eff}, \quad 1.0 < k_{eff} < 1.253 \qquad (5.2\text{-}1)$$

The calculated generation time increases from about 12 μsec at a multiplication factor of 1.25 up to 18.8 at an excess of 1.005. The reason for the change is that fissions occur more readily in the more reactive system, thereby reducing the average generation time of a prompt neutron. An average generation time in the range of expected reactivity required for pulsing is appropriate for point kinetics analysis.

The neutron losses through the test assembly for the single region Al_2O_3 driver (relatively hard spectrum) and the BeO driver (softer spectrum) are shown in Figure 5.2.2-2. These results were obtained by monitoring the fission activity in a uniformly dispersed U-235 tracer material.

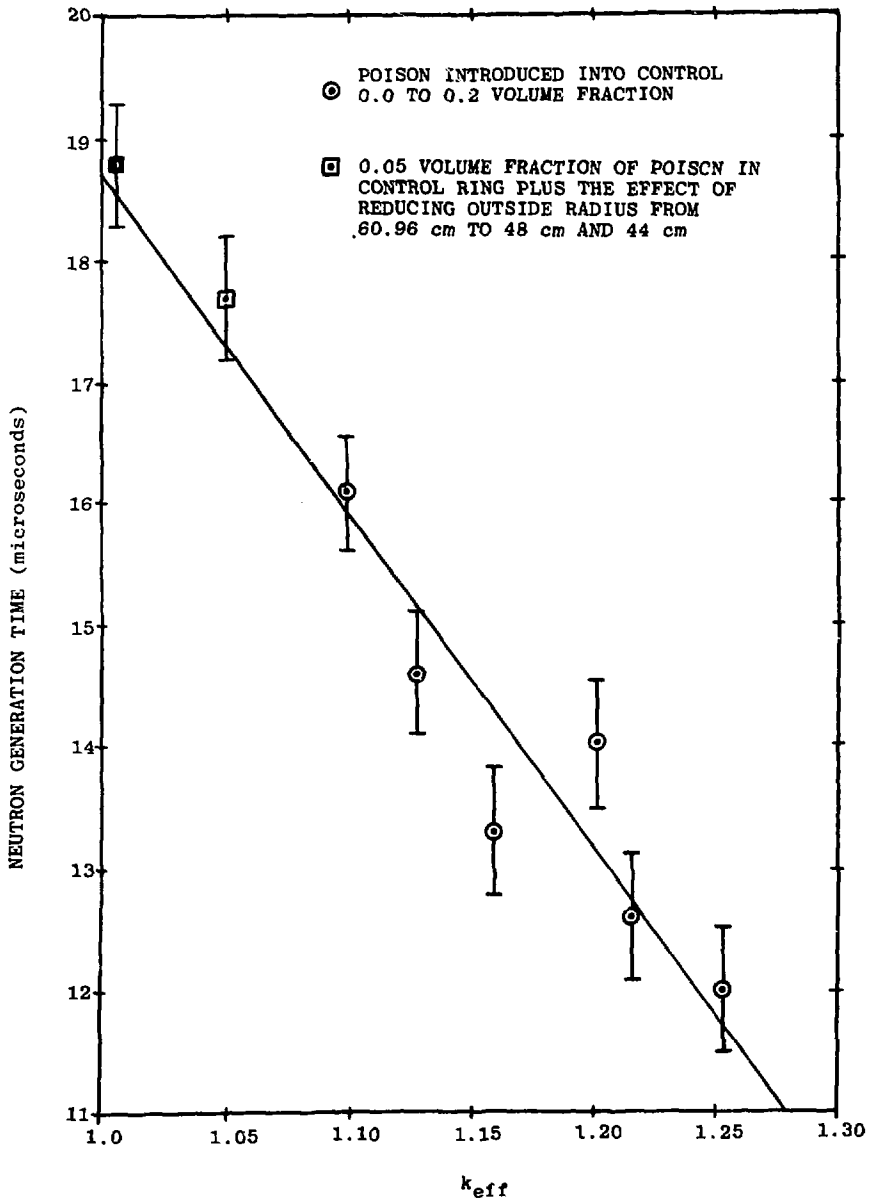

FIGURE 5.2.2-1 EFFECT OF K_{EFF} ON PROMPT NEUTRON GENERATION TIME

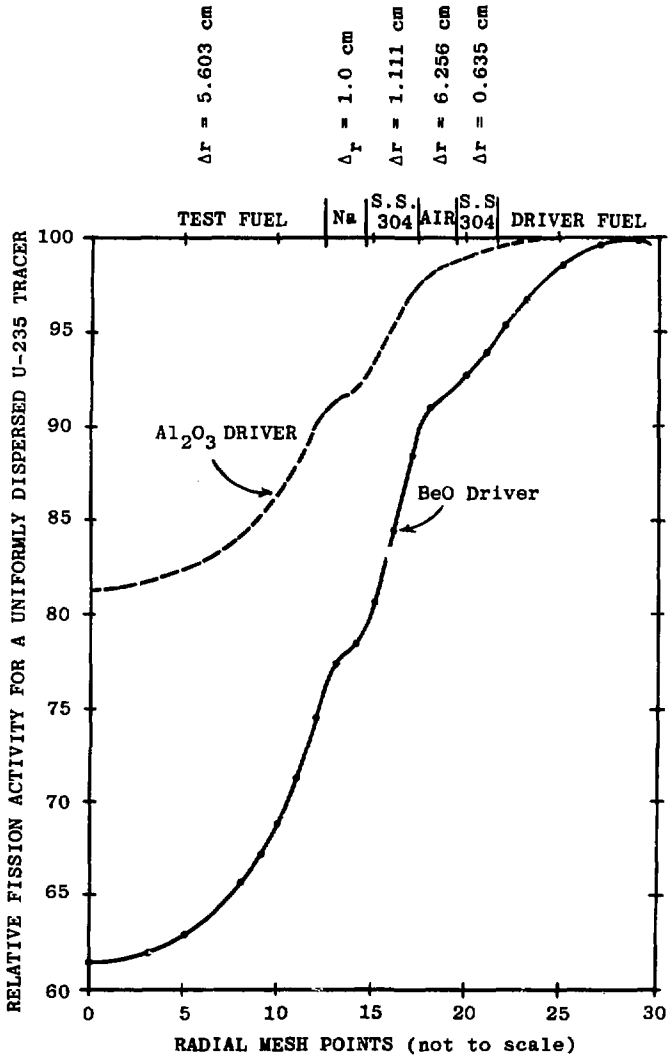

FIGURE 5.2.2-2 NEUTRON ENERGY LOSSES IN THE TEST ASSEMBLY

5.2.3 Effect of Converters

The purpose of introducing a converter region is to harden the spectrum, perhaps at some sacrifice in energy deposition, in order to reduce the radial peak-to-minimum across the test bundle. Optimally, the fissile loading in the driver and converter are appropriately matched so that the peak temperatures occur simultaneously in both regions. It is likely that performance in one or both regions may be sharply peaked due to changes in the neutron spectrum and this condition will limit performance. The severity of the peaking may be reduced by grading the enrichment. The consequence is a more evenly distributed flux profile, a higher average temperature for the driver and converter and, thus, improved cavity fluence.

Figures 5.2.3-1 through 5.2.3-2 show calculated results for two types of converters. The results were derived from 1-D S_n calculations using the HR cross sections and, therefore, indicate slightly optimistic performance compared to later, two-dimensional results with the new cross sections. The figures, however, indicate the tradeoff in radial peak-to-minimum and energy deposition in the test fuel bundle as a function of increasing converter thickness. The converter loadings were held constant in all cases shown. At these loadings, the driver and converter maximum temperatures are fairly well matched at about 2.54 cm (one inch) thickness for the Fe-Al converter and at slightly less than one inch thickness for the UO_2 converter. At a thickness of 4 inches performance was limited by the driver temperature rather than by the converter temperature. Specifically, for example, decreasing the loading in the driver could have increased the energy deposition

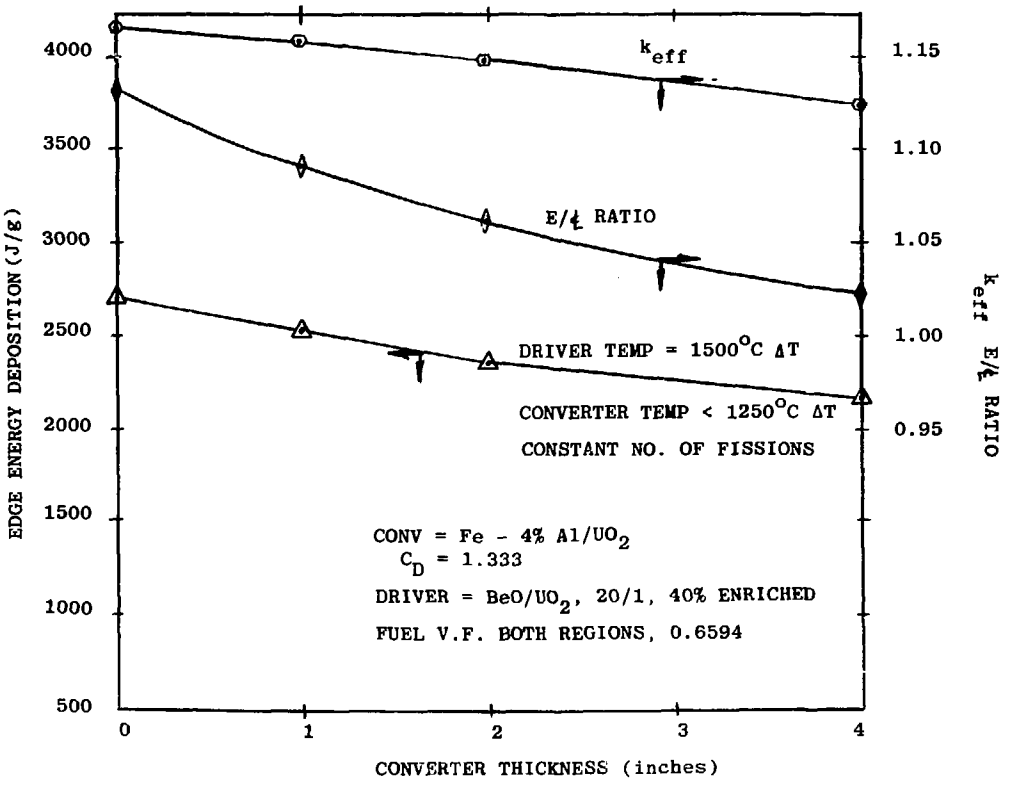

FIGURE 5.2.3-1 EFFECT OF A Fe-Al CONVERTER ON PERFORMANCE

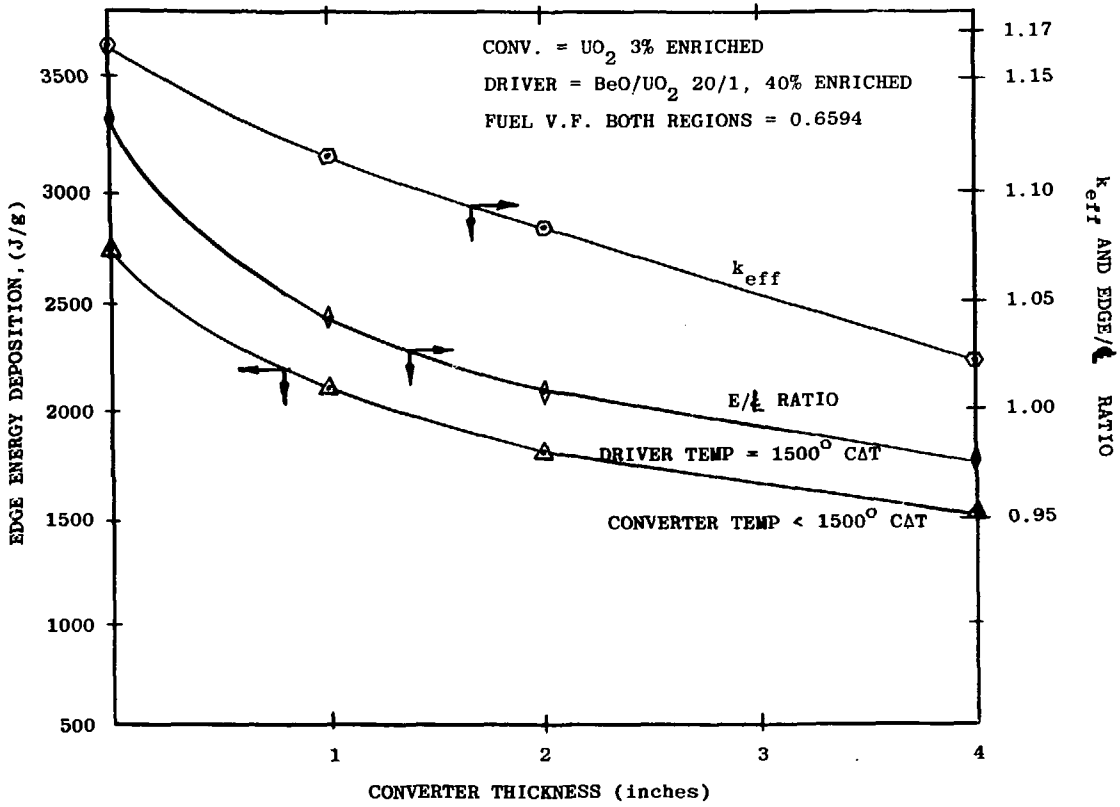

FIGURE 5.2.3-2 EFFECT OF A UO_2 CONVERTER ON PERFORMANCE

by ~180 j/gm with a 4 inch Fe-Al converter, but the core diameter would have to be increased to maintain the same excess reactivity.

Performance characteristics derived from two-dimensional parametric calculations and AMPX-processed cross sections are shown in Figures 5.2.3-3, -4, and -5. These figures include both single region and driver/converter configurations. The reflectors are graphite or nickel. Figures 5.2.3-3 and -4 show radial peak-to-minimum and energy deposition as a function of driver fuel enrichment. Converter and no converter cases are shown at two different k_{eff} values. The k_{eff} values were changed by modifying the outside core radius. The reflector thicknesses were not changed. The converter thickness (10 cm) and loading (0.001 U-235 atoms per cc in the fuel) were constant for the converter cases and, therefore, performance was limited by the converter temperature at low driver enrichments and by the driver temperature at higher driver enrichments. The upper edge of the band on Fig. 5.2.3-4 is the performance normalized to the peak temperature of the opposite fuel. At the left edge of Figure 5.2.3-4 performance near the top of the band could be obtained by reducing the fissile loading in the converter. At the right side, steps must be taken to flatten the flux in the driver more, possibly by using a larger reflector. This would help to match the driver and converter maximum temperatures for optimum performance at the top of the band.

Notice that the lower eigenvalue systems (k_{eff} = 1.0) exhibit better performance than the higher eigenvalue systems.

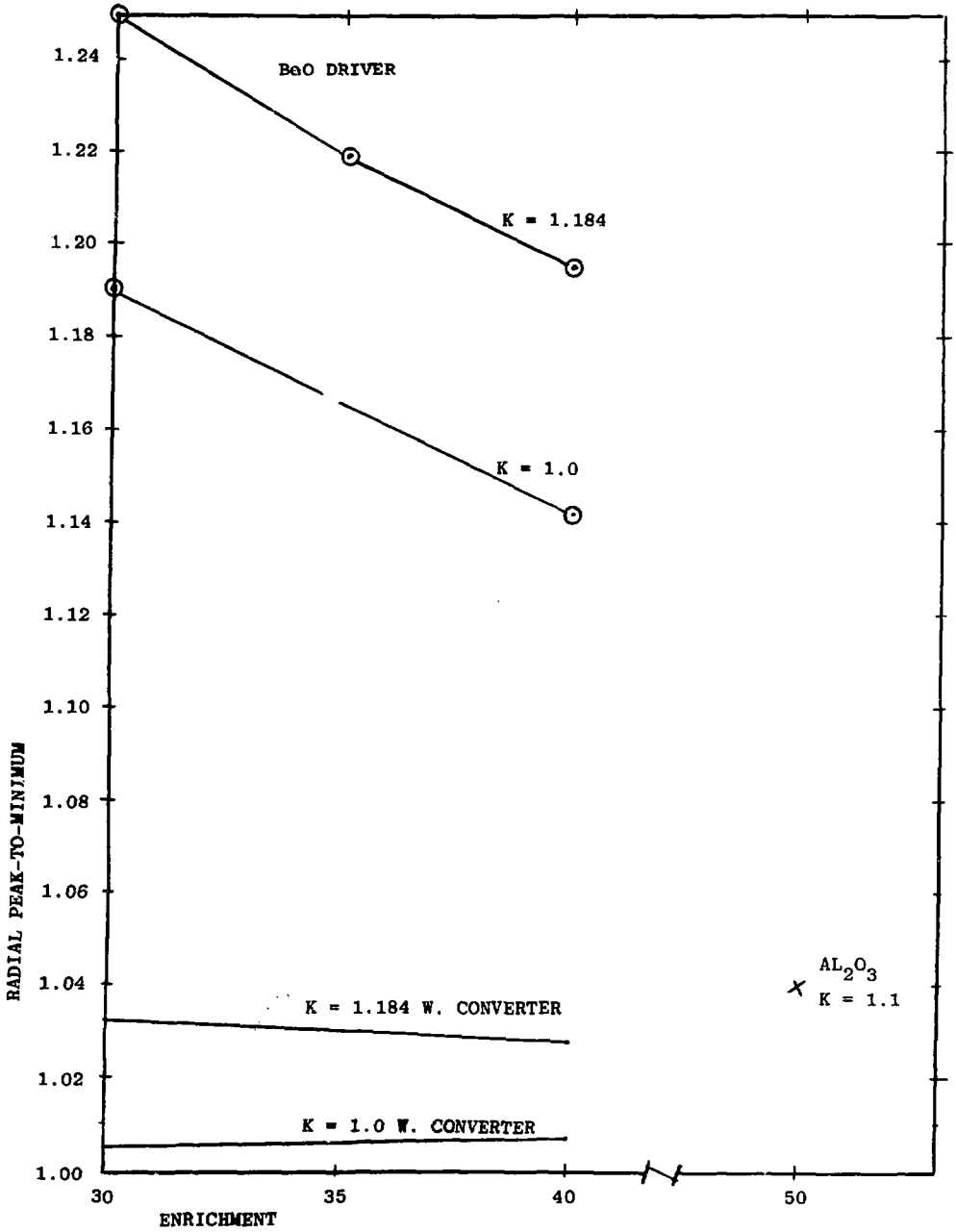

FIGURE 5.2.3-3 EFFECT OF DRIVER FUEL ENRICHMENT ON RADIAL PEAK-TO-MINIMUM

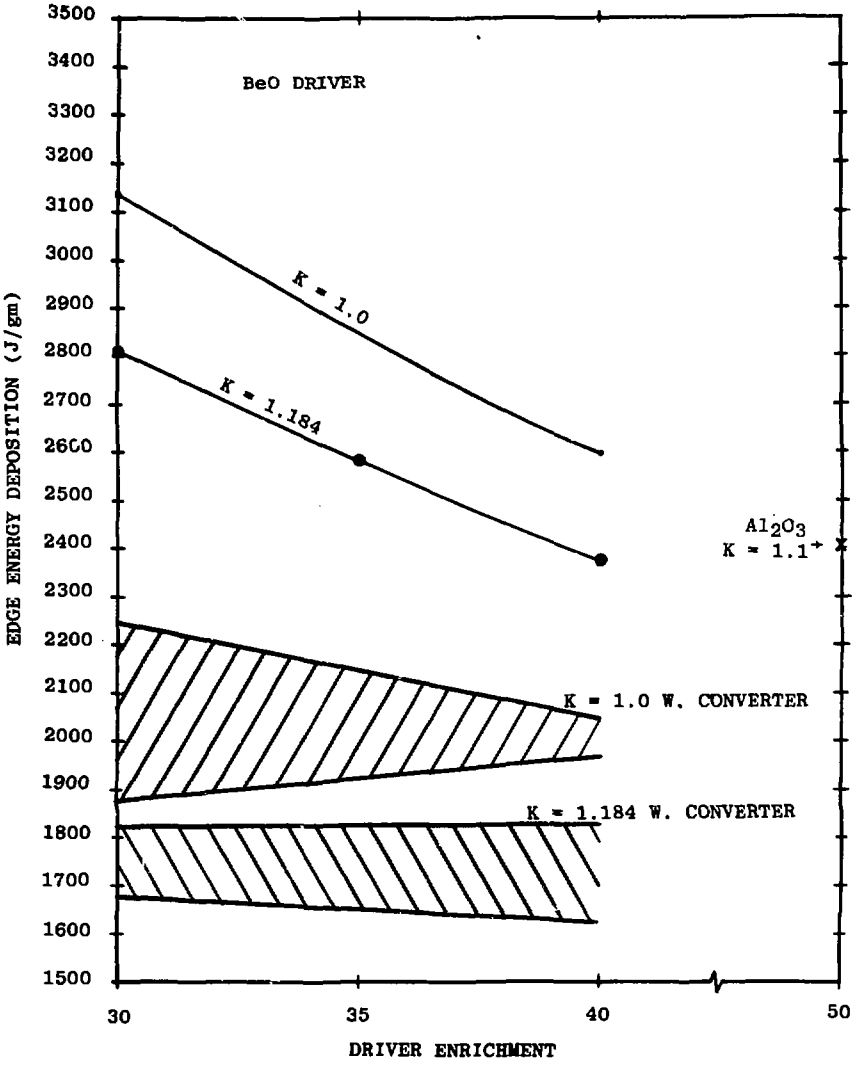

FIGURE 5.2.3-4 EFFECT OF DRIVER FUEL ENRICHMENT ON ENERGY DEPOSITION

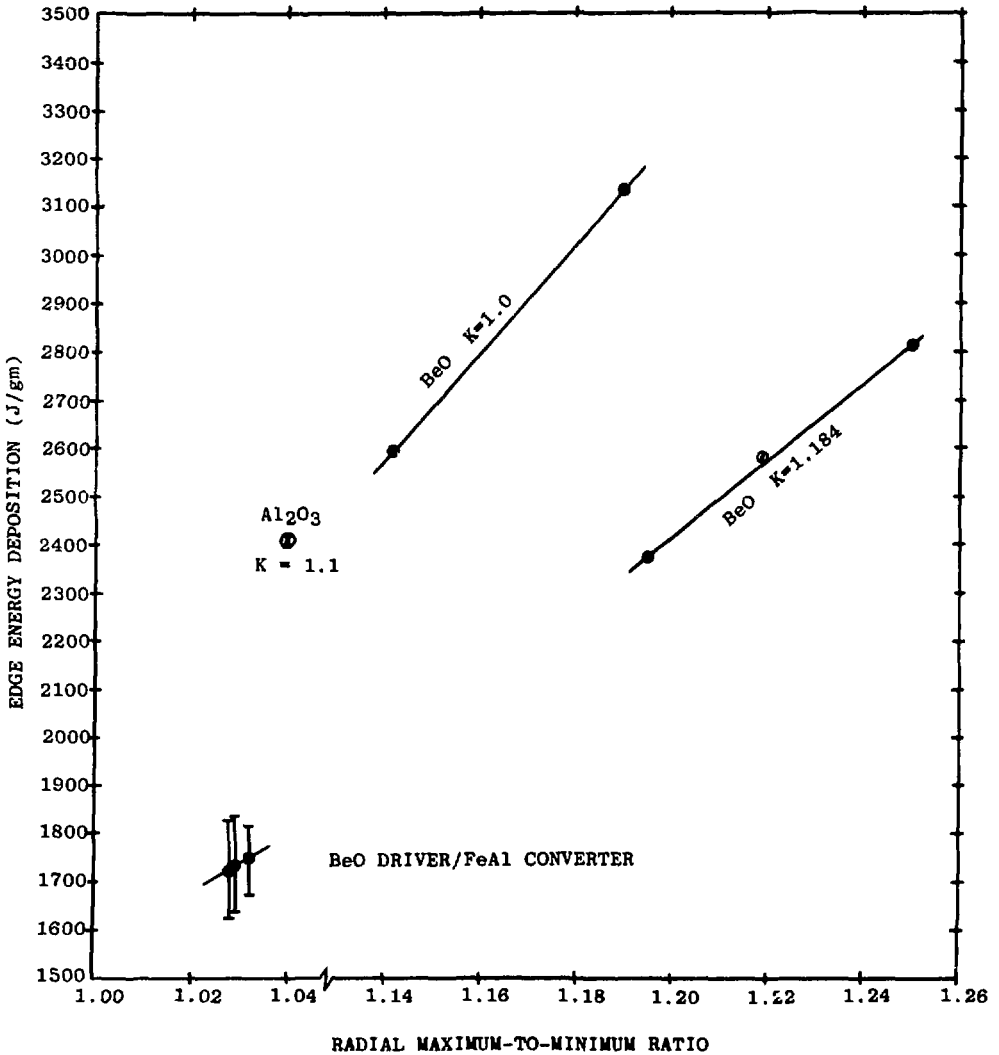

FIGURE 5.2.3-5 ENERGY DEPOSITION AND RADIAL PEAK TO MINIMUM TRADEOFFS

Figure 5.2.3-5 is a composite of Figs. 5.2.3-3 and -4. The reader can see the direct tradeoff between energy deposition (desired to be as high as possible) and radial peak-to-minimum (desired to be as close to 1.0 as possible).

The volumetric energy deposition profile in a 217 pin mixed oxide test bundle and the driver core is shown in Figure 5.2.3.-6. One set of data is for a single region BeO driver with a graphite reflector; the other curve is for the same driver and converter plus a 10 cm (4 inch) Fe-Al converter. The peak-to-minimum in the test fuel is 1.19 for the first case and 1.03 for the second case.

The self-multiplication factor, k_{eff}, as a function of the size of various driver-converter-reflector combinations, is shown in Fig. 5.2.3-7. The reference design is plotted at a core radius of 48 cm and a k_{eff} value of 1.18. Notice that addition of 5 v/o of B_4C in the core control region of this model reduces k_{eff} to 1.05.

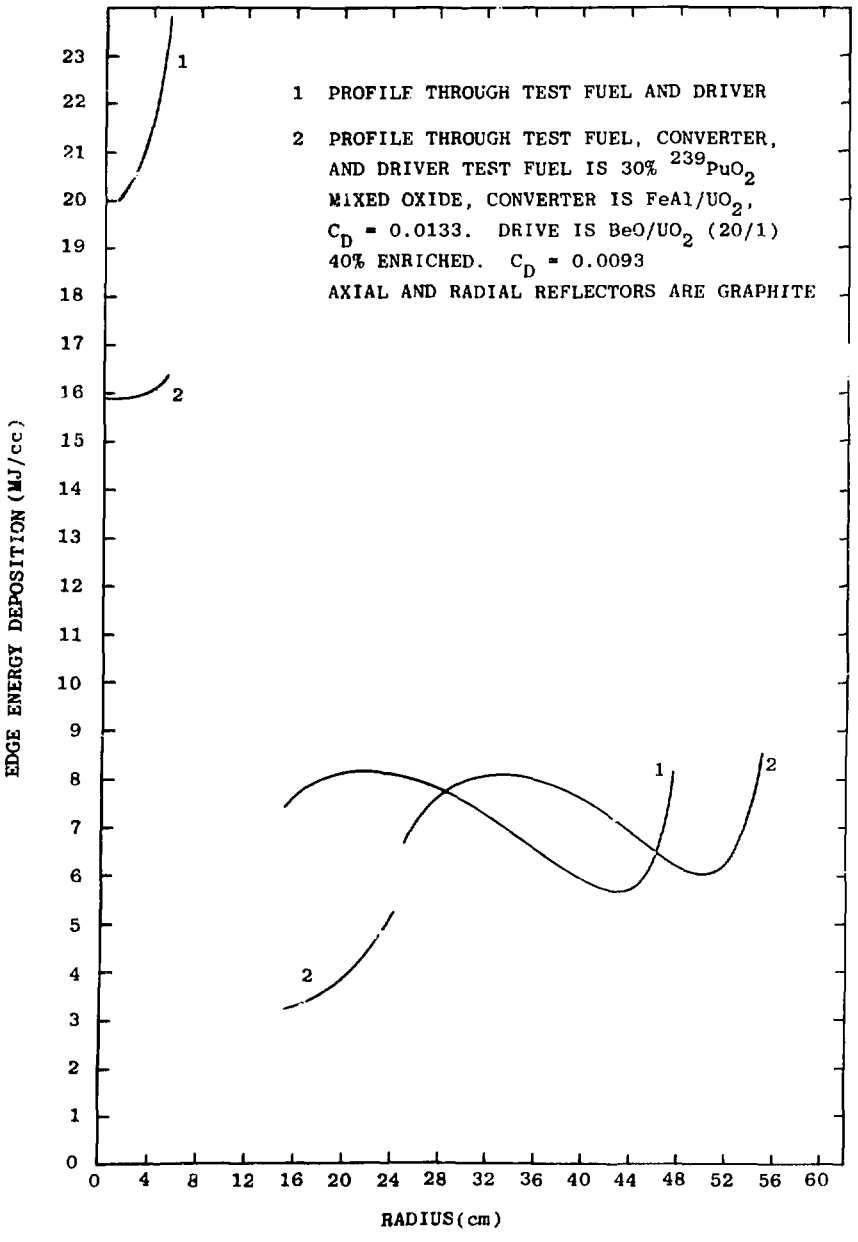

FIGURE 5.2.3-6 VOLUMETRIC ENERGY DEPOSITION PROFILE

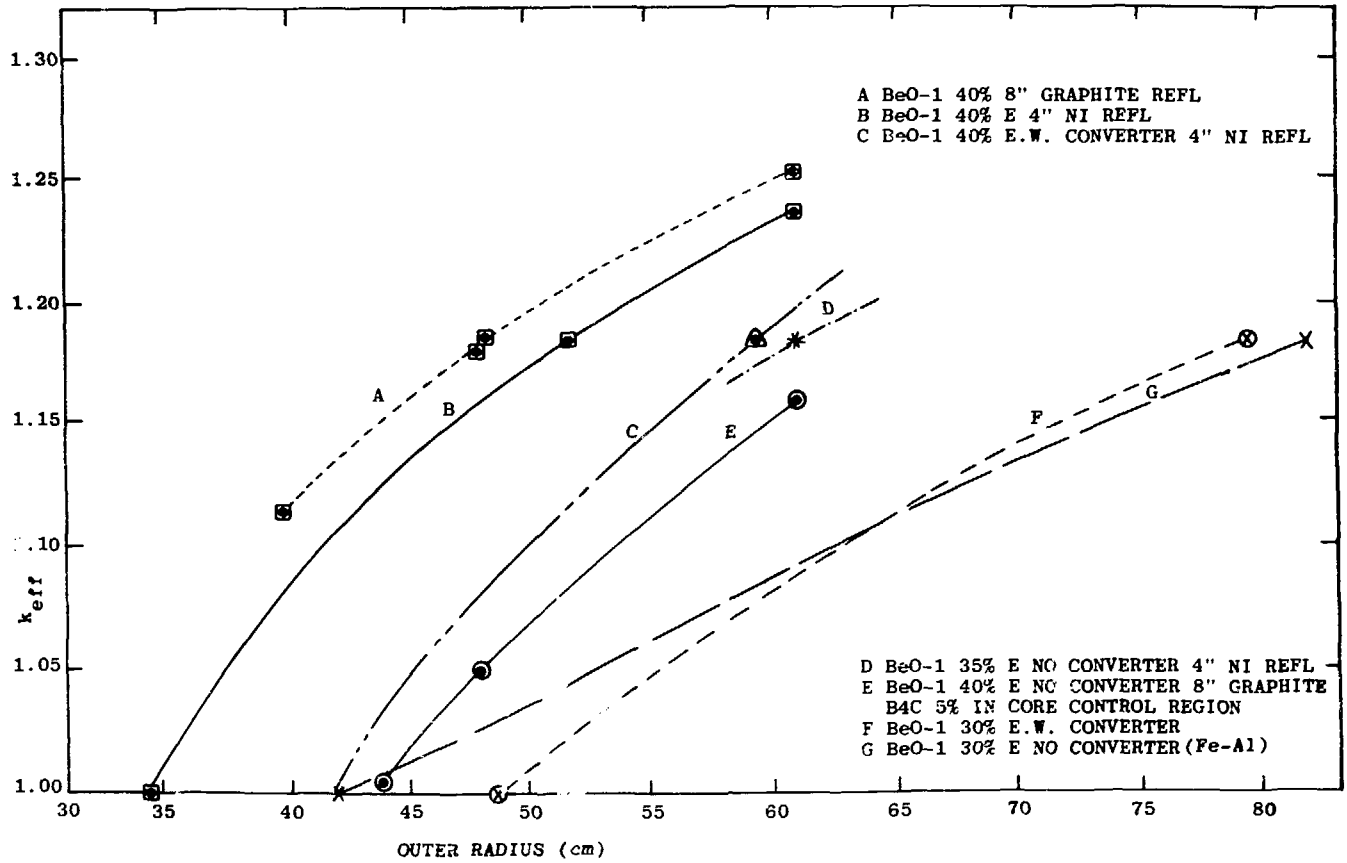

FIGURE 5.2.3-7 SELF-MULTIPLICATION FACTOR AND SIZE OF VARIOUS DRIVER REFLECTOR-CONVERTER COMBINATIONS

5.2.4 Reactivity Addition Due to Test Fuel Compaction

The reactivity addition due to test fuel compaction was calculated for 25, 50, and 100% compaction. Only one driver configuration and one test bundle loading have been investigated thus far and the results are shown in Figure 5.2.4-1. The driver fuel was BeO-1, the reflectors were nickel and the test package was a 217 pin, prototypic mixed 239 oxide fuel bundle (heavy atom fraction of Pu is 0.3). The compaction was modeled by dividing the top half of the test fuel bundle into two equal regions and moving fuel from the top region into the region above the midplane. Because of symmetry, fuel is also assumed to move from the bottom of the test subassembly into a region just below the midplane. For 100% compaction, the fuel volume fraction in the central region was doubled from 0.434 to 0.868 while it was reduced to 0.0 in the end region. Sodium is nearly all expelled from both the inner and the outer regions. The volume fraction of sodium always goes from 0.4111 to 0.0111 in both regions but is unchanged in the axial blanket. For 50% compaction only 50% of the fuel was moved from the outer to the inner region and so forth. As shown in Figure 5.2.4-1, there is a 64¢ reactivity addition at 100% compaction for a 217 pin prototypic bundle.

A 50% compaction even at very high rates will only produce an extra 30-40°CΔT in the driver fuel if the compaction occurs after the peak of the pulse. This is a performance penalty of less than 3% for 50% compaction with prototypic fuel. If the 50% compaction occurs simultaneously with the pulse, it produces an extra 280°CΔT increase in the driver fuel or a 21% performance penalty.

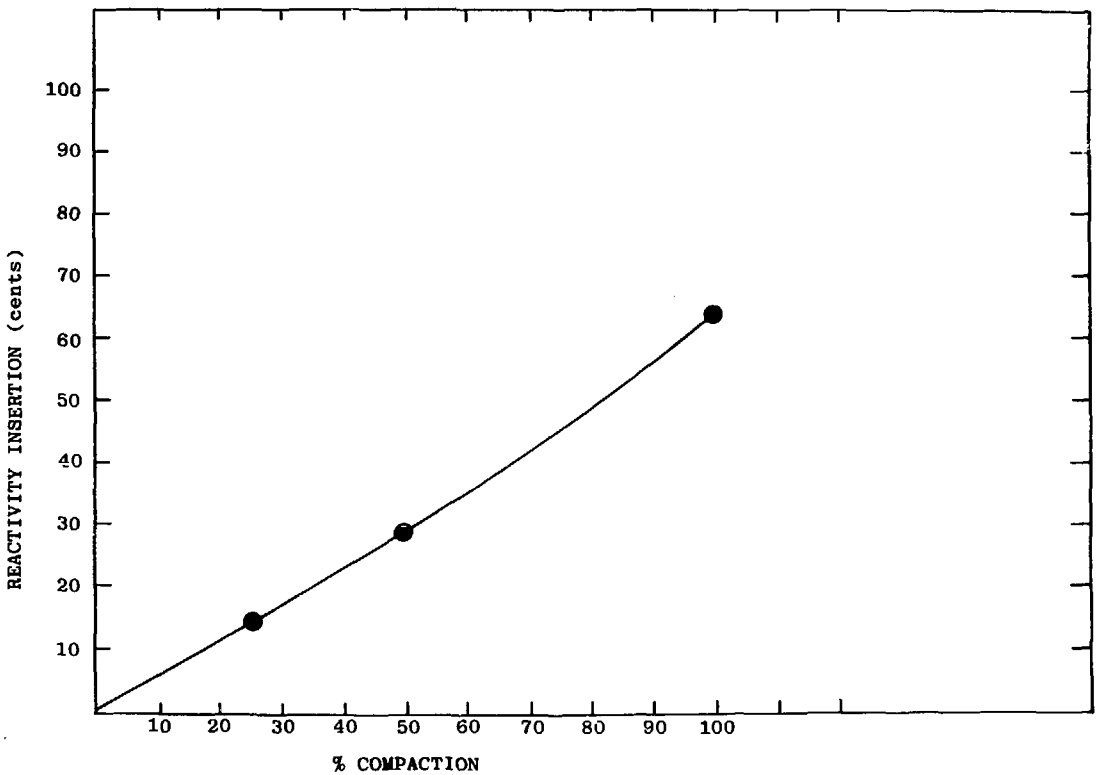

FIGURE 5.2.4-1 REACTIVITY ADDITION DUE TO TEST FUEL COMPACTION

5.3 Kinetics and Thermal Hydraulic Analysis - Gas Cooled System

5.3.1. General

BeO/UO_2 and Al_2O_3/UO_2 fueled, gas cooled systems have been analyzed and compared with respect to material properties, energy deposition, and temperature profiles. Parameter surveys to investigate the effects of fuel diameter, gap material, gap thickness, clad thickness, coolant heat transfer coefficient, and heat generation rate on the temperature distribution in the driver fuel in steady state operation, have been carried out with the TAC2D heat transfer code. Transient calculations for BeO and Al_2O_3 systems were performed with the SAK and PK1D point kinetics codes which were used to compare energy deposition, yield, and pulse width information of the two systems as well as to obtain temperature profiles and other heat transfer information.

In these models, the core is 48" to 54" high. Helium coolant at 10 atm pressure was assumed in all of these studies. The heat generation rate in the TAC2D calculations was modelled with a truncated cosine distribution in the axial direction with a peak to minimum ratio of 1.8.

In order to drive fuel elements of various diameters (from 3/4 inch to 2 inches) to operational limits on fuel and clad temperatures and stresses, the input heat generation rates (peak) ranged from about 9 watts/g (for the 2 inch diameter element with a 30 mil gap and 30 mil clad) up to 37 watts/g (for a 3/4 inch element with only a 5 mil gap and a 15 mil clad under steady state conditions. The first case is limited by fuel temperature and the second case by clad temperature. The optimum element design should not be limited too strongly by any single design parameter

(e.g. stress, fuel temperature, etc.) and the design must also satisfy limiting conditions for heat transfer under pulsing conditions as will be discussed later.

The effect of radiation on the heat transfer rate was accounted for by an emissivity in the radial direction of .5. The addition of this factor had no effect on the temperature distribution of the TAC2D calculations.

The heat transfer coefficient for a helium gas cooled system was calculated from equation 5.3-1 [11]:

$$h = .023 \frac{k}{D} (Re)^{.8} (Pr)^{.4} \quad , \text{Btu/hr-ft}^2\text{-°F} \qquad (5.3\text{-}1)$$

where k = thermal conductivity, Btu/hr-ft-°F

D = equivalent diameter, ft

$Re = \frac{DV\rho}{\mu}$, the Reynolds number — dimensionless

$Pr = \frac{c_p \mu}{k}$, the Prandtl number

$\frac{hD}{k}$ = Nu, the Nusselt number, dimensionless

The properties were taken at 600°F and 10 atm pressure. At these conditions, the heat transfer coefficient is dependent only upon coolant velocity. This dependence is graphed in Fig. 5.3.1-1.

The effect of velocity variation on fuel and clad temperatures for a fixed geometry and heat generation rate is shown in Fig. 5.3.1-2. For this figure the fuel diameter was 3.8 cm (or 0.75 inch), the gap thickness was 10 mils, the clad thickness was 15 mils, and the heat generation rate was 11.25 watts/gm at the peak of a truncated cosine distribution (P/M = 1.8).

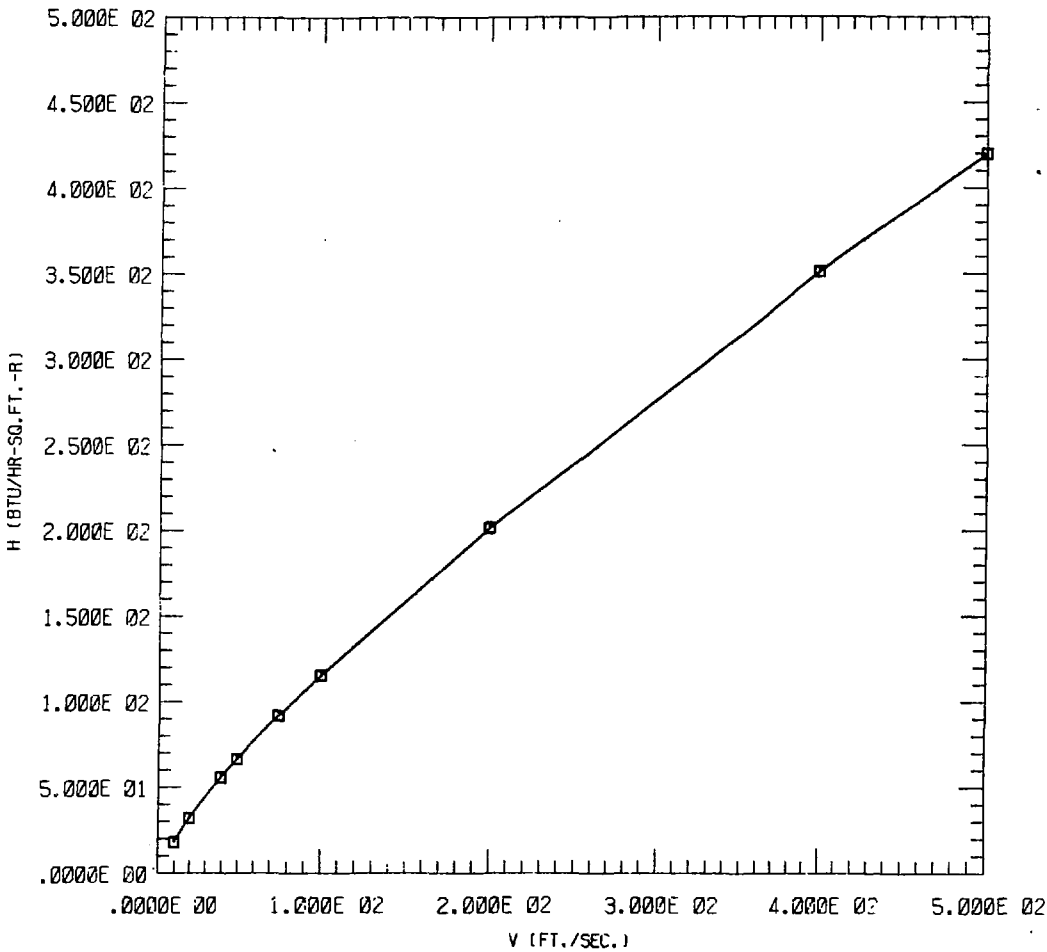

HEAT TRANSFER COEFFICIENT OF HELIUM AS A FUNCTION OF COOLANT VELOCITY

FIGURE 5.3.1-1

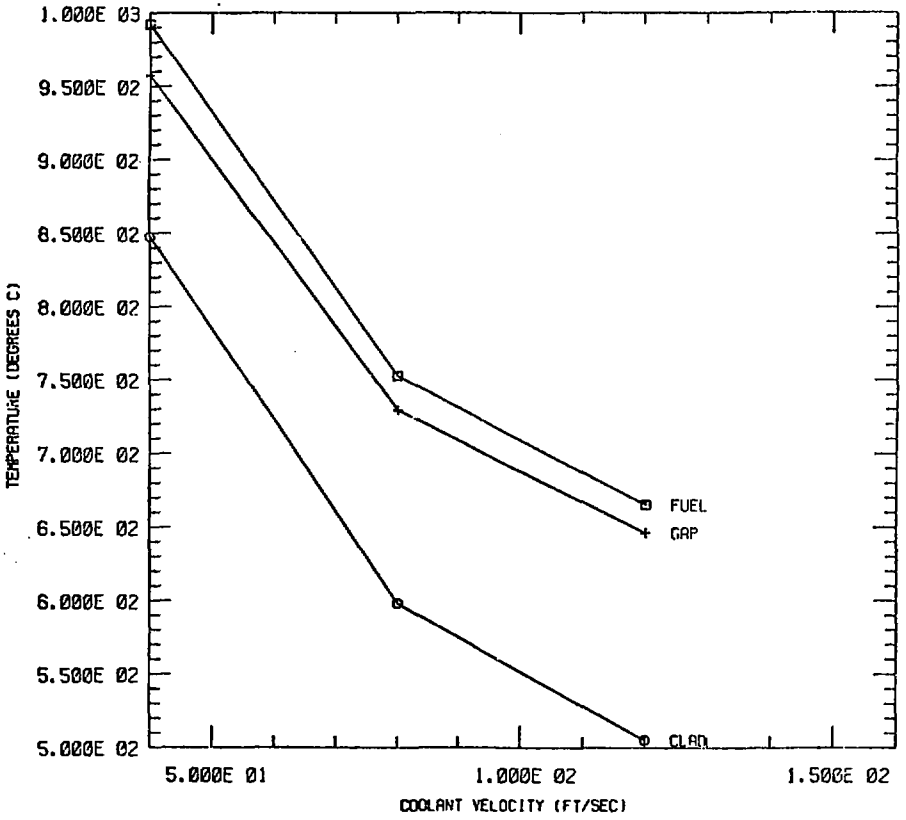

FIGURE 5.3.1-2 EFFECT OF COOLANT VELOCITY ON FUEL ELEMENT TEMPERATURES

The sonic velocity of helium at 10 atms pressure is 827 ft/sec. A helium velocity of 650 ft/sec represents an upper limit for subsequent calculations. This velocity gives an h value of 0.31 watts/cm^2-K (or 550 BTU/hr-ft^2-°F).

With helium (10 atm) as the gap filler, the heat generation rate, the fuel diameter, the SS304 clad thickness and the gap width were varied and the effect on steady state temperature distribution was determined with TAC2D. For this parametric evaluation, gap closure was not modeled; thus, the gap thicknesses are considered to be at operational temperatures rather than for clean, cold conditions.

Fuel elements with 2 inch, 1.5 inch and .75 inch fuel diameters were compared, with gap and clad widths ranging between 5 and 30 mils. The narrower fuel elements with smaller gaps are limited by clad temperatures rather than by fuel temperatures. An increase in gap thickness does increase fuel temperatures, but it does not reduce the steady state clad temperatures significantly. However, increasing the fuel diameter results in lower clad temperatures for a given fuel temperature limit.

More specifically, small (5 mils) changes in clad thickness were found to cause negligible change in the maximum clad and fuel temperatures. However, increasing the gap width by 5 mils resulted in small decreases in the maximum clad temperature (<1%) and large increases in fuel temperatures (~75°C for the larger elements and smaller increases for the smaller elements). The gap temperatures themselves increased by 6-10% for a 5 mil increase in gap width. The highest percentage increase corresponds to the narrowest gap width (5-10 mils).

Effects of power density and fuel element diameter on steady state fuel and clad temperatures are shown in Fig. 5.3.1-3. In this set of data, coolant parameters, clad thickness, and gap thickness were held constant for each fuel element diameter curve. Only the internal heat generation rate was varied to represent different power levels of the reactor. The heat generation functions are given in terms of Q, where Q represents a truncated cosine distribution with a peak value of 7.5 watts/gm.

A second graph, Fig. 5.3.1-4, shows the effect of varying clad and gap thickness for a fixed fuel diameter. Only the gap variations result in noticeable temperature changes. Two curves with the same gap (10 mils) but different clad thicknesses lie on top of one another.

These figures indicate that the best simultaneous matching of fuel and clad temperatures under steady-state operating conditions is obtained with a helium filled gap of 15 to 20 mils for the element diameters investigated. The maximum heat generation rate under optimum conditions is ~37 watts/g for the 1.9 cm element and 16 watts/gm for the 3.8 cm element. From TWØTRAN II calculations, the peak and average specific heat generation rates in the driver are 11.3 and 7.86 watts/g, respectively, at 16.7 MW total power. This power produces ~6 w/g in a debris bed of prototypic enrichment and produces a maximum cavity flux of $\sim 1.2 \times 10^{14}$ n/cm-sec at the core midplane. Thus, any element in Fig. 5.3.1-3 that can produce 1.5 Q or better without exceeding either the clad or fuel temperature limits will satisfy the steady state design criteria.

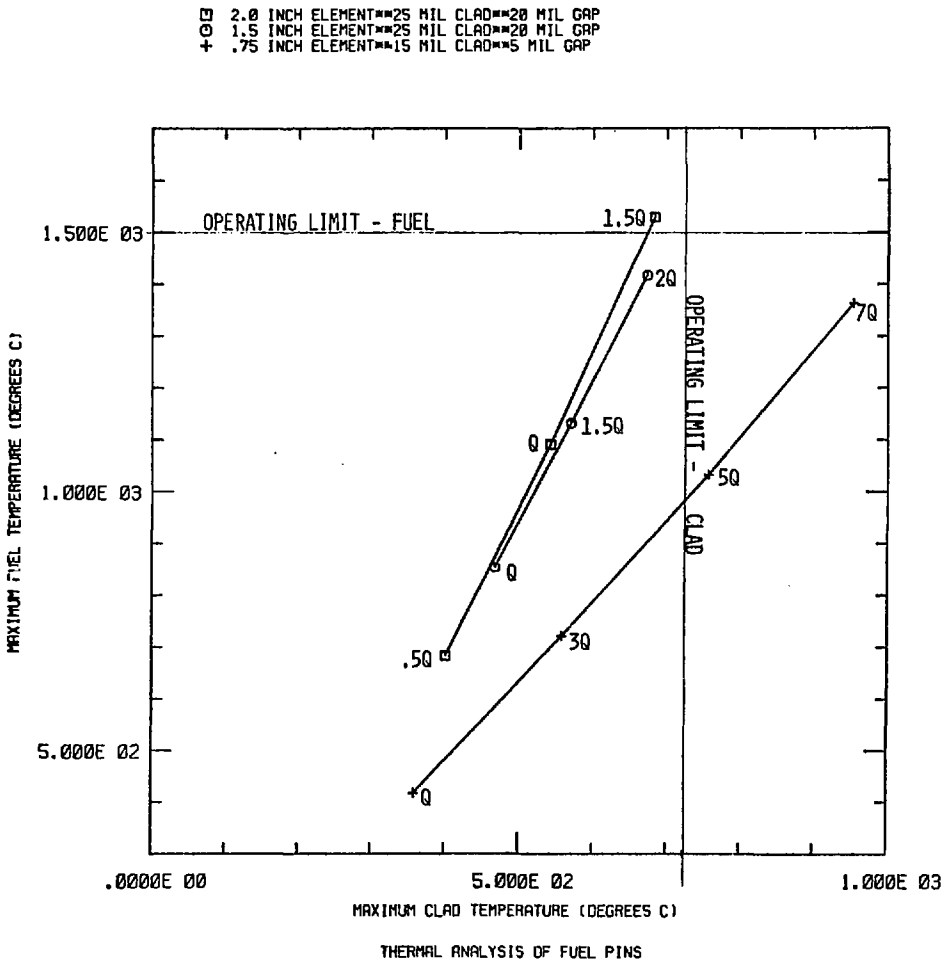

THERMAL ANALYSIS OF FUEL PINS

FIGURE 5.3.1-3

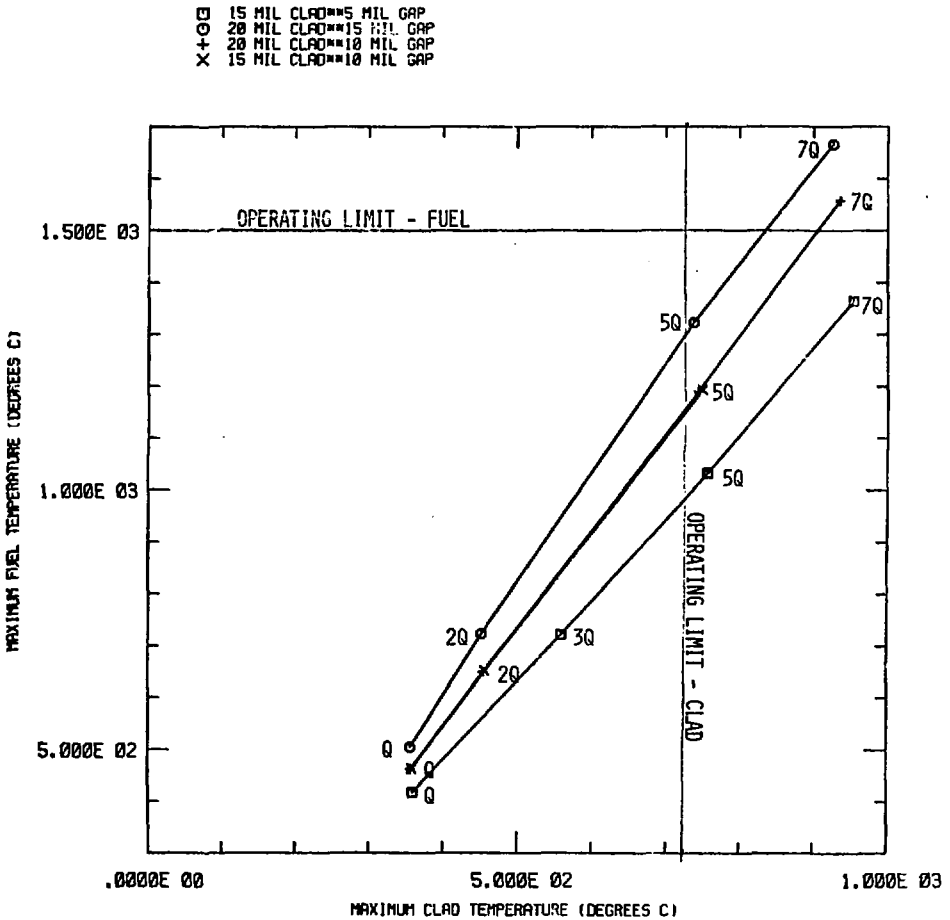

EFFECT OF GAP AND CLAD VARIATIONS ON .75 INCH FUEL ELEMENT

FIGURE 5.3.1-4

The 1.9 cm element has the largest safety margin and it was selected as the model for pulse-mode analysis. Parametric analysis of the fuel element design for pulse-mode operation was beyond the scope of this report. However, the 1.9 cm (3/4 inch) element selected for kinetic analysis (see following section) exhibited well-balanced fuel and clad behavior such that failure temperatures or yield stresses of one do not occur significantly before the other. This is important because the maximum pulse is determined by the failure threshold of either the fuel or clad (with allowances, of course, for an appropriate safety margin).

There are several conflicting design objectives that arise when a reactor is to be operated in both pulse and steady state modes. If the performance criteria in one mode is sufficiently harder to meet than the other, then the element design will be well-balanced for only one mode of operation. Although a quantitative optimization was beyond the scope of this report, the design considerations are well understood and are discussed below.

For pulse operation a larger element than the one used in our neutronic studies may be preferred for the following reasons:

1. The fuel is heated almost adiabatically so thermal resistance and cooling rates are determined by clad temperature limits and stress considerations rather than by fuel temperature.
2. A larger element generally allows for a larger fuel volume fraction and, thus, the fissile loading can be less, the clad fraction is less, and the critical size will be smaller.

3. Fabrication costs are generally lower (fewer elements).

4. Lower inner and outer clad temperatures are generally possible due to larger gap and clad thicknesses. This can be used to improve the safety margin fo clad melt in the case of a gas-cooled core or for DNB* with a liquid-cooled core.

However, the disadvantages of the larger element size are:

1. Longer cooldown time between pulses.

2. If there is a non-uniform fission profile within the element, the stress could be larger with a larger element (particularly if the element is water-cooled). If smaller elements are chosen, however, fissile loading must be increased, thereby compromising some of the advantages of going to the smaller size with respect to stresses.

3. Steady state power densities would be restricted compared to smaller elements but for HFFR steady state fluence is not the critical performance criterion.

Similar conflicts occur in specifying the thermal resistance of the gap between the fuel and the clad. A smaller gap means better heat transfer out to the clad and coolant. This is fine for steady-state operation, but not for pulsing because of the threat of clad melt or DNB. Therefore a larger gap is preferred for pulsing operations.

A parametric study performed for Sandia by the Nuclear Engineering Department of the University of Arizona [12] provided

*DNB means departure from nucleate boiling.

useful correlations with regard to stresses in the fuel and clad as the fuel diameter, clad thickness, and heat transfer coefficients are varied. For example, with a large heat transfer coefficient (h = 4000 w/m^2-K), the yield stress in the fuel may be exceeded during cooldown for BeO fuel pins greater than 2.54 cm in diameter. Maximum stress decreases with decreasing fuel diameter and heat transfer coefficient. Maximum stresses can also be controlled by increasing the thermal resistance in the gap.

In addition, peak cladding temperatures during pulse and steady state operation were determined for 3 different fuels: BeO/UO_2, Be_2C/UC, and Nb/U by the Arizona group. Peak cladding temperatures for a wide range of cooling conditions were derived and condensed into individual graphs by plotting the heat transfer coefficient as a function of the dimensionless parameter,

$$\frac{T_{clad(max)} - T_{bulk}}{T_{centerline} - T_{bulk}} ,$$

for a family of hot gap resistances. In this way, a range of fuel pin characteristics may be described on a single graph for a given material and fuel pin diameter.

A time-dependent, coupled, thermal-neutronic analysis was done at Sandia for a single element design using the SAK and PKID kinetics codes [8]. The one dimensional heat transfer model used in these codes was similar to the TAC2D model. The fuel element consisted of a 1.9 cm (3/4 inch) fuel diameter plus a cold helium gap of 10 mils and a stainless steel clad thickness of 15 mils.

The coolant was helium at 10 atmospheres pressure. A description of these results is presented in Section 5.3.3.

5.3.2 Temperature Coefficients for BeO and Al_2O_3 Systems

Temperature feedback coefficients calculated with the SAK kinetics code [8] are shown in Fig. 5.3.2-1. The cross sections were processed at 300K, 900K and 1200K. This figure illustrates the substantial difference in magnitude of the temperature coefficients of the BeO/UO_2 and Al_2O_3/UO_2 fuels. The alpha of the ACPR Upgrade is included in Fig. 5.3.2-1 as a standard for comparison. Alpha can be converted to \$/°C units by dividing the decimal units on the graph by β_{eff} = .0069. The coefficient of this gas-cooled BeO system is similar in magnitude to the Upgrade's at low temperatures while it is a factor of 3 higher than that of the Al_2O_3 system. The relatively low value of the Al_2O_3 temperature coefficient makes it impractical as a reactor fuel unless design changes are made to improve its poor kinetic performance. The low values at higher temperatures result in higher power tails and are therefore undesirable. A combination Al_2O_3 and BeO system is a possible alternative also. Parasitic resonance absorption occurs mainly in U^{238}. Thus, the negative temperature coefficient of reactivity can be increased by decreasing the enrichment of the uranium in the fuel, thereby increasing the amount of U^{238}. Another way to raise the temperature coefficient is to make the spectrum softer, t' 's increasing the potential for upscattering.

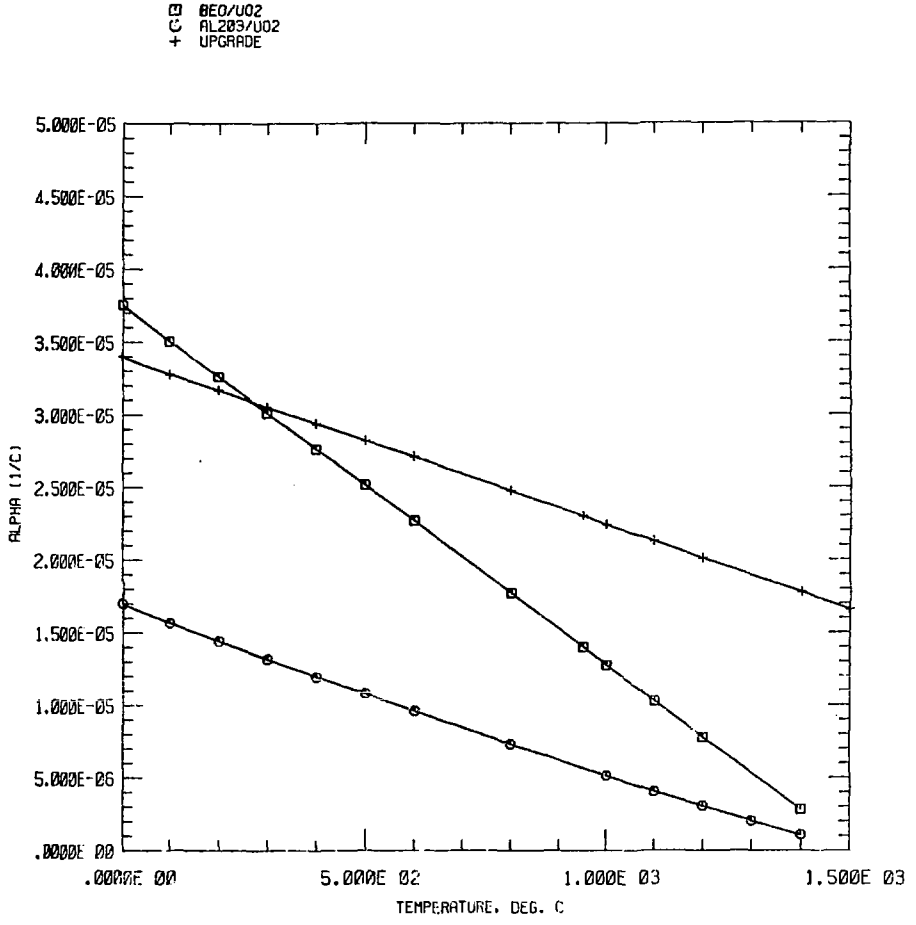

TEMPERATURE FEEDBACK COEFFICIENTS FROM SAK FOR DIFFERENT SYSTEMS

FIGURE 5.3.2-1

5.3.3 Kinetics Analysis

In the SAK and PKlD codes [8] one can specify N heat transfer models and designate how many elements of each type are present in the reactor. A relative average power density is assigned to each model. In our calculations four relative power regions were modeled but the element geometry was identical in all of the regions. One of these elements was modelled so that the peak temperature was representative of the maximum power density. Total reactor power, yield, and average fuel temperature are calculated on the basis of the number of fuel elements assigned to each region and the input power distribution specified by the user. The fuel element geometries of the BeO and Al_2O_3 fuel elements are given in Table 5.3.3-1. There were 1522 elements in the reference BeO core and 2542 elements in the Al_2O_3 core.

Maximum and average temperature histories of both types of systems were calculated for a reasonable range of neutron generation times and reactivity insertions. The two reactivity functions used are shown in Fig. 5.3.3-1. Reactivity was withdrawn according to a sine squared function:

$$\rho(t) = \rho_1 + \rho_2 \sin^2\left(\frac{\pi t}{2}\right), \qquad 0 < t < 1$$

The withdrawal was divided into two time zones so that long time steps could be used initially. In Case I the control rods were removed in 50 msecs and left out. In Case II the reactivity was withdrawn as in Case I, held out for 500 msec, and then reinserted in the next 50 msec interval. The response of the system was followed for up to 20 seconds for Case I and for ≤7 seconds for

Table 5.3.3-1

Geometry for BeO and Al_2O_3 Fuel Elements in SAK and PK1D

Parameter	Dimension
Fuel Radius, cm	0.9525
Gap Thickness, cm	0.0254
Clad Thickness, cm	0.0381
Height, cm	121.92 and 137.16

CASE I

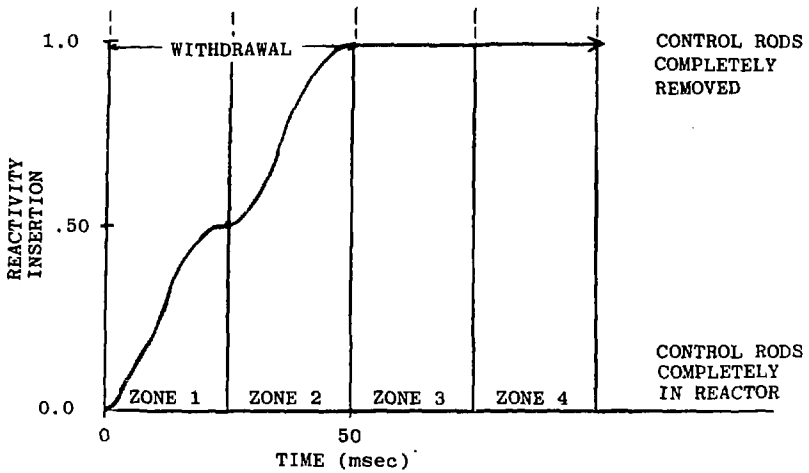

CASE II

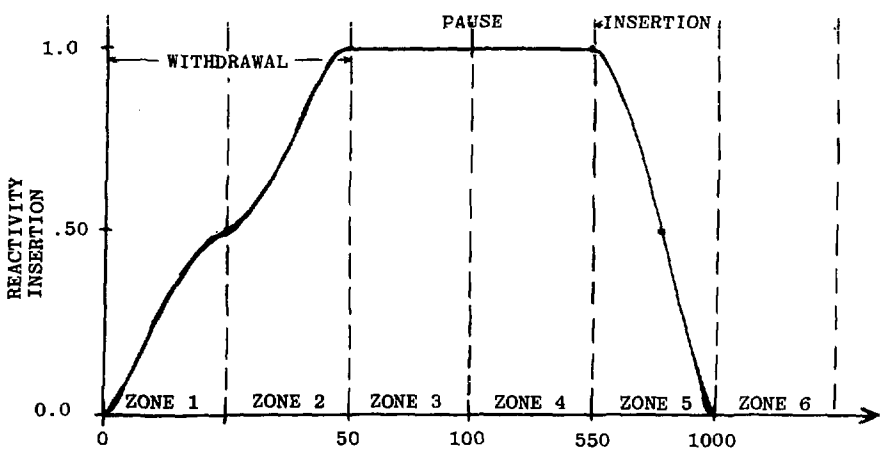

FIGURE 5.3.3-1 TIME HISTORY OF REACTIVITY INPUT

Case II in order to observe peak temperatures of both sequences. Prompt neutron generation times of 2.7 μsec, 12.0 μsec, and 20.0 μsec were modeled. These generation times correspond to reflector materials and thicknesses discussed in Section 5.2.2 and do not imply changes in the fuel material itself.

The majority of the reactor kinetics calculations were done with the PK1D point kinetics code [8]. The temperature-dependent feedback coefficient of reactivity for PK1D was derived from the spacetime SAK code [8] with temperature dependent cross sections from AMPX [3]. The prompt generation time was derived from KENØ IV, a Monte Carlo criticality code [5]. The fluence and yield normalization factors were from two-dimensional neutron transport calculations (TWØTRAN II code) [6].

5.3.3.1 BeO Kinetics

The transient characteristics of the reference BeO fuel system are described in this section. Several different prompt neutron generation times were used to simulate different reflector designs. The temperature coefficient was not varied parametrically to simulate different fuel designs. A comprehensive description of a wide range of BeO fuel design possibilities was beyond the scope of this report.

Table 5.3.3-2 summarizes the PK1D kinetics calculations for the BeO fuel. Reactivity insertions from \$2.50 to \$3.00 were modeled for systems with prompt neutron generation times of 2.7, 12.0 and 20.0 microseconds. These generation times simulate reflector designs ranging from a 4 inch metal reflector up to a twelve inch graphite reflector (see Table 5.2.2-1).

The relationship for the minimum positive period, τ_{min}, is

$$\tau_{min} = \frac{\Lambda}{\rho_o - \beta}, \text{ where } \beta = 0.0069 \qquad (5.3.2)$$

as predicted by simple kinetics models for super-prompt critical excursions. The pulse width at half maximum (as determined by PK1D) is slightly larger than that predicted by the Fuch's model due to a temperature dependent c_p, etc. There is some uncertainty in the pulse width, however, due to the choice of print frequency specified for the output. From the data we can say that

$$PWHM \geq 4.2\ \tau_{min} \qquad (5.3.3)$$

The relationship of peak fuel temperature as a function of minimum period is shown graphically in Fig. 5.3.3-2. The data is from Table 5.3.3-2.

Table 5.3.3-2

Summary of Kinetics of BeO System

Λ (μsec)	Minimum period (msec)	ρ ($)	PWHM (msec)	T max (°C) at time t(sec	Yield (MJ) at time t(sec)	Energy Deposition j/g	%Energy Deposition in tail	
2.7	0.366	2.50	~1.50	840.5 @ 1.78	1592 @ 3.0	1273	24%	rod drop
2.7	0.333	2.75	~1.75	950.5 @ 1.53	1841 @ 3.0	1472	24%	rod drop
2.7	0.310	3.00	~1.50	1060 @ 1.38	2091 @ 3.0	1672	25%	rod drop
12	1.159	2.50	~5.00	947.3 @ 1.55	1906 @ 5.0	1524	22%	rod drop
12	0.992	2.75	~4.25	1129 @ 1.25	2337 @ 5.0	1869	20%	rod drop
12	0.869	3.00	~4.00	1328 @ 1.35	2817 @ 5.0	2252	19%	rod drop
12	0.774	3.25	~3.5	1554 @ 1.2	3386 @ 5.0	2708	18%	rod drop
20	1.930	2.50	~8.25	944.9 @ 1.6	1902 @ 5.0	1521	22%	rod drop
20	1.652	2.75	~7.50	1126 @ 1.3	2331 @ 5.0	1864	20%	rod drop
20	1.449	3.00	~6.50	1323 @ 1.3	2808 @ 5.0	2245	19%	rod drop
2.7	0.366	2.50	~1.50	1022 @ 6.0	2186 @ 6.0	1748	45%	no rod drop
2.7	0.333	2.75	~1.50	1161 @ 6.0	2549 @ 6.0	2038	45%	no rod drop
2.7	0.310	3.00	~1.50	1308 @ 6.0	2941 @ 6.0	2351	46%	no rod drop
12	1.159	2.50	~5.00	1093 @ 6.0	2391 @ 6.0	1912	38%	no rod drop
12	0.992	2.75	~4.25	1281 @ 6.0	2902 @ 6.0	2320	36%	no rod drop
12	0.869	3.00	~4.00	1492 @ 6.0	3493 @ 6.0	2793	35%	no rod drop
20	1.930	2.50	~8.25	1092 @ 6.0	2389 @ 6.0	1910	38%	no rod drop
20	1.652	2.75	~7.00	1279 @ 6.0	2897 @ 6.0	2316	36%	no rod drop
20	1.449	3.00	~6.50	1488 @ 6.0	3484 @ 6.0	2786	35%	no rod drop

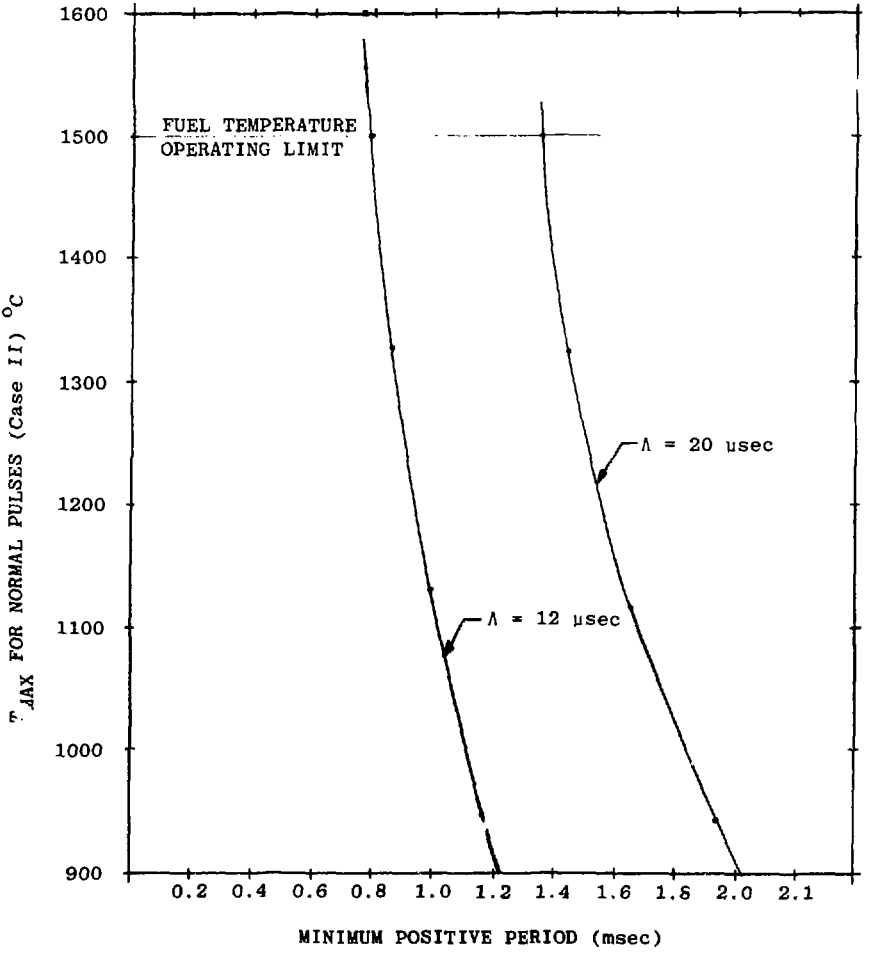

FIGURE 5.3.3-2 RELATIONSHIP BETWEEN MAXIMUM FUEL TEMPERATURE AND MINIMUM PERIOD

A power trace for a $3.00 pulse is shown Fig. 5.3.3-3 (Λ = 12 μsec). The peak power for the pulse was greater than 5×10^{11} watts. The peak occurred at 61 msec, just 10 msec after the reactivity insertion was completed. The 1522 elements in the core thus produced an average power of 3.3×10^{8} watts per element at the peak of the pulse. The hottest element produced 4.6×10^{8} watts at the peak of the pulse. The inflection in the tail of the pulse at about 600 msec is a result of reinserting the control elements. Peak powers for other reactivity values for the BeO system are given in Table 5.3.3-3.

Table 5.3.3-3 Peak Power for Selected Pulses, Λ = 12 μsec
BeO Core, 1522 elements

ρ_o, $	Peak Power, watts	Time at Peak Power, msec
2.50	2.6×10^{11}	66
2.75	3.7×10^{11}	63
3.00	5.0×10^{11}	61
3.25	6.5×10^{11}	59

The average and maximum temperature history of the BeO fuel is shown in Figures 5.3.3-3a and -3b for the $3.00 reactivity insertion. A $3.00 pulse is expected to be slightly below the maximum pulsing level. Figure 5.3.3-3a depicts the temperatures resulting from the normal pulsing mode (Case II) where the control elements are reinserted. When the control elements are held out of the reactor (Case I), the maximum and average fuel temperatures are higher by about 150°C. Figures 5.3.3-3a and 5.3.3-3b are for a

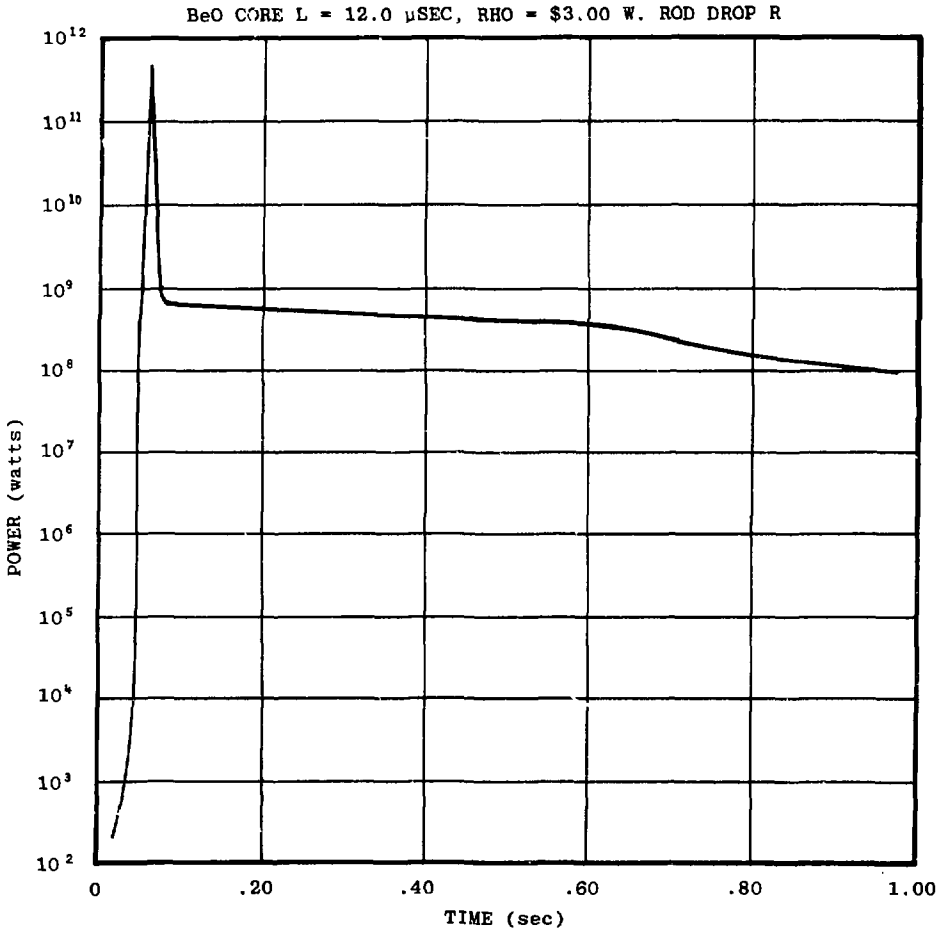

FIGURE 5.3.3-3 POWER HISTORY FOR A $3.00 PULSE WITH THE BeO FUEL, Λ = 12 μsec

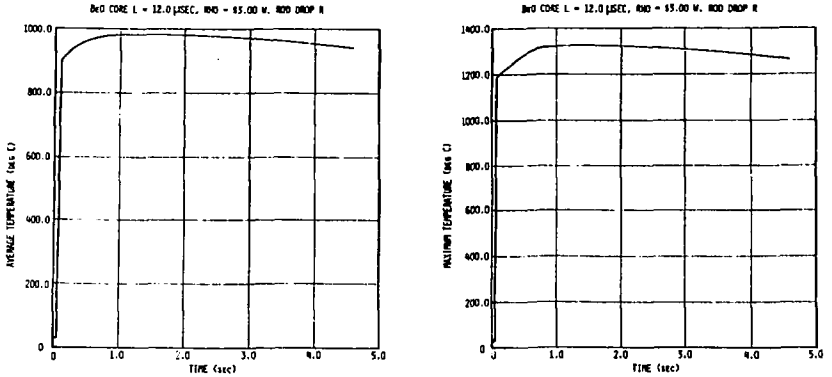

FIGURE 5.3.3-3a BeO FUEL TEMPERATURES FOR A $3.00 PULSE WITH CONTROL ROD DROP

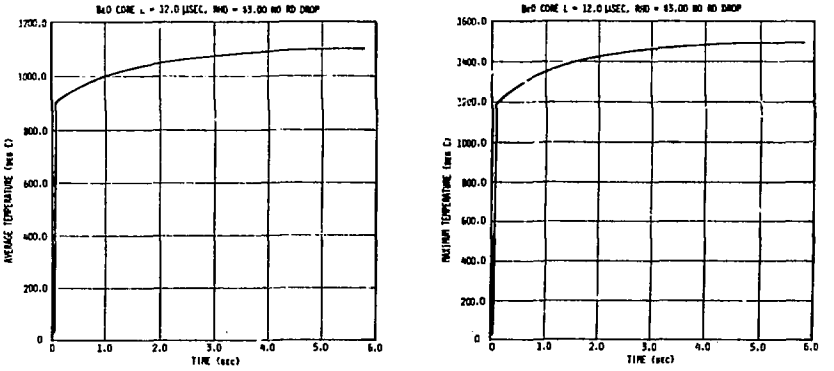

FIGURE 5.3.3-3b BeO FUEL TEMPERATURES FOR A $3.00 PULSE WITHOUT CONTROL ROD DROP

prompt neutron generation time of 12 microseconds, but the energy yield and peak temperatures do not vary much over the range of prompt neutron generation times of interest for HFFPR, 12 to 20 microseconds. Simple relationships derived from the Fuch's model for reactor kinetics explain why this is so.

$$E = \frac{2(\rho_o - \beta)}{\alpha K} \quad , \text{ cal/gm of fuel} \qquad (5.3.4)$$

also,

$$E = c_p \Delta T_{fuel} \qquad (5.3.5)$$

where ρ_o is the input reactivity, decimal units of reactivity

α is the temperature coefficient of reactivity, decimal units per °C

β is the effective delayed neutron fraction, 0.0069

K is the inverse heat capacity, $1/c_p$, gm-°C/cal

c_p is the heat capacity of the fuel, cal/gm-°C

ΔT is the average temperature rise of the fuel, °C

The Fuch's model predicts that energy yield and temperature rise are independent of lifetime and depend only on reactivity if the fuel parameters, α and c_p, are not changed. We found this to be true except for the shortest neutron generation time, 2.7 μsec. In that case the power began to rise sufficiently fast that some heating took place in the fuel before all the reactivity was inserted. This will be described in more detail later in this section.

The clad temperature history following a $3.00 pulse is shown in Fig. 5.3.3-4. The heat transfer coefficient representing an

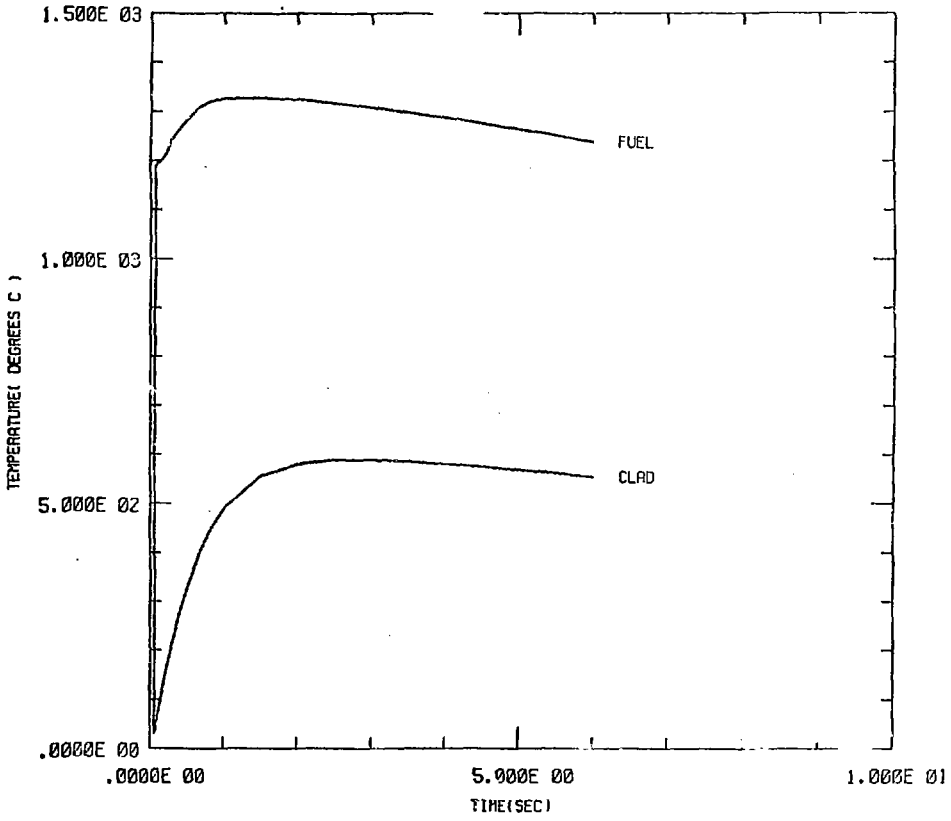

FIGURE 5.3.3-4 BeO FUEL AND CLAD TEMP. HISTORIES, $3.00 PULSE

upper limit of .8 sonic velocity for the helium coolant was assumed here. The pressure was 10 atmospheres. The reactivity function was that of a normal pulse (Case II). The maximum fuel temperature is reproduced here for comparison. The operating limits of the fuel and clad are 1500°C and 725°C, respectively. For a $3.00 pulse, the fuel reaches a maximum temperature of 1328°C at 1.3 sec and the clad reaches a maximum temperature of 588°C at 2.5 sec. The important feature to be pointed out here is that for large pulses, fuel failure will not occur appreciably before clad failure and vice versa. The dependence of peak clad temperature on coolant velocity is illustrated in Figure 5.3.3-5. The effect on fuel temperature is negligible. This figure shows that the helium coolant must flow at a velocity of at least 350 ft/sec in order not to exceed the clad operating limit.

The radial temperature profile across the BeO fuel is described in Fig. 5.3.3-6 for three time frames following a $3.00 pulse. One profile is before the fuel reaches its peak temperature (at t = 1 second) and the second profile is at 3.4 seconds, 2.1 seconds beyond the peak fuel temperature. The clad temperature has peaked but considerable heat is still being transferred to the clad and its temperature is 580°C. The third profile is at 5.9 sec and the clad temperature has decreased to 555°C.

The performance of the BeO systems in terms of maximum energy deposition in a prototypic test bundle, minimum positive period, and reactor yield are graphed in Fig. 5.3.3-7. The Case II reactivity function was used for all cases in this figure. The maximum pulse limit of $3.19 produces a peak fuel temperature of 1500°C

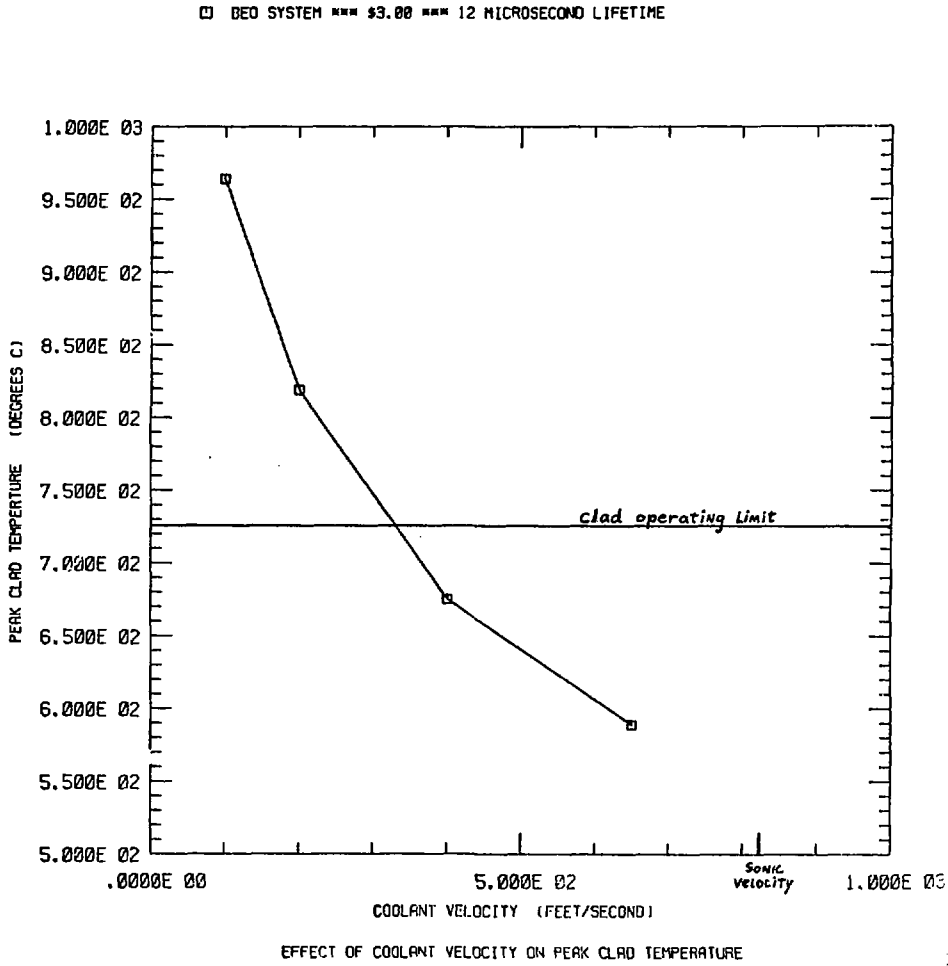
BEO SYSTEM *** $3.00 *** 12 MICROSECOND LIFETIME
1.000E 03
9.500E 02
9.000E 02
8.500E 02
8.000E 02
7.500E 02
7.000E 02
6.500E 02
6.000E 02
5.500E 02
5.000E 02
PEAK CLAD TEMPERATURE (DEGREES C)
clad operating limit
.0000E 00
5.000E 02
Sonic Velocity
1.000E 03
COOLANT VELOCITY (FEET/SECOND)
EFFECT OF COOLANT VELOCITY ON PEAK CLAD TEMPERATURE

FIGURE 5.3.3-5

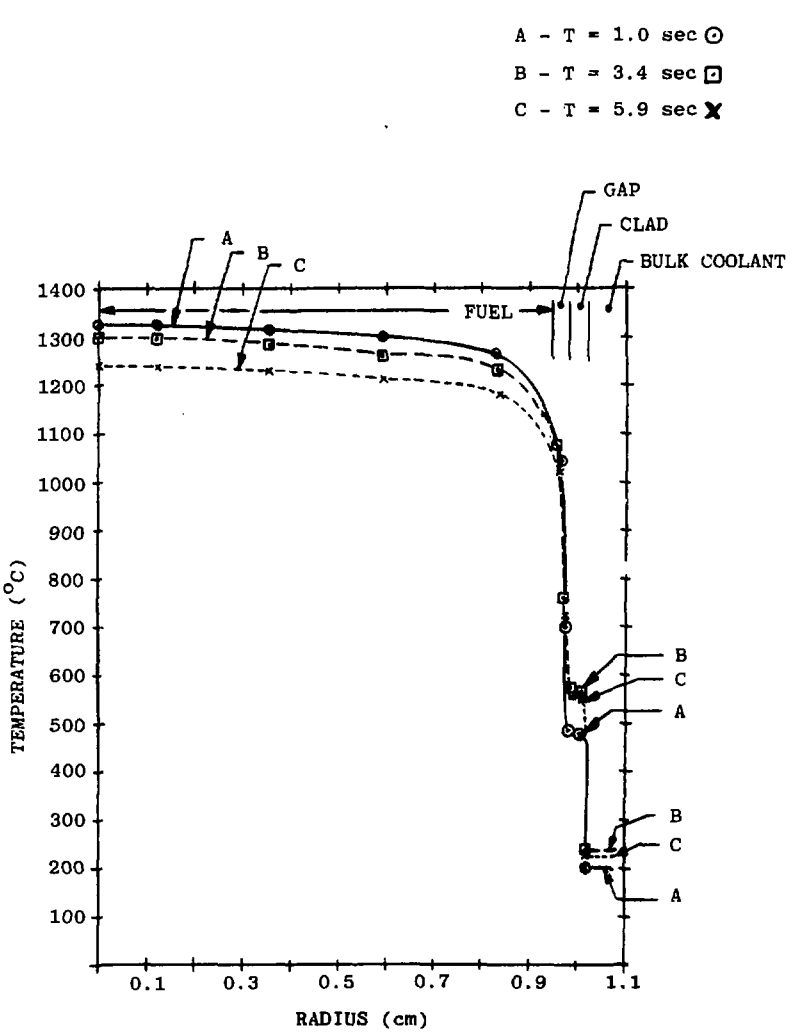

FIGURE 5.3.3-6 TEMPERATURE PROFILES IN A BeO ELEMENT FOR A $3.00 PULSE (CASE II)

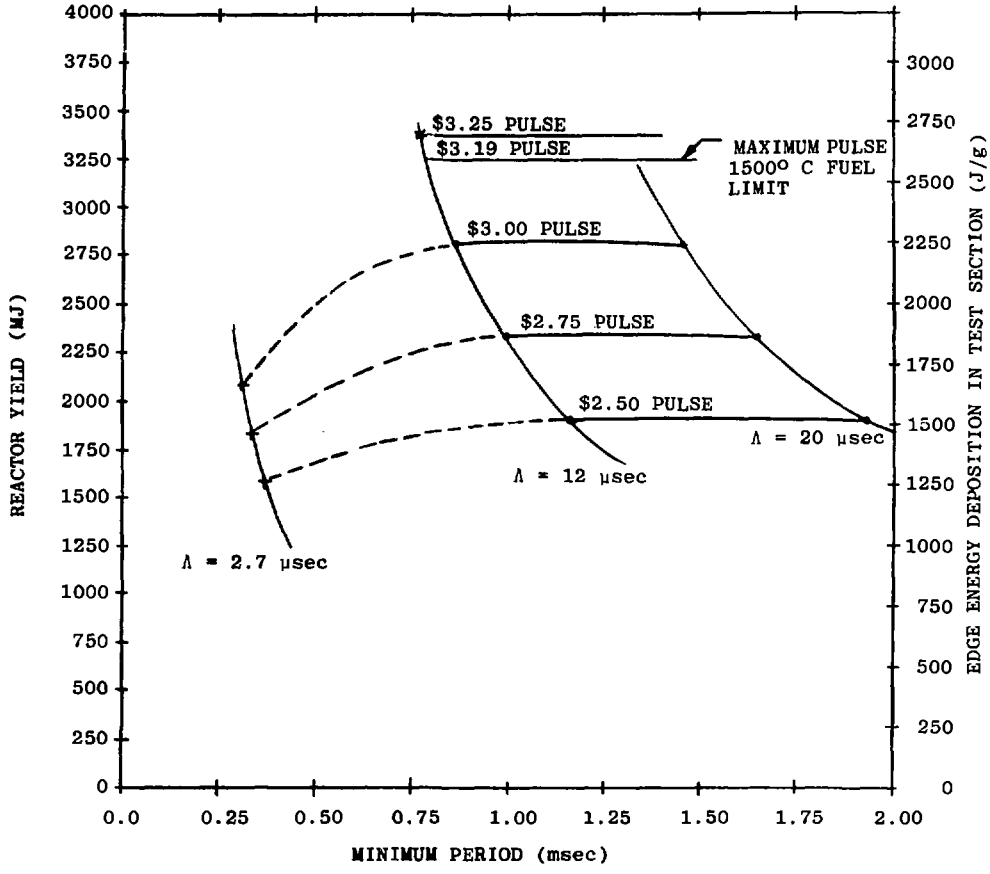

FIGURE 5.3.3-7 BeO REACTOR PERFORMANCE, NORMAL PULSES

and a peak clad temperature of 693°C (the clad limit is 725°C). Peak temperatures for the $3.00 pulse were given previously in Fig. 5.3.3-3. Minimum periods in the range of 0.8 to 1.2 msec produce energy depositions of 2600 j/gm on a $3.19 pulse. Approximately 20% of this energy is in the tail (i.e., t > 100 msec). The short generation time (2.7 μsec) curve is lower than expected because not all of the reactivity was inserted before fuel heating took place. At peak power only $2.56 of the $3.00 input reactivity function had been introduced. The peak occurred at 45 msec and the reactivity function was programmed for a 50 msec insertion time. The effective reactivity value of the preinitiated pulse was probably somewhere between $1.75 (prior to any fuel heating) and $2.56. Such phenomena are characteristic of short generation time systems and, therefore, such systems are impractical for a test reactor that must produce predictable, reproducible pulses. (Fast burst reactors such as the Sandia Pulse Reactors, Λ = 10 nanosec, operate on stochastic kinetics and are pulsed from zero power to avoid this preinitiation problem). This was not a problem with the longer generation times. Therefore, our main interest is in systems with $\Lambda > 12$ μsec. For these systems maximum reactor yields are on the order of 3000 MJ, a factor of 10 over the ACPR Upgrade.

Performance of BeO systems for the Case I reactivity function is shown in Fig. 5.3.3-8. Since the rods are held out, the total yield and energy depositions are higher than in the previous figure by about 25%. This additional energy is generated in the tail of the pulse and represents a hypothetical situation where all

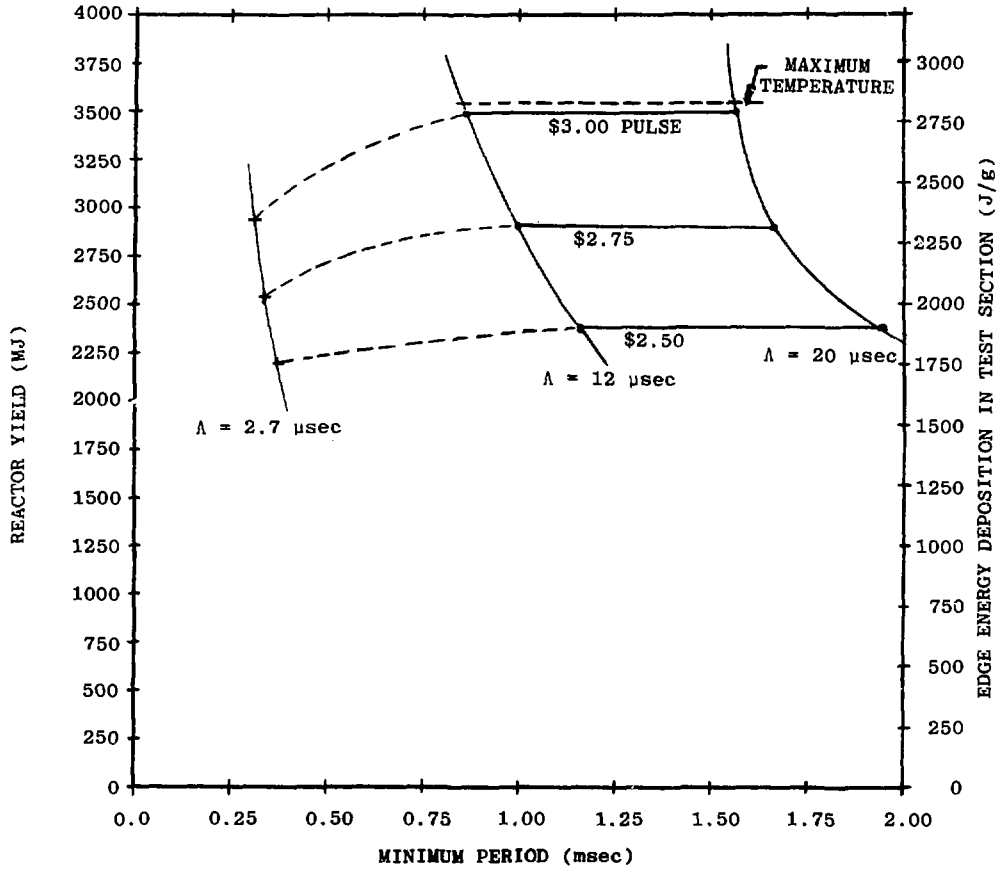

FIGURE 5.3.3-8 BeO REACTOR PERFORMANCE WITH NO ROD DROP

of the rods might be jammed after ejection preventing planned reinsertion. This type of scenario may dictate the maximum allowable reactivity insertion for pulse operation. This would be approximately $3.05.

In using the results from PK1D the following assumptions were made to simplify production runs for a large number of cases. It was assumed that neither the temperature coefficient of a given driver fuel, the conversion factor used to calculate the energy deposition for test fuel (not modeled in PK1D), nor the yield of the driver reactor depended too strongly on the neutron generation time, which was varied. The neutron generation time depends on the reflector, however, and the reflector alters the flux distribution which in turn affects the yield.

The first two assumptions can probably be justified particularly since a representative flux distribution was used as a base case (e.g., the 12 μsec lifetime for the BeO fuel). The yield of the driver will depend strongly on flux distribution, however. Thus, the yield may be high by ~20% for the 2.7 μsec system and low by ~15% for the 20 μsec system. The energy deposition in the test fuel was derived from the yield through a conversion factor obtained from the TWØTRAN II calculations. There is less error in the energy deposition than in the yield, however, since the 12 μsec conversion factor was used for all three different generation times. The actual conversion factors for the 2.7 μsec and 20 μsec cases vary inversely to the actual yield from those cases, so the product is not in error as much as the yield itself. The adiabatic energy deposition values from TWØTRAN II provide a

conservative lower limit energy deposition value for comparison. The estimated error in the PK1D depositions is less than 9%. These considerations do not affect the 12 μsec base case.

Similar assumptions are applicable to the Al_2O_3 systems which are described in the next section.

5.3.3.2 Al_2O_3 System Kinetics

Table 5.3.3-4 summarizes the kinetics calculations for the Al_2O_3 fuel systems. As with the BeO systems, three prompt neutron generation times represented different reflector designs. See Table 5.2.2-1 for a description of the reflector types.

Power history for three reactivity insertions are shown in Fig. 5.3.3-9. The generation time for all three cases was 12 μsec.

The maximum temperature history of the Al_2O_3 fuel for a 12.0 μsec lifetime is graphed in Fig. 5.3.3-10 for reactivity insertions of $1.15, $1.25 and $1.50. At 18 seconds, all the temperatures in Case I situations had either reached a maximum or were rising slowly (≤10°C/sec). Since the temperature coefficient for Al_2O_3 is so small (See Fig. 5.3.2-1), the response of this system to reactivity insertion was relatively slow. Reactivities of $2.00 and over exceeded the temperature range within which the material properties were valid. The BeO system, on the other hand, reaches a maximum temperature in about 6 seconds for the Case I reactivity function and in about 1.2 to 1.8 seconds for the Case II reactivity function. The temperature profile across a 2 cm OD fuel pin as a function of radius is depicted in Fig. 5.3.3-11 for PK1D Al_2O_3/UO_2 fuel. The normal pulse reactivity function (Case II) was used for three reactivity insertion values. The neutron lifetime was 12.0 μsec. A 20.0 μsec lifetime gave similar final temperatures for $1.15 and $1.25. These temperature profiles are shown at a time of 19 sec. The fuel temperature is at its maximum value or is rising slowly (<10°C/sec).

TABLE 5.3.3-4: Summary of Kinetics of Al_2O_3 System

LIFETIME (μSEC)	τ MIN (MSEC)	REACTIVITY ($)	T MAX (°C)	TIME OF T MAX (sec)	YIELD (MJ)	ENERGY DEPOSITION (joules/gm)	% ENERGY IN TAIL	CONTROL RODS IN OR OUT
2.7	2.236	$1.15	1199	21.4	3925	3300	89%	OUT
2.7	1.519	$1.25	out of range	--	--	--	--	OUT
2.7	.732	$1.50	out of range	--	--	--	--	OUT
12.0	6.004	$1.15	1197	21.4	3903	3280	88%	OUT
12.0	4.979	$1.25	1394	21.4	4685	3940	84%	OUT
12.0	3.244	$1.50	2450	20.2	7114	5980	76%	OUT
20.0	8.303	$1.15	1197	21.5	3892	3270	87%	OUT
20.0	7.113	$1.25	1393	21.4	4676	3930	83%	OUT
20.0	4.998	$1.50	2075	21.1	7096	5970	75%	OUT
2.7	2.236	$1.15	461	5.7	1171	1000	62%	IN
2.7	1.519	$1.25	625	5.7	1660	1400	55%	IN
2.7	.782	$1.50	1060	5.7	3017	2500	43%	IN
2.7	.534	$1.75	1747	7.0	4738	3990	37%	IN
12.0	6.004	$1.15	428	5.7	1067	900	57%	IN
12.0	4.973	$1.25	608	5.7	1592	1340	45%	IN
12.0	3.244	$1.50	1048	5.7	2975	2500	41%	IN
12.0	2.288	$1.75	1600	6.0	4736	3980	36%	IN
20.0	8.303	$1.15	397	5.7	976	820	51%	IN
20.0	7.113	$1.25	584	5.7	1532	1290	48%	IN
20.0	4.999	$1.50	1033	5.7	2930	2460	39%	IN
20.0	3.697	$1.75	1554	5.9	4652	3910	34%	IN

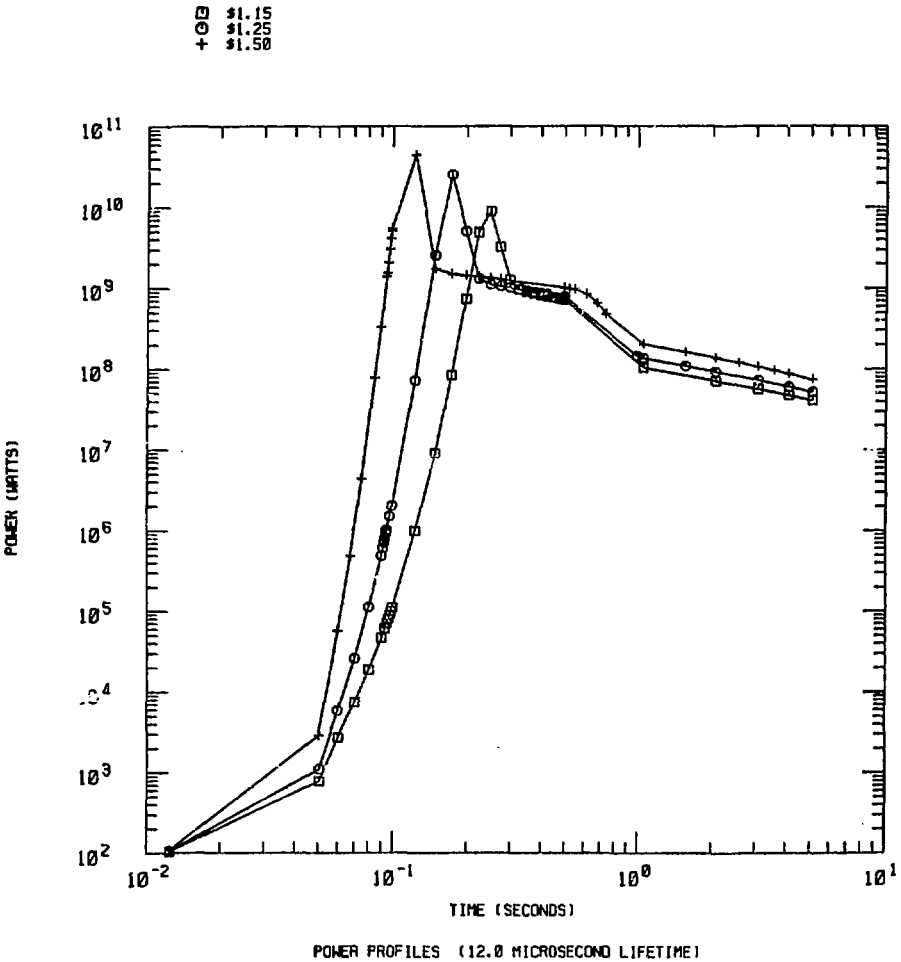

POWER PROFILES (12.0 MICROSECOND LIFETIME)

FIGURE 5.3.3-9

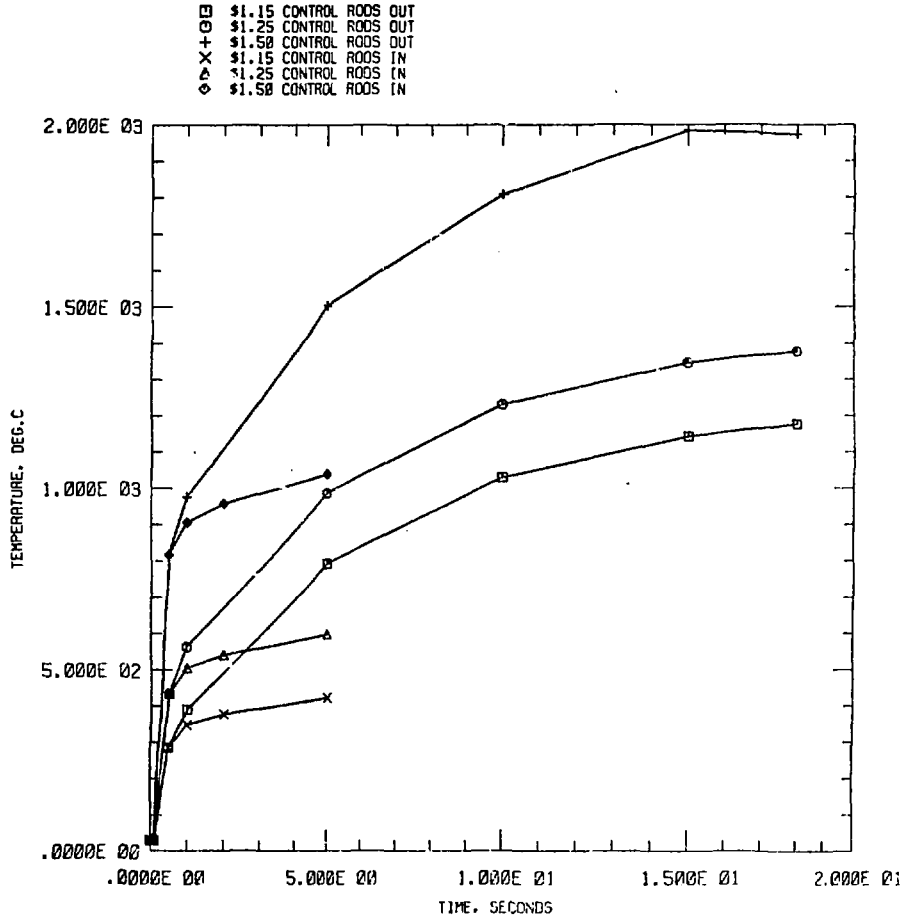

FIGURE 5.3.3-10 TEMPERATURE HISTORY OF Al_2O_3 FUEL AT HOT SPOT CENTERLINE

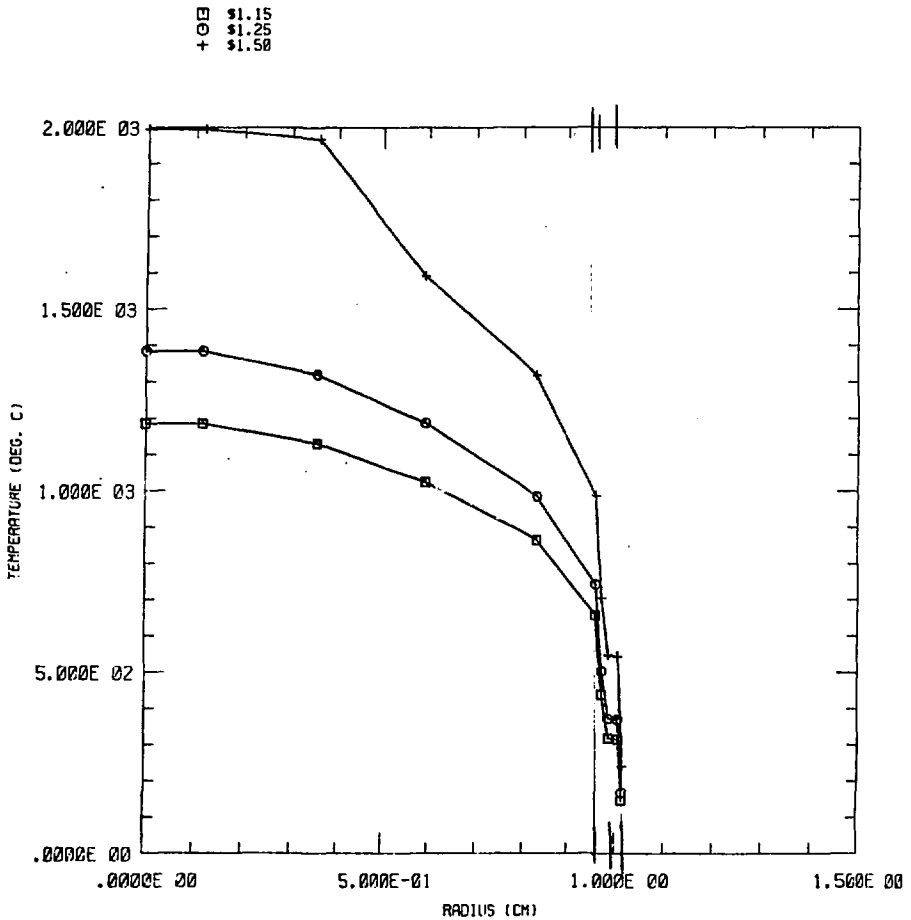

FIGURE 5.3.3-11

Temperature histories of the fuel and clad for a 1.9 cm element and a $1.50 normal reactivity insertion are shown in Fig. 5.3.3-12 (Λ = 12 μsec). A heat transfer coefficient representing an upper limit for coolant flow (.8 sonic velocity) was assumed here. These curves illustrate the effects of a sustained high power tail on the fuel and clad temperatures. The temperatures do not start decreasing in a reasonable time after the peak of the power pulse. The fuel temperature is also proportionately much closer to its operating limit (1250°C) than the clad temperature is to its limit (725°C).

The effect of coolant velocity (and thus heat transfer coefficient) on the maximum clad temperature is illustrated in Fig. 5.3.3-13. The helium is required to flow at velocities no smaller than 200 ft/sec in order for clad temperatures to remain within reasonable limits.

The performance of the Al_2O_3 systems in terms of yield, minimum period and energy deposition in a test bundle are shown in Figures 5.3.3-14 and 5.3.3-15 for Case II reactivity functions. The reactor yields are larger than in the BeO systems for two reasons. First, the system is larger (more fuel); and secondly, the feedback coefficient is smaller, resulting in wider pulses and higher power tails for any given maximum temperature of the fuel.

The energy depositions for the test section are misleading since 35-40% of the energy is in the tail. This is unacceptable from the standpoint of performance requirements. In an attempt to explain the poor pulse performance of these systems and suggest possible improvements, we artificially varied the heat transfer

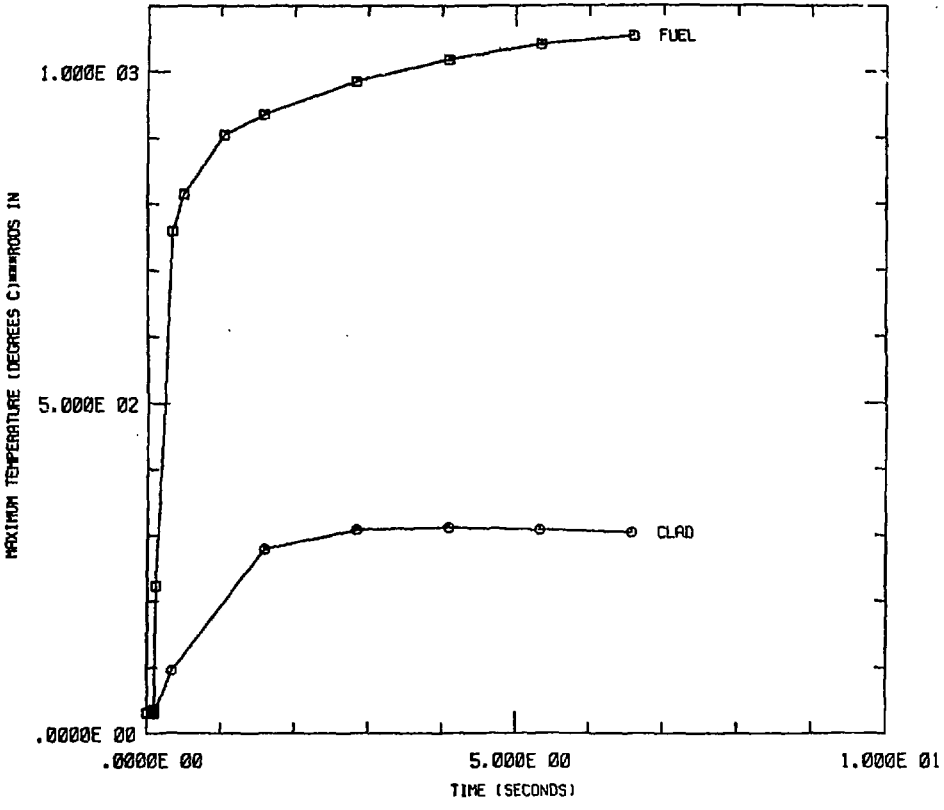

TEMPERATURE HISTORY OF FUEL AND CLAD FOR MAXIMUM PULSE

FIGURE 5.3.3-12

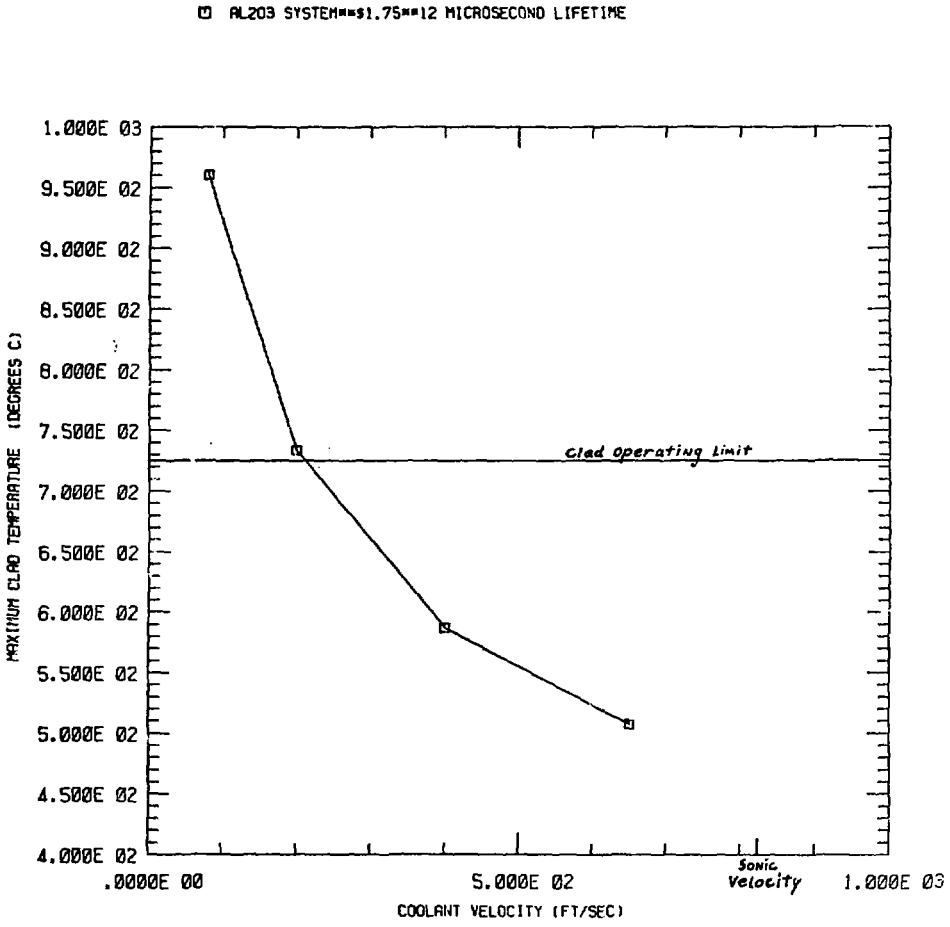

EFFECT OF COOLANT VELOCITY ON PEAK CLAD TEMPERATURE

FIGURE 5.3.3-13

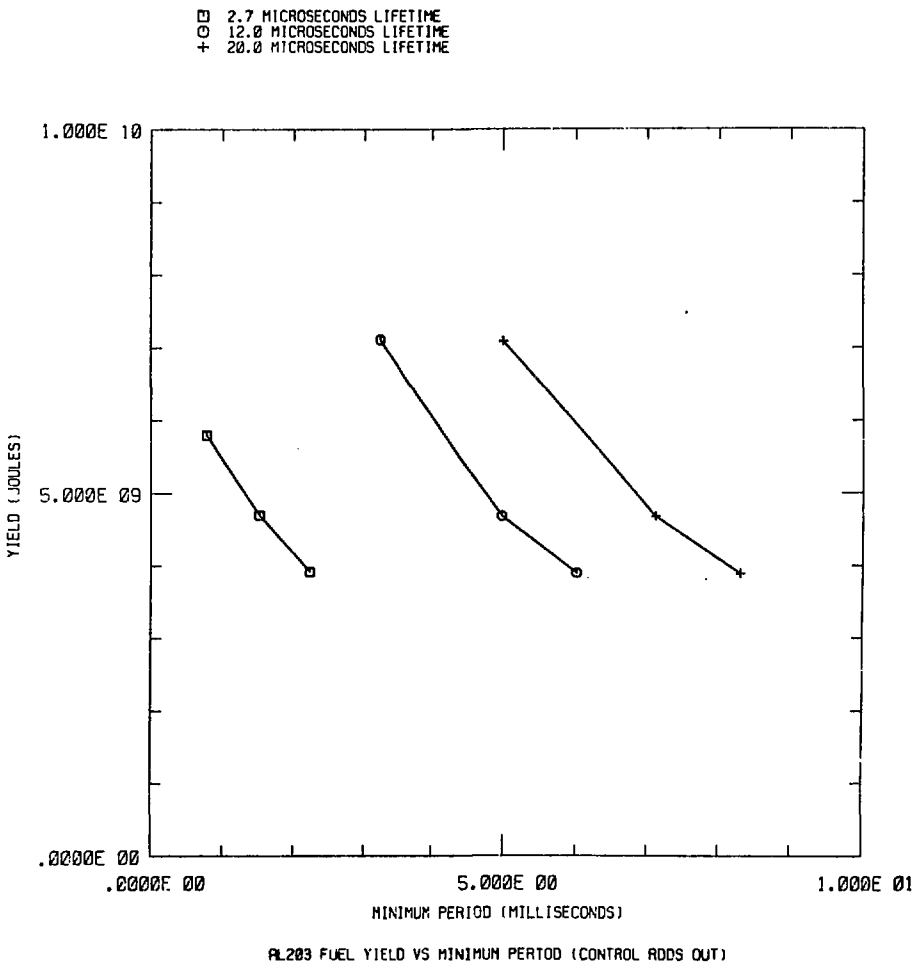

RL203 FUEL YIELD VS MINIMUM PERIOD (CONTROL RODS OUT)

FIGURE 5.3.3-14

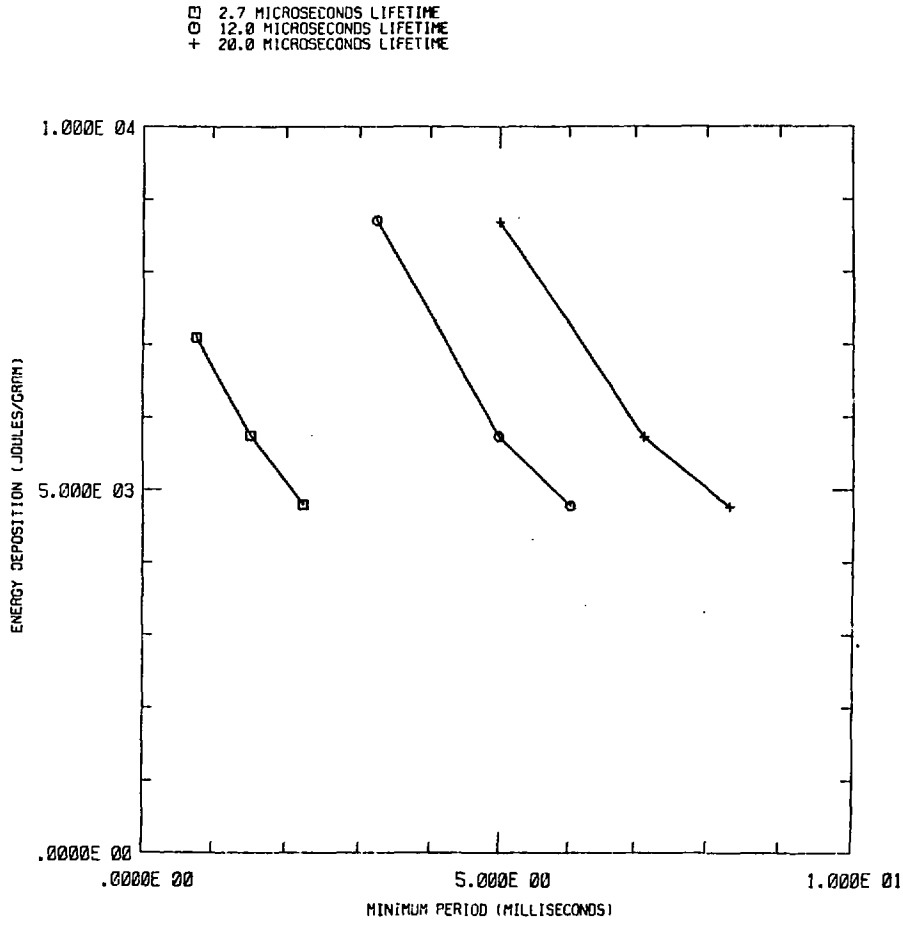

AL203 FUEL ENERGY DEPOSITION VS MINIMUM PERIOD (CONTROL RODS OUT)

FIGURE 5.3.3-15

coefficient and the reactivity coefficient, α. The results of this analysis are tabulated in Table 5.3.3-5. It can be concluded that raising the heat transfer coefficient to even as high as 5 times its value does not influence the temperature response strongly enough to change the slope of the temperature before 6.5 sec. Increasing α, however, had a far greater effect and produced an eventual temperature decay for the reactor, although the behavior was still sluggish. Multiplying α by 5 caused the temperature to peak at 4.35 sec, but at low temperatures. It can be concluded that our problems with the Al_2O_3/UO_2 fueled reactor were due to the low value of the temperature coefficient, and that a higher one is necessary to make this concept practical.

Possible design modifications that would improve the Al_2O_3 performance are suggested below:

1. Use a reactivity control function to shape the pulse and reduce the high power tail.
2. Soften the spectrum in the outer core, grade the enrichment or use a completely different fuel type (e.g. BeO, ZrH) in the outer core to improve the feedback coefficient.
3. Design in a strong axial expansion feedback to supplement the Doppler feedback.
4. Decrease the enrichment to increase the Doppler feedback from U-238.

Table 5.3.3-5: Effect of Varying the Heat Transfer Reactivity Coefficients*

Condition	Reactivity Insertion $1.75	Reactivity Insertion $2.00
1) Same α; doubled h		
Temperature at 6.5 sec	1595°C	(out of range)
Temperature rise at 6.5 sec	11°C/sec	
2) Same α, 5h		
Temperature at 6.5 sec	1594°C	(out of range)
Temperature rise at 6.5 sec	10°C/sec	
3) Original h; doubled α		
T_{max}	670°C	874°C
Time at T_{max}	6.23 sec	6.29 sec
4) Original h; 5α		
T_{max}	265°C	327°C
Time at T_{max}	4.19 sec	4.35 sec

*A Case II reactivity function was used and the neutron generation time was 12 μsec.

5.4 Neutronics Calculation - Water Cooled Systems

5.4.1 General

Initial studies of the water cooled systems, infinite media and 1-D S_n calculations, were performed using the H-R cross section sets. These studies were involved mainly with light water moderated, BeO/UO_2 ceramic fuel, two region cores of the driver/converter type. One of the main concerns was the matching of the driver and converter such that operating temperatures in the two regions were close to the desired maximum operating temperatures of 1500°C in the driver and 1200°C in the converter.

Because of the steep profiles across large test bundles with the light water cooled, BeO/UO_2 ceramic fuel, two region driver/converter cores, it was decided to investigate other systems. The first was a one region core with a cadmium filter and the second, a heavy water moderated core. Two other fuel types, Al_2O_3/UO_2 and $Fe\text{-}Al/UO_2$, were also investigated.

The water moderated systems showed poor performance and because of this the studies were limited to mainly one dimensional parametric studies. It was concluded that two dimensional studies of the water cooled systems were not warranted at the present time.

5.4.2 Parametric Studies

The parameters that were taken into consideration include (1) the moderator; (2) fissile atom fraction; (3) core size; (4) method of hardening the cavity spectrum; and (5) fuel type. Variations in these parameters lead to variations in (1) energy deposition in the test package; (2) edge to center line ratio of the energy deposition in the test package; and (3) k_{eff} of the system.

5.4.3 General Trends in the Parametric Studies

The following general trends were observed. An increase in fissile atom fraction produced a decrease in energy deposition in the test package and an increase in k_{eff}. An increase in core size for a fixed driver fuel loading resulted in a decrease in energy deposition and an increase in k_{eff}. An increase in the hardness of the cavity spectrum resulted in a decrease in both the energy deposition and edge to center ratio in the test package. A change in moderators from H_2O to D_2O produced an increase in energy deposition and a decrease in both the edge to center ratio and k_{eff}.

5.4.4 Results of Parametric Studies - Water Cooled Systems

Figure 5.4-1 shows the results of the parametric study of the H_2O moderated core and variable width converter. The fuel is BeO/UO_2 (35/1) with a 20% U-235 enrichment. It can be seen that an increase in either core outer diameter or converter thickness leads to a decrease in edge energy deposition. A decrease in the edge to center line ratio is achieved by increasing the converter thickness. An increase in k_{eff} is observed with increasing outer diameter.

As an example of the use of Figure 5.4-1 suppose one wishes to have a k_{eff} of 1.17 and an edge to center line ratio of 1.20. One finds that a k_{eff} of 1.17 occurs at an outer diameter of 4 ft, and an edge to center line ratio of 1.2 corresponds to a 2 inch converter. Looking to the edge energy deposition line for a 2 inch converter, one finds that at an outer diameter of 4 ft the edge energy deposition is approximately 1100 j/g with a k_{eff} of 1.17.

It is evident from Figure 5.4-1 that for an outer diameter less than 10 feet, it is not possible to achieve an edge energy deposition of 2500 j/g in prototypic fuel with an edge to center line ratio that

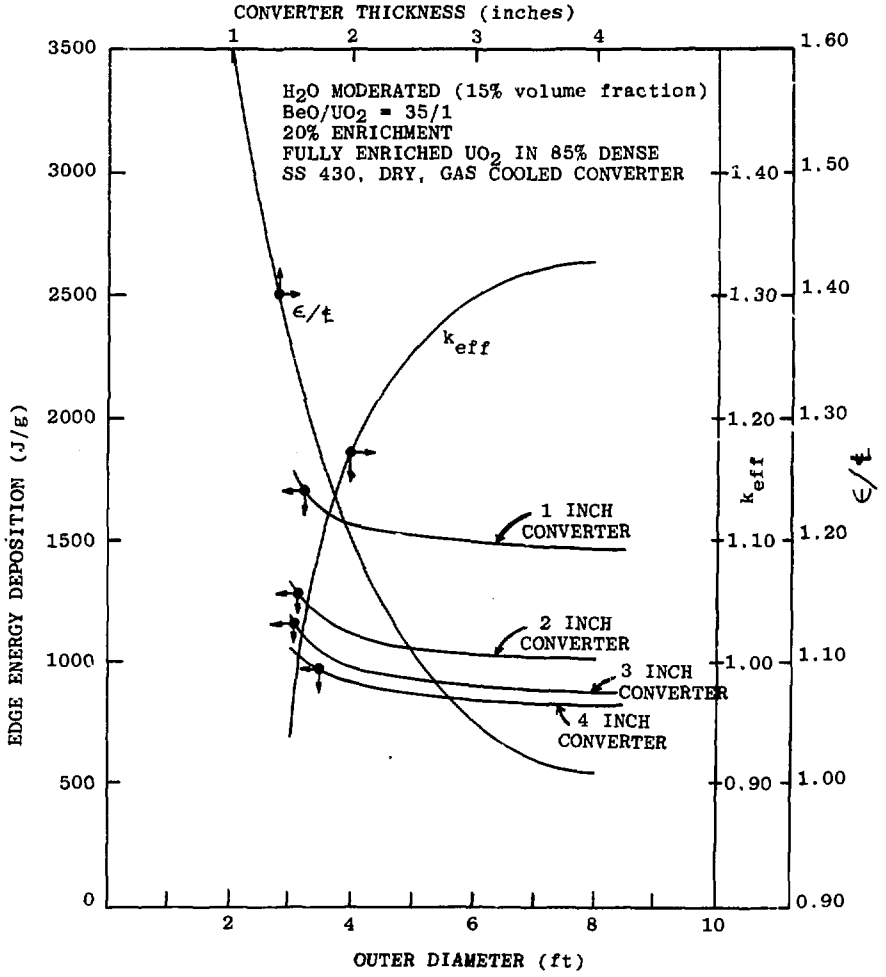

FIGURE 5.4-1 EDGE ENERGY DEPOSITIONS OF H_2O MODERATED CORE FOR CONVERTERS OF VARIOUS THICKNESSES

is acceptable ($E/\phi \leq 1.25$). In order to meet these criteria, the fissile atom fraction of both the driver core and converter would have to be lowered. This would then entail increasing the outer diameter of the core in order to achieve a large enough k_{eff}.

An alternative to the dry converter for hardening the cavity spectrum is the use of a filter material. Figure 5.4-2 shows the results of the parametric study of the H_2O moderated core of BeO/UO_2 fuel with a molecular ratio of 35/1 and variable U-235 enrichment. To use Figure 5.4-2 one needs to supply at least one of the following variables: k_{eff}, edge energy deposition, outer diameter, or fissile atom fraction, to get an estimate of the range of the other variables of interest.

Figure 5.4-2 exhibits the general trends that were discussed earlier. It is evident that in order to achieve an edge energy deposition of at least 2500 j/g one needs to go to even lower fissile atom fractions and larger core than are shown in Figure 5.4-2. It should also be evident from Figure 5.4-2 that the edge to center line ratio is greater than would be acceptable.

In an attempt to increase the edge energy deposition and lower the edge to center line ratio, it was decided to investigate a system with a less effective moderator such as D_2O. D_2O is still a very effective moderator and with its lower absorption cross section would result in a leakier system. In Table 3-4 one can see that the D_2O moderated core does have a slightly harder spectrum than the H_2O moderated core.

Figures 5.4-3, 5.4-4, and 5.4-5 show the results for the D_2O moderated cores with driver fuels of BeO/UO_2, $Fe\text{-}Al/UO_2$, and Al_2O_3/UO_2. The same general trends again hold for each of the three fuel types.

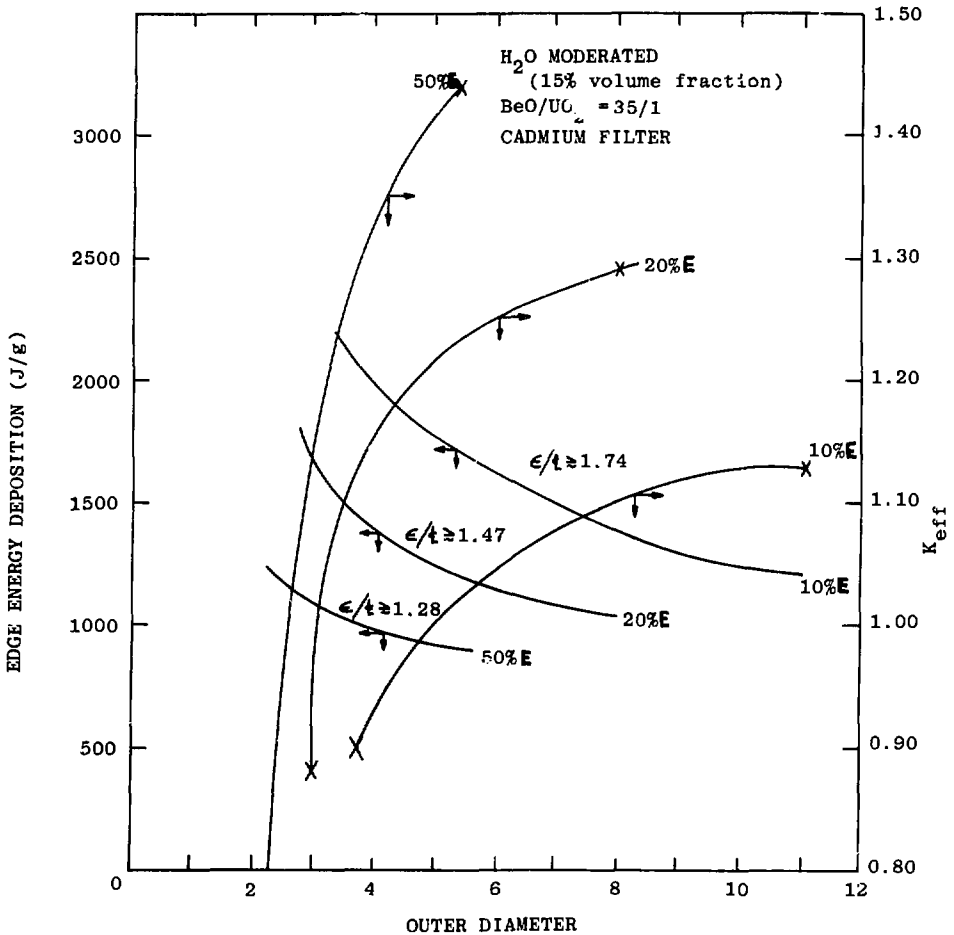

FIGURE 5.4-2 PARAMETRIC STUDY OF H_2O MODERATED CORE USING CADMIUM FILTER

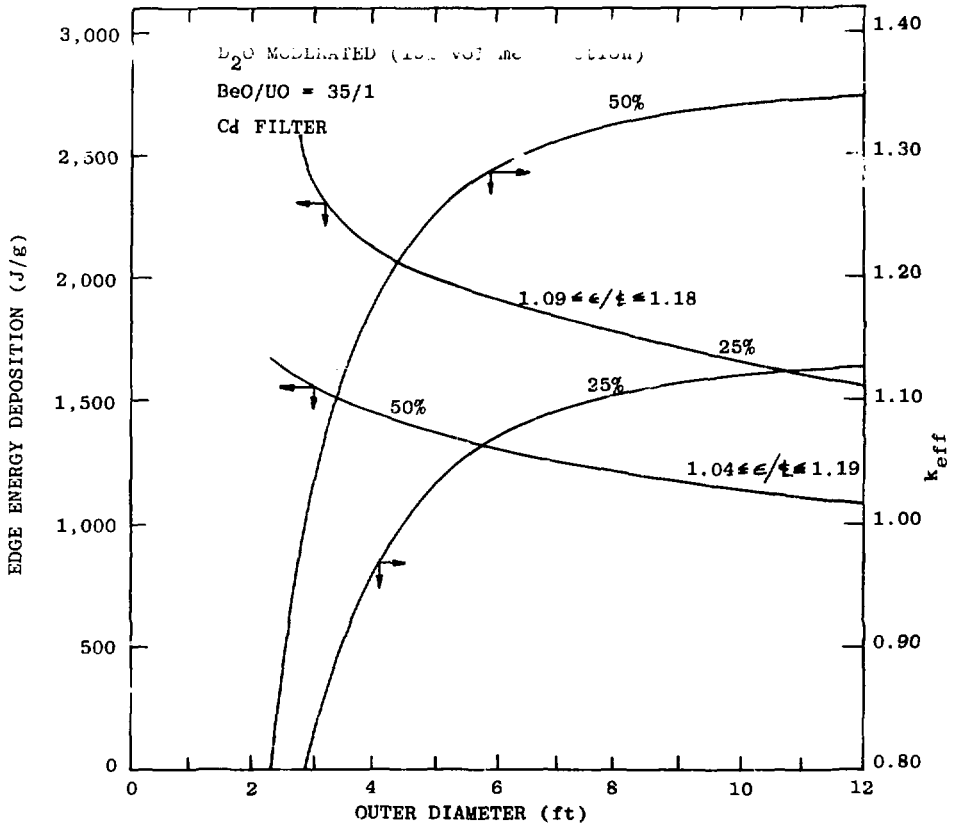

FIGURE 5.4-3 PARAMETRIC STUDY OF D_2O MODERATED CORE USING CADMIUM FILTER

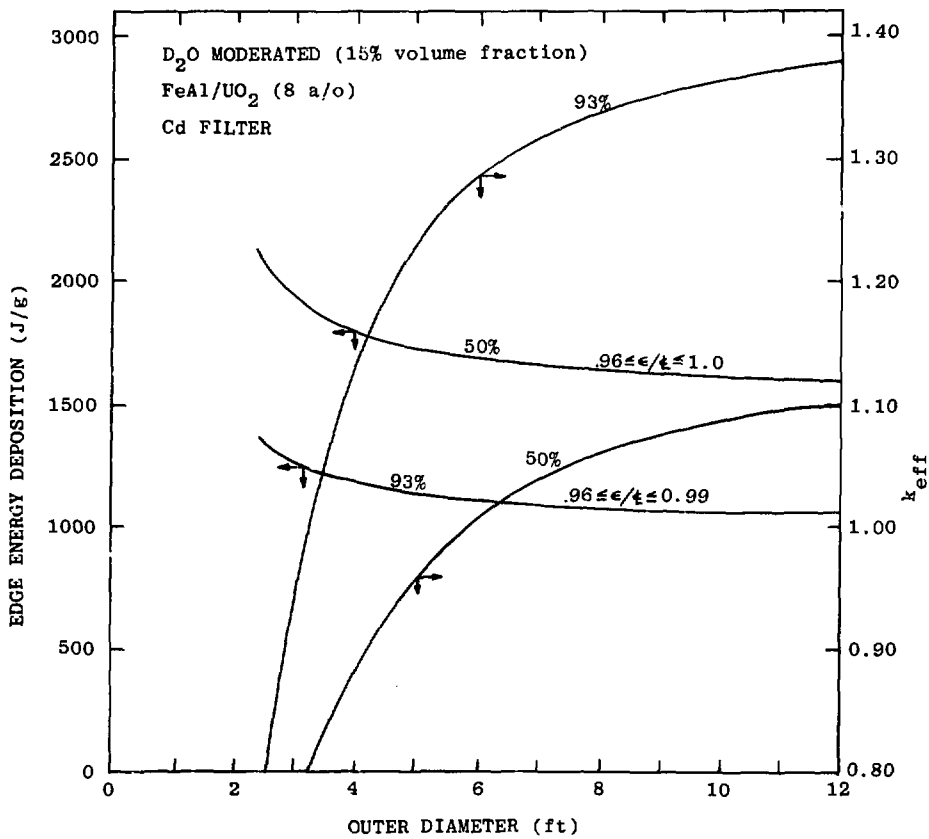

FIGURE 5.4-4 PARAMETRIC STUDY OF D_2O MODERATED CORE FOR Fe-Al/UO_2 SYSTEM WITH CADMIUM FILTER

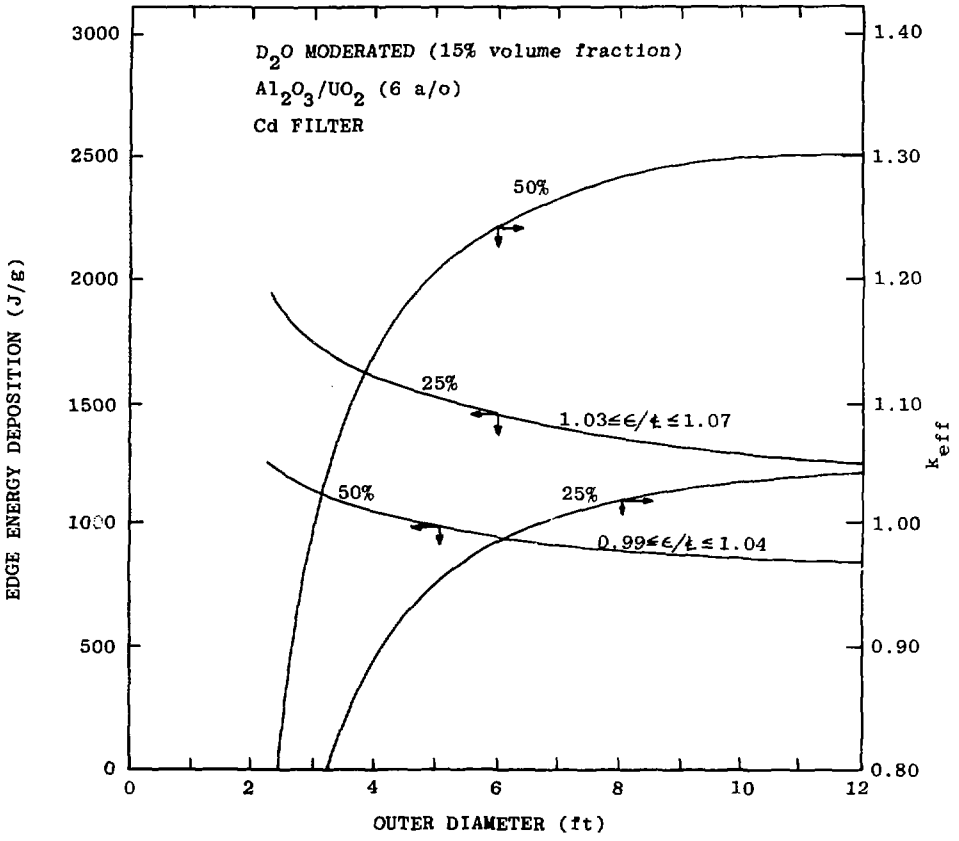

FIGURE 5.4-5 PARAMETRIC STUDY OF D_2O MODERATED CORE FOR Al_2O_3/UO_2 SYSTEM WITH CADMIUM FILTER

To show the improvement in edge energy deposition that is achieved by going to a D_2O moderated core a comparison of Figures 5.4-2 and 5.4-3 will be made. Assuming that one would like a k_{eff} of approximately 1.10, from Figure 5.4-2 it is found that the maximum edge energy deposition is about 1400 j/g with H_2O as the moderator, while for the D_2O moderated core the maximum edge energy deposition is about 1800 j/g with a 2% enriched fuel of BeO/UO_2 with a molecular ratio of 35/1. Along with an improvement in edge energy deposition, there is also a vast improvement in edge to center line ratio for the D_2O moderated core. Since the filter on both the D_2O and H_2O moderated cores is the same, the edge energy deposition of the D_2O moderated core can be increased even more by decreasing the amount of filter material. This, of course, would also increase the edge to center line ratio and care would have to be taken to insure that this ratio did not become unacceptable.

One can see from figures 5.4-4 and 5.4-5 that the $Fe-Al/UO_2$ fuel and the Al_2O_3/UO_2 fuels do not perform as well as the BeO/UO_2 fuels. Although the edge to center line ratios are very low, their edge energy depositions are much lower than for the BeO/UO_2 fuels. Their lower edge energy depositions are due in part to their much lower volumetric heat enthalpies. The enthalpy for BeO/UO_2, molecular ratio = 35/1, at 1500°C is about 1900 cal/cc while for the $Fe-Al/UO_2$ fuel at 1250°C the enthalpy is about 1370 cal/cc and for the Al_2O_3/UO_2 fuel at 1250°C is about 1324 cal/cc. Peaking in the harder spectrum fuels is much more severe than with the BeO fuel and could well act to further limit the performance of these fuels.

5.4.5 Kinetics Analysis of BeO/UO_2 Core for D_2O Moderated HFFPR, Nordheim-Fuchs Model

In order to get an estimate of the kinetic performance of the water cooled HFFPR, it was decided to look at the D_2O moderated HFFPR with a BeO/UO_2 core. The BeO/UO_2 ratio is 35/1, and the U-235 enrichment is 25%. The core outer diameter is 8 ft, and the cavity spectrum hardening system is a cadmium filter.

Table 5.4-1 is a listing of k_{eff} versus fuel temperature. These points were fitted to a quadratic. However, since the initial slope of this equation was positive, it was necessary to estimate the range of α, the temperature coefficient of reactivity. The high end of the estimate was taken to be the slope of the straight line connecting the 300°K and 900°K points. The low end of the estimate was taken as the average of the quadratic and linear approximations. This procedure can be seen visually in Figure 5.4-6.

Table 5.4-1

k_{eff} versus Temperature for BeO/UO_2 = 35/1, 25% enrichment. D_2O Moderated, 8 ft outer diameter core.

Temperature (°K)	k_{eff}	$\rho = \frac{k_{eff} - 1}{k_{eff}}$
300	1.104	0.0942
900	1.076	0.0706
1200	1.030	0.0291

$$\alpha = -\alpha_T = -\frac{d\rho}{dT} \Rightarrow 1.178 \times 10^{-5} \lesssim \alpha \lesssim 3.932 \times 10^{-5}$$

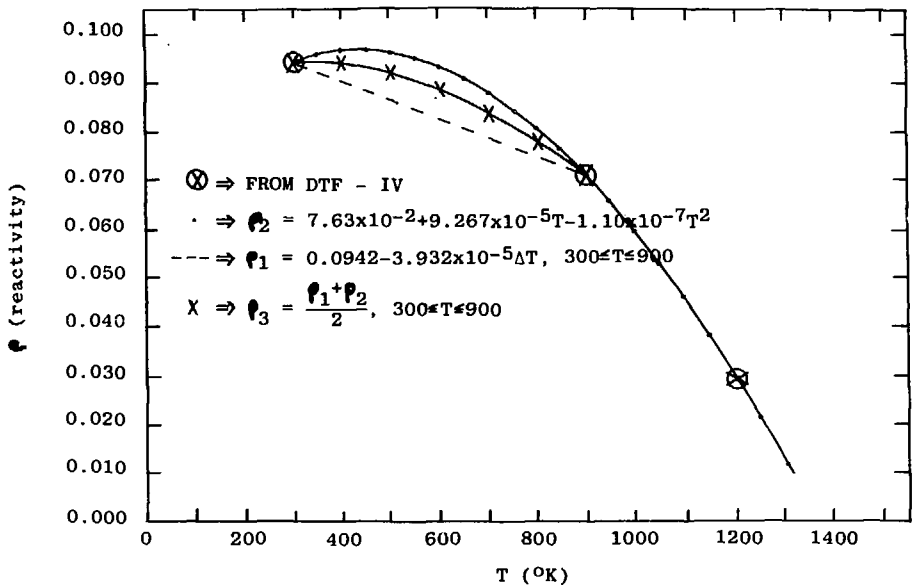

FIGURE 5.4-6 QUADRATIC AND LINEAR APPROXIMATIONS FOR ESTIMATION OF TEMPERATURE COEFFICIENT OF REACTIVITY

The generation time was computed by using the Monte Carlo code KENO-IV. From KENO-IV, the generation time, ℓ, is $2.02982 \times 10^{-5} + 2.88718 \times 10^{-7}$.

From Hetrick [13] the initial excess reactivity, ρ_o, is given as

$$\rho_o = \frac{\alpha K E}{2} + \beta \,, \qquad (5.4\text{-}1)$$

where,

$\alpha \equiv$ negative of the temperature coefficient of reactivity [$°C^{-1}$],

$K \equiv$ reciprocal heat capacity [g-°C/cal],

$E \equiv$ core hot spot energy [cal/g],

$\beta \equiv$ Delayed neutron fraction.

Before the feedback of the system becomes significant the power rise is small, but rises exponentially with a short period. The reciprocal period, ω, during this interval is given in Hetrick as

$$\omega = \frac{\rho_o - \beta}{\ell} \,, \qquad (5.4\text{-}2)$$

where,

$\ell \equiv$ generation time [sec].

The period, T, is thus

$$T = 1/\omega \,. \qquad (5.4\text{-}3)$$

The width, τ, of the power burst at half height is given in Hetrick as

$$\tau = \frac{4}{\omega} \cosh^{-1}\sqrt{2} = \frac{3.524}{\omega} . \qquad (5.4\text{-}4)$$

The peak power of the burst, E_{peak}, can be estimated as

$$E_{peak} = \frac{\ell\omega^2}{2\alpha K} . \qquad (5.4\text{-}5)$$

Table 5.4-2 contains a listing of input values for the Nordheim-Fuchs model and a listing of the results from the analysis.

TABLE 5.4-2

Nordheim-Fuchs Analysis - Input Parameters and Results

Input parameters

$E = 550$ cal/g

$\beta = 0.0075$

$K = 2.727$ g-°C/cal

$\ell = 2.030 \times 10^{-5}$ sec

Results

Case #1 ($\alpha = 3.932 \times 10^{-5}$)

$\rho_o = 0.0370$ or \$4.93

$\omega = 1452.56$ sec^{-1}

$T = 6.88 \times 10^{-4}$ sec = 688 μsec

$\tau = 2.426 \times 10^{-3}$ sec = 2.426 msec

$E_{peak} = 0.836$ MW/g fuel

Case #2 ($\alpha = 1.178 \times 10^{-5}$)

$\rho_o = 0.0163$ or \$2.18

$\omega = 434.99$ sec^{-1}

$T = 2.30 \times 10^{-3}$ sec = 2.30 msec

$\tau = 8.101 \times 10^{-3}$ sec = 8.101 msec

$E_{peak} = 0.2503$ MW/g fuel

Chapter 6

Cooling System Considerations

6.1 Heat Exchangers and Pumps

A thorough analysis of the heat exchangers required for a gas cooled system has been carried out in Ref. 14. The helium to water heat exchanger is of the U-tube type because of its simplicity and ability to withstand thermal stresses. The structural design guide for the helium heat exchanger is code case 1592 (Class 1 components in elevated temperature service), Section III of the ASME Boiler and Pressure Vessel Code.

The analysis of the water heat exchanger has also been carried out in Ref. 14. The mass flow rates through both heat exchangers are given in Fig. 6-1. The results of the linear analysis, as well as the manufacturer's results, indicate that the size of both heat exchangers will be on the order of 3 feet in diameter and 10 feet in length.

Mechanical Technology Incorporated (MTI) has considerable experience in the manufacture of helium pumps. MTI manufactured the helium blowers for the UHTREX reactor [15] and is now designing similar blowers for Union Carbide and ORNL.

The circulator can easily handle 26,000 lb/hr of helium at 150 psia and 600°F with a head rise between 2.5 and 5 psi. The approximate horsepower would be 110 at 2.5 psi head and 220 at 5 psi head.

Water pump 1, located between the two heat exchangers, will operate at a speed of 1750 RPM and will have about 7-1/2 horsepower. Water pump 2, serving the cooling tower, will be about 50 horsepower

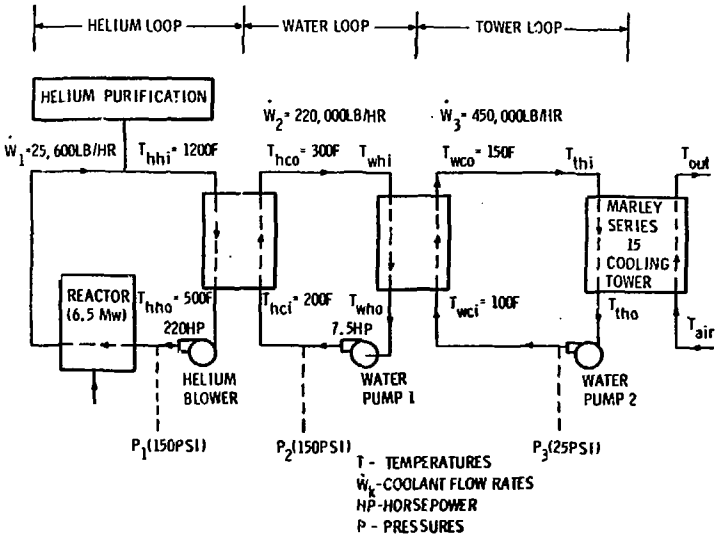

FIGURE 6-1 BLOCK DIAGRAM OF GAS COOLING SYSTEM

and will run at 1750 RPM. Further details on the pumps are given in Ref. 14.

6.2 The Cooling Tower

The cooling tower is a Marley series 15 forced drought tower. It is able to handle 450,000 lb/hr of water and drop the water temperature from 150°F to 100°F. It will cover an area of 20 feet by 16 feet and will stand 17 feet tall. The fan will be powered by a 20 horsepower motor.

6.3 The SERF Reactor Vessel as a Component of the HFFPR

A preliminary survey was made of the SERF reactor vessel to determine if it might be used with the HFFPR. Analysis indicated [14] that the design stresses of this vessel will be greatly exceeded if it is subjected to temperatures on the order of 1200°F.

The vessel is locked in strong concrete with very little room for expansion. It should not be subjected to a temperature higher than 350°F. Even if a design scheme is devised whereby the vessel can be retained and not subjected to temperatures greater than 350°F, it should be cut off at the concrete so that there will be no overhang. Extreme pressures would be present in an overhang if it was present.

It may be possible to devise a scheme where the existing water cooling system for the vessel can be modified to keep its temperature below 350°F. If this is possible, then the vessel may be usable for the HFFPR.

6.4 HFFPR System Layout in the Sandia SERF Building

It is suggested that the helium/water heat exchanger be placed in the Beam Room north of the irradiation cell and on the same level. Here it will be adequately shielded while being sufficiently close to the reactor.

The secondary heat exchanger may be placed in the pump house together with the two water pumps. The pump house is a new addition to the SERF building.

Finally, the helium purification system should be constructed as a modular unit and placed in lock 1, west of the irradiation cell and on the same level, after it has been provided with a gas-tight liner. Further details may be obtained from Ref. 14.

Appendix A

Performance Requirements and Design Criteria for HFFPR

For the purpose of a preliminary design evaluation, a table of performance requirements and features is given in Table A-1.

TABLE A-1

Performance Requirements and Features for HFFPR

Adiabatic Energy Deposition in Prototypic Mixed Oxide Test Fuel (20-30% Pu-239 Fraction)	~2500 j/g
Energy Deposition Capability for Fully Enriched Test Fuel	5000-7000 j/g*
Radial Peak-to-Min Across Large ($61 \leq$ pins ≤ 217) Bundle	<1.15
Steady-State Power Generation for PAHR-Type Tests	6 w/g
Minimum Period/Minimum Pulse Width	1 ms/5ms
Radial Fuel Motion Slots	2 slots
Cavity Size	0.28 m diameter x 1.22 m
Overall Core Size	Less than 1.25 m (diameter) by 1.8 m

Delivering such performance repeatedly and consistently places severe demands on the driver or driver/converter combinations. Desirable properties useful for screening potential driver fuels are given in Table A-2.

---

*The lower figure is derived from a short period pulse performance requirement; the high figure is the upper limit for some shaped-burst accident scenarios.

Table A-2 Desirable Neutronic, Thermal, and Mechanical Properties of Driver Fuels[a]

General Category	Desired Property	Advantage
Neutronic	low absorption cross section high scattering cross section moderate-to-low slowing down power	a hard spectrum with fair-to-good reactivity
	high packing density of matrix atoms	reduced leakage, improved volumetric heat capacity
	high k_∞ with only moderate-to-low fissile atom densities	and best FOM at a fixed core size
	good negative temperature coefficient of reactivity	safety, control, reduced effect of experiments
	short neutron generation time (<35 μsec)	short pulse capability
Thermal	high melting or failure temperature	high performance
	high thermal conductivity	low steady state operating temperatures and resistance to thermal cycling
	high heat capacity of matrix material	high deposition per °C temperature rise of the driver
Mechanical	strength and stability at high temperature	reduced fuel failure
	low thermal expansion coefficient	resistance to thermal cycling

[a] In addition to these desired properties, the fuel must be compatible with the clad and coolants selected.

An ideal material possessing all of these properties probably does not exist. However, this set of general criteria is helpful in comparing and narrowing down the types of fuels best suited for a given set of performance requirements and the modes of operations required.

When applying these criteria and making comparisons one can quickly eliminate a number of fuel candidates from the list. A LASL STF design study [16] contains a good discussion of this subject and although their performance requirements included a more stringent Class III operation*, their comparison of fuel properties is valid for our case as well. Independent investigations at Sandia concentrated initially on Niobium-Uranium cermet fuel, UO_2 fuels (for fully enriched tests only), and BeO/UO_2 fuels. This was later expanded to include Al_2O_3/UO_2 and UO_2 dispersions in iron and iron-alloys. We did not devote any effort to the graphite based fuels investigated by both Argonne and LASL because of disadvantages of system size and inability to perform the short period pulses that were of interest in our experimental program.

By dropping the requirement for Class III operation, helium gas became the preferred coolant for our study. This is consistent with Argonne's choice of gas cooling in their proposal for STF. Watercooled concepts were also investigated, however, and these results are discussed in Chapter 3 and Section 5.4.

---

*A Class III facility is defined as one which has the capability of running for an indefinite period of time at full power before the initiation of a burst or any other experiment, such as loss of flow.

Infinite medium calculations coupled with a simplified analytical model derived by Ostensen [17] were used to zero in on the molecular loadings and enrichments for driver fuel candidates that would yield acceptable energy depositions in the test fuels. The infinite media multigroup calculations were performed using the CHILE code [18] which includes an optional leakage correction term. CHILE also estimates the prompt neutron generation time of the fuel. The Ostensen model was used to estimate the approximate upper limit for the fissile atom fraction in the driver fuel matrix necessary to match the most stringent performance requirement in the test fuel without exceeding an acceptable temperature rise for the driver fuel.

The general criteria established to evaluate the infinite media parametric studies are shown in Table A-3. The limits on k_∞ shown in Table A-3 were based partially on some one-dimensional calculations that permitted estimation of finite geometry leakage effects and partly on qualitative evaluations* of the excess required for slot worths, control, etc. The excess reactivity alotted for radial slots and control was 7 to 10% $\Delta k/k$ each for a total of 14-20%. The leakage effects were estimated to be worth 15 to 25% $\Delta k/k$ for nominal core diameters and reflector thicknesses. To be conservative, the k_∞ lower limits were set at 1.4 for the lower-leakage BeO fuels and 1.45 for other fuels.

---

*Monte Carlo calculations by LASL for maximum negative slot worths on their sodium cooled Class III design [16] and on their softer spectrum Phoebus design [19] were 0.006 $\Delta k/k$ for 3 slots and 0.134 $\Delta k/k$ for two wider slots, respectively. The Class III design slots were ~9 cm and ~5 cm wide and the Phoebus slots were 12 cm wide.

TABLE A-3

Criteria for Zero Dimensional Analysis of Fuel Candidates

Description	Desired Value
Normalized Spectra:	
Peak Energy Range	100 - 400 keV
Fraction in Peak Group	>20%
Fissile Atom Fraction Required to deposit 2500 j/g in 20% enriched UO_2 test fuel:	
BeO/UO_2 driver fuel[a]	<0.011
Other fuels[b]	<0.0093
Fissile Atom Fraction required to deposit 5000 j/g in 93% enriched UO_2 test fuel:	
BeO/UO_2 driver uel	<0.026
Other fuels (Al_2O_3/UO_2, Nb-U, $FeUO_2$)	<0.022
k_∞	
BeO/UO_2[c]	>1.4
Others (see above)	>1.45
Prompt Generation time	~1 μsec to 30 μsec
Desired Kinetics:	
Minimum positive period	1 msec
Pulse width	5 msec

[a] 1500°CΔT Operating limit was assumed.

[b] 1250°CΔT Operating limit was assumed.

[c] The atom density of the BeO fuel is relatively high and these fuels therefore have higher non-leakage probabilities in finite geometries.

Appendix B

Material Properties

The driver fuel should ideally have a low parasitic absorption cross section, a high scattering cross section, a hard spectrum, high melting point, high thermal conductivity, and stability at high temperatures. The thermal conductivities and specific heats of BeO, UO_2, and Al_2O_3 are compared in Figs. B-1 and B-2. It can be seen that BeO is the best conductor of the fuels and that the contribution of UO_2 is so small that it can be virtually neglected in both BeO/UO_2 and Al_2O_3/UO_2 fuels. The physical properties used in this design study are from References 11, 20 and 21.

Stainless steel 316 and 304 have been modeled as the cladding in this study. Recent papers [22,23,24], however, have emphasized a preference for high nickel austenitic steel (35-60% nickel). Inconel 718 and a Nimonic alloy, PE16, have been of particular interest. These have an operating temperature of 825°C, which is ~100°C higher than that of SS316.

Two gap filler materials have been considered for this design: nitrogen and helium. A comparison of the physical properties of these two gases at 10 atm pressure in Figs. B-3, B-4, and B-5 indicates that helium has significantly better heat transfer properties than nitrogen. A comparison of one set of otherwise identical TAC2D runs gave the results indicated in Table B-1.

Table B-1

	He	N
Max. BeO/UO_2 fuel temp:	975°C	2002.2°C
Max. gap temp:	886.11°C	1990.55°C
Max. SS clad temp:	369.44°C	368.3°C

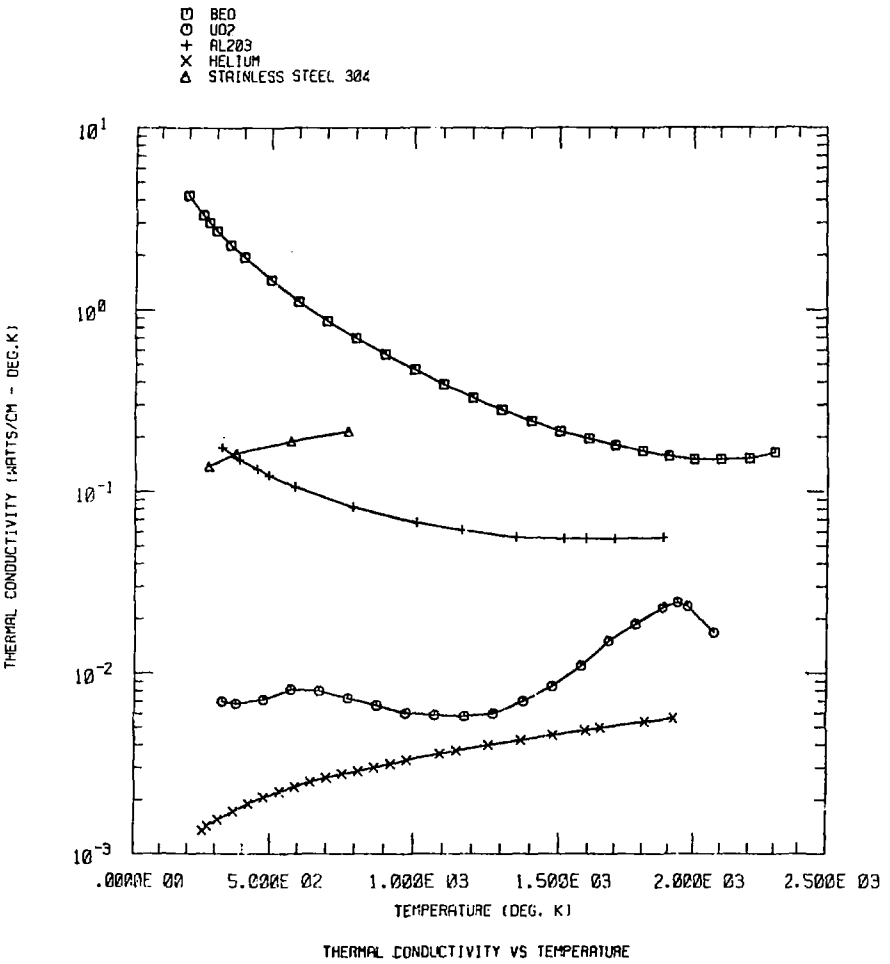

THERMAL CONDUCTIVITY VS TEMPERATURE

FIGURE B-1

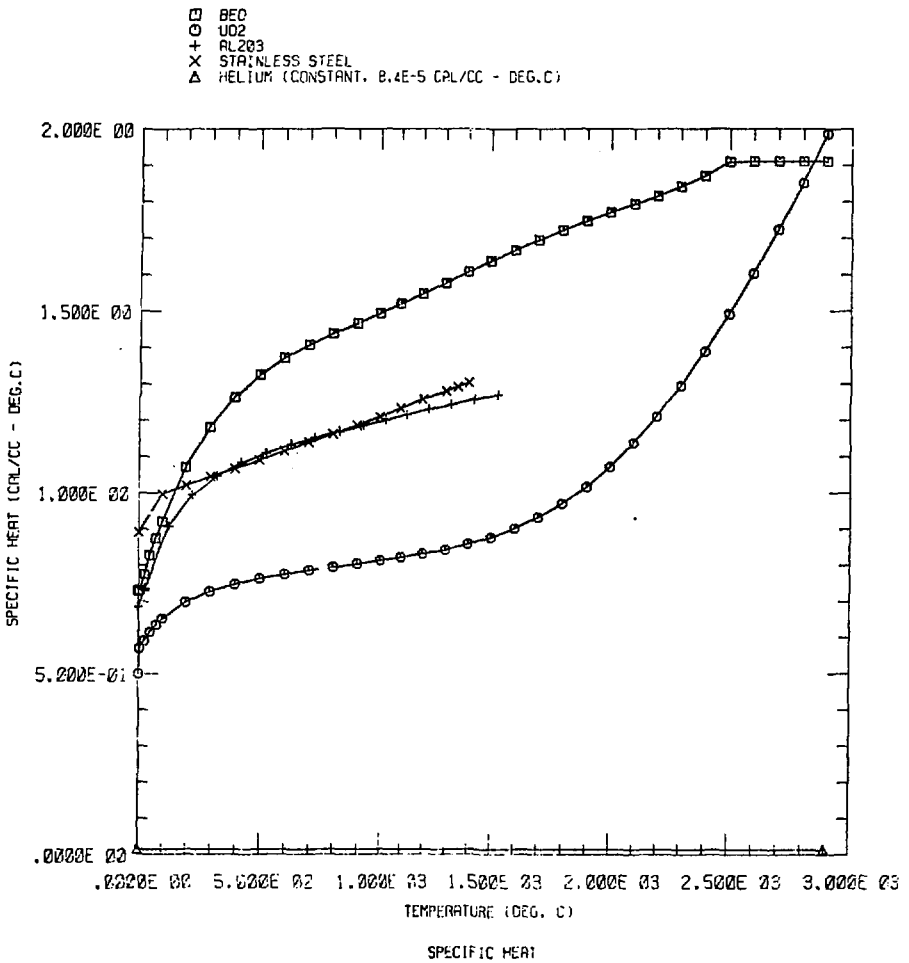
BEO
UO2
AL2O3
STAINLESS STEEL
HELIUM (CONSTANT, 8.4E-5 CAL/CC - DEG.C)
2.000E 00
1.500E 00
1.000E 00
5.000E-01
.0000E 00
SPECIFIC HEAT (CAL/CC - DEG.C)
.0000E 00
5.000E 02
1.000E 03
1.500E 03
2.000E 03
2.500E 03
3.000E 03
TEMPERATURE (DEG. C)
SPECIFIC HEAT

FIGURE B-2

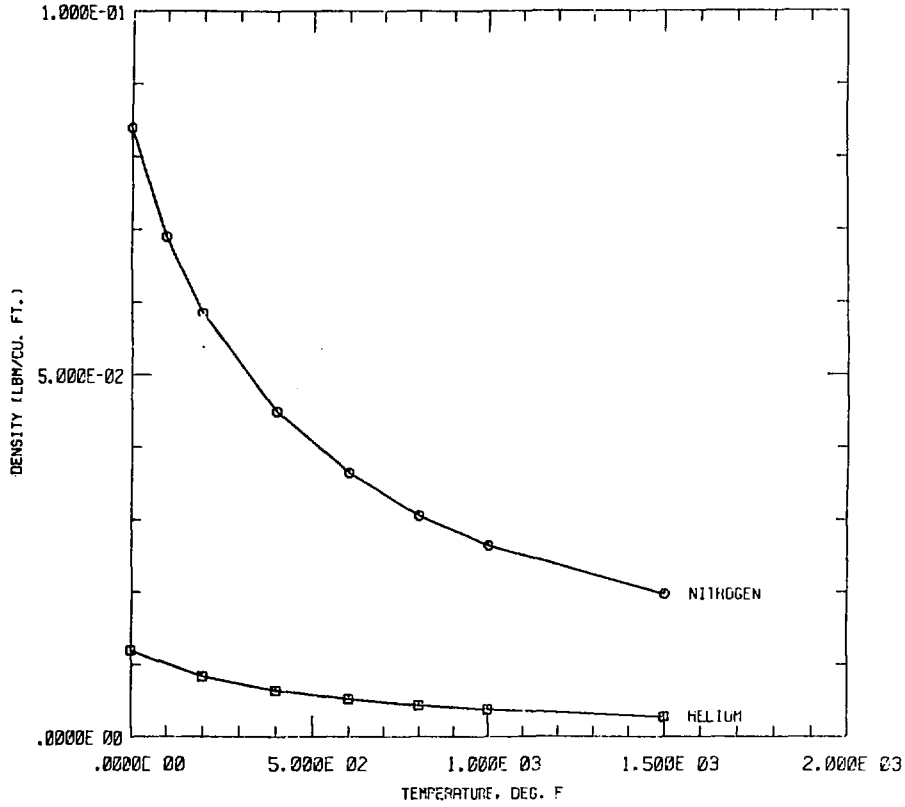

FIGURE B-3 COMPARISON OF THE DENSITIES OF NITROGEN AND HELIUM

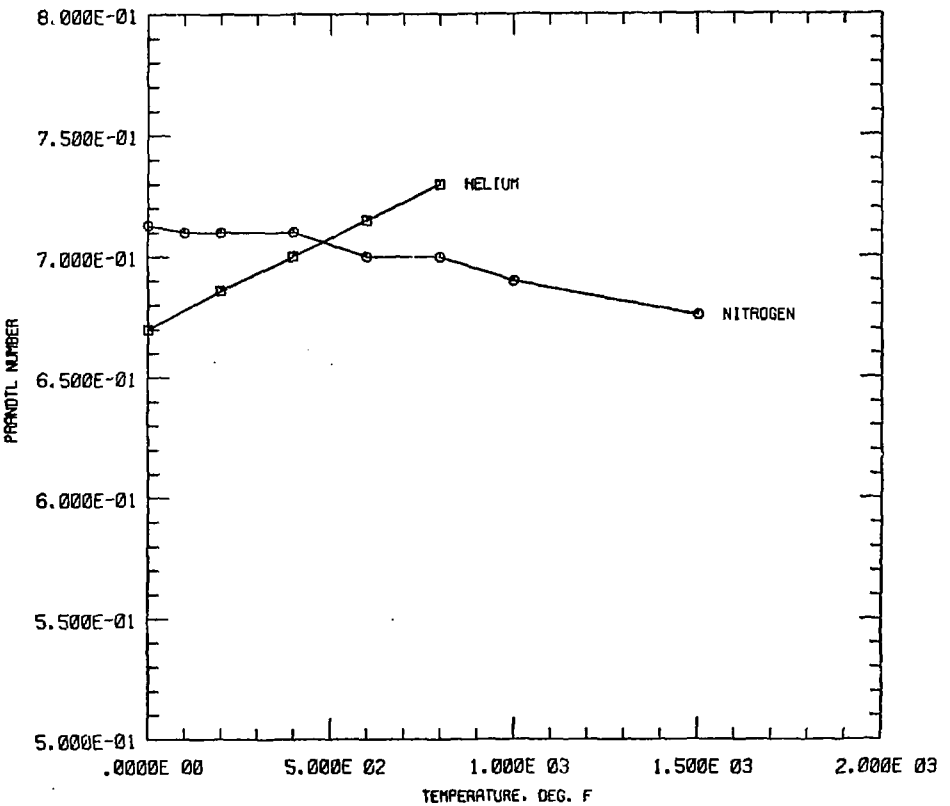

FIGURE B-4 COMPARISON OF THE PRANDTL NUMBER OF NITROGEN AND HELIUM

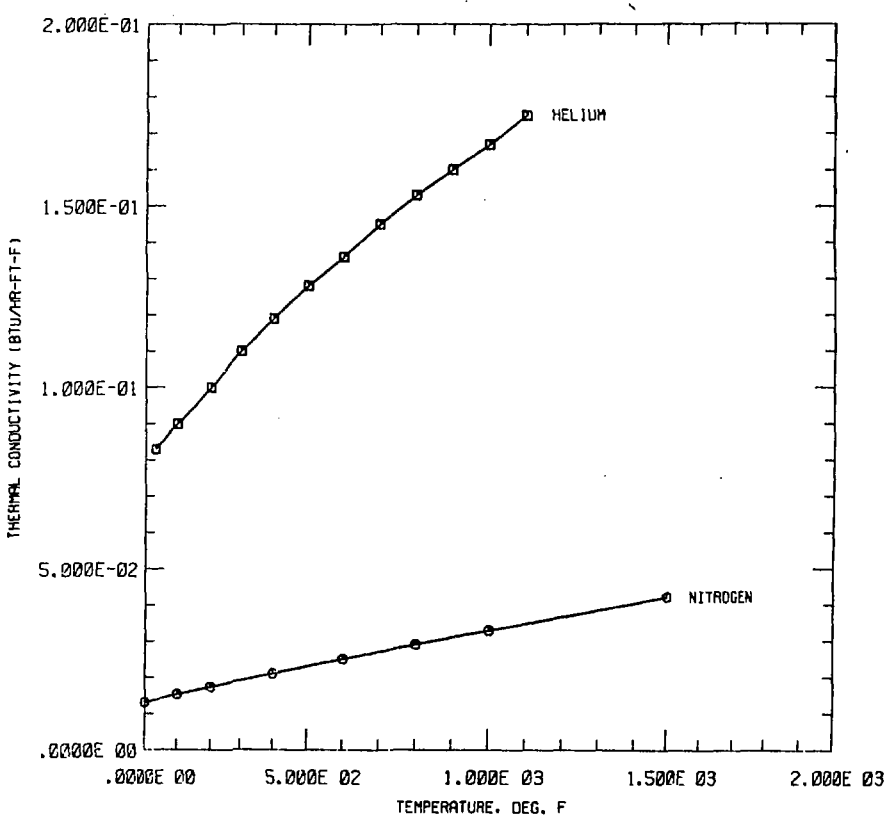

FIGURE B-5 COMPARISON OF THE THERMAL CONDUCTIVITY OF NITROGEN AND HELIUM

Appendix C

Material Compositions and Mixture Specifications

Material compositions and mixture specifications for the gas-cooled reference reactor and test assembly are given in Tables C-1 and C-2, respectively.

Table C-1 Material Composition for the Reference Gas-Cooled HFFPR and Test Assembly Regions

Region	Material	Volume Fraction	Density (g/cc)
Test Assembly Core Region	Mixed Oxide Fuel	0.434	10.0
	Na Coolant	0.4111	0.82
	Gap (void)	0.0113	--
	Clad-Stainless Steel*	0.1436	7.92
Test Assembly Axial Blanket	Depleted UO_2	same as above	same as above
	Na Coolant		
	Gap		
	Clad		
Test Assembly Coolant	Na	100%	0.82
Test Assembly Stainless Steel* Containment	Fe 71 w/o Ni 10 w/o Cr 19 w/o	100%	7.92
Air	N 76.7 w/o O 23.3 w/o	100%	0.976×10^{-3}
Reactor Cavity Liner	Fe 71 w/o Ni 10 w/o Cr 19 w/o	100%	7.92
Homogenized Driver Core Cell	BeO/UO_2 Fuel	0.6592	4.0
	Gas Coolant	0.25	--
	Gap (Void)	0.0356	--
	Clad-Stainless Steel*	0.0552	7.92
Homogenized Axial Blanket of Driver	Graphite	0.6592	1.7
	Gas Coolant	0.25	--
	Gap (void)	0.0356	--
	Clad-Stainless Steel*	0.0552	7.92
Radial Reflector	Graphite	100%	1.7

*Stainless steel 304 was substituted for stainless 316 in the neutron transport calculations because our molybdenum cross section tape was defective.

Table C-2

Mixture Specifications for the HFPPR and Test Assembly Regions

Region	Nuclide	Heavy Atom % (where applicable)[a]	Atom Densities (Atoms per Barn-Centimeter)
Homogenized Test Assembly Region	Pu-239	30.16	2.917 E-3
	Pu-240	4.06	0.393 E-3
	Pu-241	0.59	0.057 E-3
	Pu-242	0.07	6.9 E-6
	U-238	64.97	6.284 E-3
	U-235	0.15	0.014 E-3
	O-oxide		19.34 E-3
	Na-coolant		8.834 E-3
	Fe		8.711 E-3
	Ni		1.167 E-3
	Cr		2.503 E-3
	Mo		--
	Mn		--
Test Assembly Axial Blanket	U-238	99.3	9.661 E-3
	U-235	0.7	0.069 E-3
	O-oxide		19.46 E-3
	Na		8.834 E-3
	Fe		8.711 E-3
	Ni		1.167 E-3
	Cr		2.503 E-3
	Mo		--
	Mn		--
Sodium in Test Section at 1000°F	Na		0.02149
Steel Containment and cavity liner	Fe		0.06066
	Ni		0.00813
	Cr		0.01743
1 atm air at 5000 ft elevation	N		3.222 E-5
	O		0.8563 E-5
Fuel converter region (not used in reference design and not optimized)	Fe		0.04761
	Al		0.00198
	U-235	50	0.00072
	U-238	50	0.00072
	O		0.00288
	N		9.2 E-6 (1.1 E-6)[b]
	O		2.4 E-6 (0.3 E-6)[b]
	Fe		0.00335
	Ni		0.00045
	Cr		0.00096

[a] mixture for beginning of equilibrium cycle (BOEC)

[b] see footnote next page

Table C-2--Cont'd

Region	Nuclide	Heavy Atom % (where applicable)	Atom Densities (Atoms per Barn-Centimeter)	
Driver Core	U-235	40	0.00083	
	U-238	60	0.00123	
	Be		0.04129	
	O		0.04542	
	He		--	
	N		9.2 E-6	(1.1 E-6)[b]
	O		2.4 E-6	(0.3 E-6)
	Fe		0.00335	
	Ni		0.00045	
	Cr		0.00096	
	Mo		--	
	Mn		--	
Homogenized Driver Axial Reflector	C		0.05636	
	He		--	
	N		9.2 E-6	(1.1 E-6)[b]
	O		2.4 E-6	(0.3 E-6)
	Fe		3.35 E-3	
	Ni		0.45 E-3	
	Cr		0.96 E-3	
	Mo		--	
	Mn		--	
Radial Reflector	C		0.0855	

[b]Numbers in brackets represent air in gap of fuel element. Total value represents gap plus 1 atm air in the coolant channel.

References

1. Fast Reactor Safety Research Program Quarterly Report, SAND 77-0611, NUREG-0181-2, Sandia Laboratories, Albuquerque, NM, p.55, January-March 1977.

2. Advanced Reactor Safety Research Program Quarterly Report, SAND 77-1134, NUREG-0181-3, Sandia Laboratories, Albuquerque, NM, p.88, April-June 1977.

3. N. M. Greene, G. L. Lucius, L. M. Petrie, et al, AMPX: A Modular Code System for Generating Coupled Multigroup Neutron-Gamma Libraries from ENDF/B, ORNL/TM-3706, Oak Ridge National Laboratory, Oak Ridge, Tennessee, March, 1976.

4. P. S. Pickard and W. H. Vandevender, User's Manual for the CDC-6600 Version of AMPX, SAND 77-1148, Sandia Laboratories, Albuquerque, NM, November 1977.

5. L. M. Petrie and N. F. Cross, KENO IV--An Improved Monte Carlo Criticality Program, ORNL-4938, Oak Ridge National Laboratory, Oak Ridge, Tennessee, November 1975.

6. K. D. Lathrop and F. W. Brinkley, TWOTRAN II: An Interfaced, Exportable Version of the TWOTRAN Code for Two-Dimensional Transport, LAS-4848-MS, Los Alamos Scientific Laboratory, Los Alamos, NM, July 1973.

7. K. D. Lathrop, DTF-IV-A FORTRAN IV Program for Solving the Multigroup Transport Equation with Anisotropic Scattering, LA-3373, Los Alamos Scientific Laboratory, Los Alamos, NM, July, 1965.

8. Paul S. Pickard and Jay P. Odom, Sandia Reactor Kinetics Codes: SAK and PK1D, SAND 77-1211, Sandia Laboratories, Albuquerque, NM, 1977.

9. J. P. Peterson, et al, TAC2D--A General Purpose Two-Dimensional Heat Transfer Computer Code, GA-8868, Gulf General Atomic, Inc., San Diego, CA, September 1969.

10. Gordon E. Hansen and William H. Roach, Six and Sixteen Group Cross Sections for Fast and Intermediate Critical Assemblies, LAMS-2543, Los Alamos Scientific Laboratory, Los Alamos, NM, December 1961.

11. M. M. El-Wakil, Nuclear Heat Transport, International Textbook Company, Scranton, Pennsylvania, 1971.

12. R. L. Brehm, et al, High Flux Fast Pulsed Reactor Fuel Pin Thermal-Hydraulic Stress and Heat Removal Study for Sandia Laboratories Contract No. 06-3877, College of Engineering, The University of Arizona, Tucson, Arizona, 1977.

13. David L. Hetrick, Dynamics of Nuclear Reactors, University of Chicago Press, Chicago, Illinois, 1971.

14. Henry C. Monteith, Preliminary Design of the Cooling System for the High Fluence Fast Pulsed Reactor (HFFPR), Sandia Laboratories, Albuquerque, NM, SAND 77-0963, to be published.

15. Ultra High Temperature Reactor Experiment (UHTREX) Facility Description and Safety Analysis Report, LA-3556 (Rev.), Los Alamos Scientific Laboratory, Los Alamos, NM.

16. John D. Allen, George E. Cort, et al, Conceptual Design for a Fast Reactor Safety Test Facility, LA-6031-MS, Los Alamos Scientific Laboratory, Los Alamos, New Mexico, October 1975.

17. R. W. Ostensen, Design Considerations for Epithermal Pulsed Reactors, SAND 77-1470, Sandia Laboratories, Albuquerque, NM, January 1978.

18. Jeffrey S. Philbin and Byron M. Carmichael, An Application of the Lagrangian Functional to Collapsing Reactor Cross Sections, LA-3992, Los Alamos Scientific Laboratory, Los Alamos, NM, December 1968.

19. PHOEBUS/UHTREX: A Preliminary Study of a Low-Cost Facility for Transient Tests of LMFBR Fuel, LA-NUREG-6501-MS, Los Alamos Scientific Laboratory, Los Alamos, New Mexico, October 1975.

20. Thermophysical Properties of Matter, TPRC Data Series, Purdue University, Vols. 1 and 4, IFI/Plenum Corp., New York, 1970.

21. Frank Kreith, Principles of Heat Transfer, Intext Educational Publishers, New York, Appendix 3, 1973.

22. R. Fazzolare, "Gas-Cooled Fast Breeder Reactor Designs with Advanced Fuel and Cladding," Nuclear Engineering and Design, Vol. 40, pp. 191-201, 1977.

23. LMFBR Alloy Development Program, Hanford Engineering and Development Laboratory Report, 7405-117.66 (1974).

24. A. R. Veca, et al, "Fuel Element Design for the 300 MW(e) Gas-Cooled Fast Breeder Reactor," Nuclear Engineering and Design, Vol. 40, pp. 81-99, 1977.

Distribution:

4400 A. W. Snyder (2)
4420 J. V. Walker (15)
4422 R. L. Coats
4423 J. E. Powell
4424 P. S. Pickard
4424 B. Rosenstroch (15)
4425 W. J. Camp
4430 R. M. Jefferson
4450 J. A. Reuscher
4451 T. R. Schmidt
4452 L. D. Posey (5)
4452 J. S. Philbin (15)
8266 E. A. Aas

3141 T. L. Werner (5)
3151 W. L. Garner (3)
for DOE/TIC, Unlimited Release

3172-3 R. P. Campbell (25)
for DOE/TIC, Unlimited Release